In response to **2014 ESA's Call for a M-4 Mission** to be launched in 2025

Nitrogen Ion TRacing Observatory (NITRO)

M. Yamauchi, I. Dandouras, and H. Rème

A comprehensive study of Nitrogen dynamics in the upper atmosphere, inner magnetosphere and auroral region with astrobiological perspectives
(Cosmic Vision theme 1.3 and 2.1)

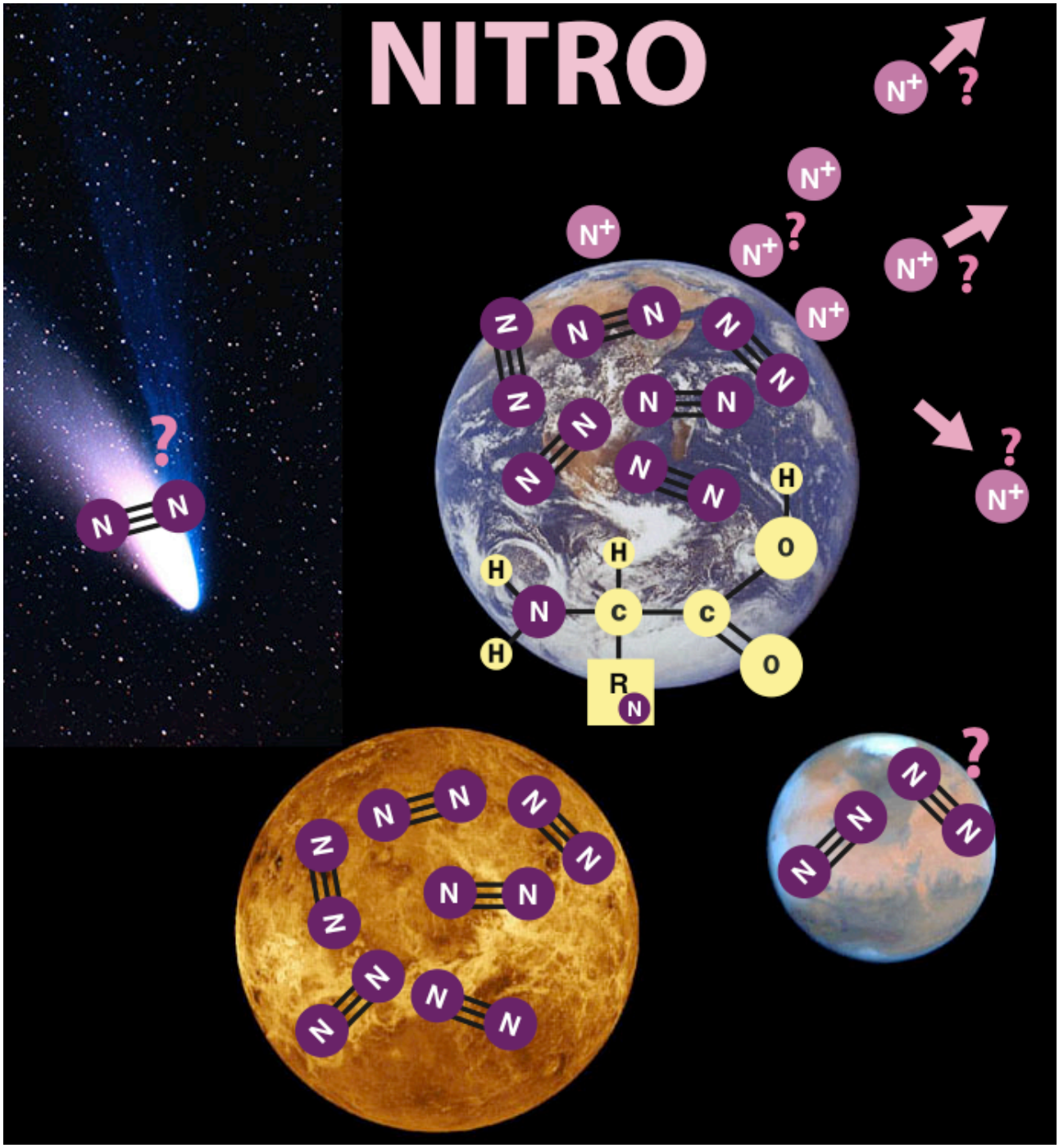

Proposing team for the NITRO mission

Core (comitting >20% working time)

M. Yamauchi <M.Yamauchi@irf.se> **(single-point contact)**
Swedish Institute of Space Physics (IRF), Box 812, S-98128 Kiruna, Sweden
telephone: +46-980-79120 / fax +46-980-79050

I. Dandouras <Iannis.Dandouras@irap.omp.eu> and **H. Rème** <Henri.Reme@irap.omp.eu>
CNRS and Paul Sabatier Toulouse University, Institut de Recherche en Astrophysique et Planétologie (IRAP), 9 avenue du Colonel Roche, BP 44346, F-31028 Toulouse, Cedex 4 France

Spacecraft design

P. Rathsman <peter.rathsman@ohb-sweden.se>, OHB-Sweden, Kista, Sweden

PI, PI institute, & main national funding agency for scientific payload (blue=LoE or acknowledment)

PI	PI institute	Funding
(a) I. Dandouras	IRAP (above)	**CNES**
(b) M. Wieser	IRF (above)	**SNSB**
(c) P. Wurz	University of Bern, Physikalisches Institut, Bern, Switzerland (UBern)	**SSO**
(d) L. Kistler	University of New Hampshire, Durham, USA (UNH)	**NASA**
(e) J. De Keyser	Belgian Institute for Space Aeronomy, Brussels, Belgium (BIRA-IASB)	**BELSPO**
(f) R. Nakamura	Institut für Weltraumforschung, Graz, Austria (IWF)	**ALR**
(g) B. Grison	Institute of Atmospheric Physics, Academy of Sciences, Prague, Czech Republic (ASCR/IAP)	**PRODEX**
(h) J.-L. Pincon	Laboratoire de Physique et Chimie de l'Environnement et de l'Espace, Orléans, France (LPC2E)	**CNES**
(i) A. Fazakerley	Mullard Space Science Laboratory, Uiversity of College London, Surrey, UK (MSSL)	**UKSA**
(j) J. Sample	Space Sciences Laboratory, U. California, Berkeley (UCB), USA (UCB/SSL)	**NASA**
(k) E. Quemerais	Laboratoire ATmosphères Milieux Observations Spatiales, Paris, France (LATMOS)	**CNES**
(l) N. Paschalidis	NASA Goddard Space Flight Center, Greenbelt, USA (GSFC)	**NASA**
(m) T. Sakanoi	Tohoku University, Sendai, Japan (TohokuU)	JAXA*
(n) S. Yokota	Institute of Space and Austronautic Studies, Sagamihara, Japan (ISAS)	JAXA*
(o) J.-M. Jahn	Southwest Research Institute, San Antonio, USA (SwRI)	**NASA**
(y) I. Daglis	University of Athens, Greece (UAthens)	**GRST**
(**) O. Marghitu	Institute for Space Sciences, Bucharest, Romania (ISS)	**ROSA**

* under application process. ** Interdisciplinary Analyses Coordinator

CoI institute for subsystem and programming, & main national funding agency for scientific payload

CoI institute	Funding
Space Research Center, Warsaw, Poland (SRC-PAS)	**IID**
University of Sheffield, UK (USheffield)	**UKSA**
Laboratoire de Physique des Plasmas, Polythechnique, Paris, France (LPP)	
Geoforschungszentrum Potsdam, Germany (GFZ)	
University of Tokyo, Japan (UTokyo)	JAXA*
Finish Meteorological Institute, Helsinki, Finland (FMI)	
Aalto University, Helsinki, Finland (AaltoU)	

PI and PI institute Science coordinator and ground-based optical observations

country	PI	PI institute
Norway	F. Sigernes	University Centre in Svalbard, Longyearbyen (UNIS)
Finland	K. Kauristie	FMI
Sweden	U. Braendstroem	IRF

Executive Summary (2 pages)

The **NITRO** mission for the first time studies the distribution, budget, dynamics and escape rate of nitrogen around the Earth, by monitoring magnetospheric nitrogen ions (N^+ and N_2^+) and exospheric nitrogen and by distinguishing N^+ from O^+ in the inner magnetosphere, polar cap, and just above the ionosphere at all relevant energies.

With a two-spacecraft configuration, using both in-situ plasma measurements and line-of-sight integrated remote sensing measurements of emissions, the **NITRO** mission will shed light on major questions from six different disciplines related to the Cosmic Vision themes CV1.3 and CV2.1 multi-disciplinary objectives:

* **Ancient Earth** (amino acid formation depends on relative abundance of atmospheric N, O, & H).
* **Planetary Evolution** (why is the N/O ratio on Mars only 0.1% of Earth, Venus, or Titan).
* **Exospheric Morphology** (no direct measurement exists of the exosphere above 1500 km).
* **Ionospheric Physics** (ionization at the topside ionosphere at different solar forcing/geomagnetic conditions determines ion escape and ionosphere-exosphere-magnetosphere coupling).
* **Magnetospheric Dynamics** (the global consequences of the circulation of plasma of ionospheric origin and the dependency of the N-O-H ratio on solar coronal and wind conditions are not well understood).
* **Space Plasma Physics** (tracing ions with similar masses but different initial topside ionosphere velocities gives extra information on energization mechanisms in space).

Nitrogen dynamics in the magnetosphere has not been thoroughly investigated in the past due to the difficulty in separating N^+ from O^+. However, our limited knowledge of the behavior and energization of N^+ and N_2^+ in the magnetosphere (<20 eV and > 50 keV) indicates that N^+ and N_2^+ escape is more strongly dependent on the solar UV and solar wind conditions than the escape of O^+, although N and O have very similar masses, indicating that the outflow dynamics may be quite different. The mass resolution of ion instruments has recently improved for such N/O separation. In addition, the sensitivity of telescopes in the UV-visible range has also improved so as to allow detecting emission lines of magnetospheric N^+ and N_2^+. Thus now is the time for these important questions to be addressed.

Just detecting and distinguishing nitrogen from oxygen is a task that could be performed by one small spacecraft. However, a much richer result can be achieved with two spacecraft because the relationship between source conditions (topside ionosphere) and the outflow can be determined, and temporal/spatial structures can be differentiated. Without understanding the source conditions, knowledge of the nitrogen budget and dynamics would not be very complete.

The **NITRO** mission consists of two spacecraft, one of which is Sun-pointing and spinning (spin period of 20-30 sec) at an 800 km x 33000 km altitude orbit (apogee at about 6 R_E geocentric distance) with 68.5° inclination for in situ plasma measurements in the magnetosphere (the "in-situ SC"). The other spacecraft is three-axis stabilized at a 500 km x 2400 km altitude orbit with 88.35° inclination for optical measurements of line-of-sight integrated emissions from the magnetospheric plasma and monitoring of plasma and neutral conditions just above the ionosphere and the exosphere (the "remote-sensing SC").

The 68.5° inclination of the in-situ SC orbit makes the apogee drift by about 24°/year in latitude and -53°/year in longitude (about 413°/year with respect to the Sun), covering the inner magnetosphere three-dimensionally in three years, with minimal risk of the instruments being adversely affected by the radiation belt (expected total dose less than 50 krad after 5.5 mm / 5 mm Aluminum for the in-situ and remote sensing SC, respectively). The longitudinal (RAAN) drift rates of these two spacecraft are the same with maximum 5°/year separation with maximum error in the orbit insertion (0.15° in inclination).

Such drift phase locking allows the ultraviolet and visible telescopes (NUVO) onboard the remote-sensing SC to have the in-situ SC in the NUVO's field-of-view (FOV) the majority of the time, with about 850 hours/year of visibility of the in-situ SC from the apogee traversals (> 1800 km altitude, below which the density contribution from the upper ionosphere is significant) in the polar region outside the radiation belts (invariant latitude (Inv) >60°), although the observation will be made at even lower altitude to obtain the altitude dependence. This allows comparison of the column densities and the local densities of N^+, N_2^+ and O^+, to separate temporal variations and spatial structures in the in-situ observations during the full mission time of three years. Although the remote-sensing SC has optical telescopes (NUVO) with narrow FOV, the pointing does not require more than 1° accuracy because the remote target region is less than 10 R_E away.

The remote-sensing SC also allows to directly detect the ion and neutral population and outflow at and above the upper ionosphere and in the exosphere. The two spacecraft do not have to be magnetically conjugate to detect the same ion population at both spacecraft. However, ions that enter the inner magnetosphere start drifting in the longitudinal direction by magnetic and ExB drifts, while the in-situ SC

covers a longitudinal range of more than 20°, the in-situ SC can detect the same ion population if ions are bouncing between both hemispheres as a bonus.

The payloads are classified into four categories: core scientific instruments (SIs) that directly measure nitrogen ions; supporting SIs that are required to understand the nitrogen measurements; supporting non-scientific payloads that should be included as a spacecraft subsystem; and optional SIs. The core SIs measure magnetospheric nitrogen ions (cold, hot, and energetic), upper ionospheric cold ions, and exospheric neutral nitrogen, by detecting ions and neutrals directly, or indirectly through nitrogen emission lines (UV 91 nm, 108 nm, 123-139 nm, visible 391 nm, 428 nm).

Supporting SIs on the in-situ SC include Langmuir probes for spacecraft potential measurements (the potential is most likely small on the remote sensing SC), a magnetometer to provide approximate pitch angle information and for determination of the existence of O^+/N^+ cyclotron waves, electron instruments that define the local magnetospheric region of the in-situ SC as well as the connectivity to the ionosphere through the photoelectrons, and wave measurements to help understand the energization of the ions to more than the escape velocity. Supporting SIs on the remote sensing SC include a CCD camera that monitors ionospheric airglow and the auroral conditions, and a low-energy ion analyser (< 100 eV) for the source ion energies at the topside ionosphere and the spacecraft potential that is better determined by a Langmuir probe.

Supporting non-scientific payload includes active spacecraft potential control for the in-situ SC and a scanner for the UV/visible telescopes on the remote sensing SC. Finally, the optional measurements take advantages of the unique orbital configuration of the two-spacecraft mission, significantly widening the science beyond the original requirements. These measurements include: ENA at the in-situ SC; hot precipitating heavy ions above the ionosphere; electrons; and waves including a Langmuir probe at the remote sensing SC.

Mission success strongly relies on the ability to distinguish the masses of heavy ions (N^+, O^+ and N_2^+) when and where their energy flux is only about $10^{5\text{-}7}$ keV cm^{-2} s^{-1} str^{-1} keV^{-1} (cf. Figure 1.4), and on removing penetrating background contamination from the radiation belt particles. Ion data from recent space missions (Cluster, Mars Express, Rosetta, and Prima) indicate that such mass separation in the bulk hot-plasma energy range is possible with two ion instruments: one for heavy ions (M/q = 10 - 40 amu) that examines N^+, O^+ and N_2^+ only and masks H^+ and He^+, and the other for lighter ions (M/q = 1 - 20 amu). Therefore, the core SIs include multiple complementary ion instruments with mass separating ability. The "one instrument measures everything" concept was the major reason why N^+ behavior was never fully determined in the past and is a pitfall that we avoid with the NITRO mission.

Information on the energetic particle flux is transferred separately in housekeeping (HK) data so that the spacecraft can react autonomously to a high radiation belt flux by switching off (or putting into a safe mode) various instruments as needed. Real-time analysis of the high-energy and penetrating particle count rates thus constitutes a "virtual instrument", that is able to identify the traversals of the radiation belt boundaries.

The other requirements are:

* A conductive surface for the spacecraft bodies.
* No requirement for real-time positioning.
* Free field-of view of particle instruments on board the in-situ spacecraft from solar panels and booms.
* 3D coverage of the tophat type particle instruments every spin for the in-situ spacecraft.
* Free field-of view of the optical instruments from solar panels and booms.
* Attitude of the remote-sensing SC should enable NUVO looking the in-situ SC's apogee with one-dimensional scanner.
* Moderate magnetic cleanliness (10 nT at magnetometer sensor locations on a boom at 5 m and 3 m).
* Minimum EMC cleanliness (at only 1-10 Hz, and three times easier than Cluster).
* Particle cleanness of the spacecraft from propulsion system nitrogen (and firing only during perigee).
* Temporal measurement resolution of 2 min for the in-situ SC and 30 sec for the remote-sensing SC
* More than 0.5 GByte/day data telemetry for each SC, which can be achieved by a 5W transmitter for the in-situ SC (equatorial station) and a 2 W transmitter for the remote sensing SC (high-latitude station).
* All instruments should have correct radiation shielding that amounts to a nearly 50 krad upper limit in three years with 5.5 mm Aluminum for the in-situ SC and 5 mm Aluminum for the remote sensing SC.

The total mass and power of scietific payloads including shielding is 50 kg/75 W for in-situ SC and 27 kg/44 W for remote sensinf SC. The three-year mission cost with baseline design would be about 430 MEUR, including two VEGA launches (45 MEUR x 2), two spacecraft with a kick motor (70 MEUR + 75 MEUR), integration tests (10 MEUR x 2), supporting payloads and subsystems (25 MEUR), operations and arichiving (90 MEUR), and 13% management cost of ESA (60 MEUR).

1. Scientific Objectives (9.5 pages)

Nitrogen constitutes 78% of Earth's atmosphere and is also essential for life as a key element in amino acids and living organism, e.g., the Redfield-Brzezinski stoichiometric ratio for diatomic plankton in the terrestrial ocean is C:Si:N:P = 106:15:16:1 (Brzezinski, 1985). Atmospheric molecular nitrogen is cycled into the Earth's surface by various biological and inorganic processes, and returned mainly by bacterial denitrification. However, we have very little knowledge of the fate of atmospheric nitrogen and its direct products (atomic nitrogen N, ionized nitrogen N^+ and N_2^+) compared to oxygen and its products (O and O^+) above 1000 km altitude. Since the chemical bonding for the nitrogen molecule (triple bonding) is different from the oxygen molecule (double bonding), the ionization height is quite different for these two abundant elements, although they have similar molecular masses. Thus one cannot use our knowledge of O^+ behavior to understand N^+.

1.1. Introduction: Past Observations of Magnetospheric Heavy Ions

Missing observations

Already more than three decades ago, Chappell et al. (1982) found cold (< 30 eV) N^+ and N_2^+ in the magnetosphere. In subsequent years, observational knowledge gradually expanded on the nitrogen ions N^+ and N_2^+, as separated from O^+ and O_2^+, in the geospace environment. Dynamics Explorer 1 (DE-1: 1981 launch, polar orbit with apogee altitude about 16600 km) and Akebono (1989 launch, polar orbit with apogee altitude about 4000 km) carried suprathermal ion mass spectrometers. Both of these instruments, RIMS on DE-1 (Chapell et al., 1982; Craven et al., 1985) and SMS on Akebono (Yau et al., 1991) have shown non-contaminated N^+ and N_2^+ measurements above the ionosphere, but the measurement energy is limited to only < 50 eV for RIMS and < 30 keV for SMS. The Canadian e-POP mission (Enhanced Polar Outflow Probe, launch 2012, polar orbit with apogee altitude about 1500 km) also carries a suprathermal ion mass spectrometer (IRM) measuring up to 90 eV, and has identified N^+ and N_2^+ at the upper ionosphere according to PI of IRM, but results of the analyses are not yet available.

Energetic nitrogen ions of > 10 keV have also been detected by the AMPTE (launch 1984, equatorial orbit with apogee altitude about 50000 km) CHEM instrument (Hamilton et al., 1988), the WIND/STICS instrument (Mall et al., 2002), the Geotail/STICS instrument (Christon et al., 2002) and the CRRES/MICS instrument (Liu et al, 2005). However, these past magnetospheric missions have never separated N^+ or N_2^+ respectively from O^+ or O_2^+ over the energy range of 50 eV- 10 keV. For Mars, we will eventually have more knowledge (pending publication of cold ion mass spectrometer data from the MAVEN Mars orbiter), but no matter what the result will be, the importance of Earth observation increases.

This lack of measurements creates a significant gap in our knowledge because the measured velocity of the cold N^+ is lower than the escape velocity, i.e., these observations do not give information on how much is lost. Furthermore, we also do not have the theoretical predictions of Jeans escape or other neutral forms (both cold and energetic) of escape for nitrogen loss. This contrasts with the terrestrial oxygen ion (O^+) measurements that have been intensively studied during past decades (e.g., Peterson et al., 2008, Slapak et al., 2013). The oxygen measurements are not limited to the Earth, and we have substantial knowledge on the O^+ dynamics even on Mars and Venus (Nilsson, 2011, Fedorov et al., 2008).

One reason for the lack of N+ observations is the difficulty in separating N^+ from O^+ in the time-of-flight (TOF) instruments flown to date. The modern instrumentation for the magnetospheric missions has been mainly aimed at higher temporal resolution and angular coverage (from 2D to 3D) with lighter weight, and not at better mass resolution. Although many mass-resolving ion instruments for hot plasma in the 0.01-10 keV range (on board AMPTE-CCE, CRRES, FAST, POLAR, and Cluster) have a design of $m/\Delta m > 10$, actual data have not yet reached such an ideal specification. Cluster/CODIF (launch 2000, 0.03-40 keV, $m/\Delta m \sim 4$ to 7, Rème et al., 2001) resolves H^+, He^{++}, He^+, O^+, and molecular ions, but does not resolve N^+ from O^+. This is also true for the low energy range of CRRES/MICS (launch 1990, 1-430 keV/q), and for AMPTE-CCE/HPCE (< 17 keV/q).

What do past N^+ and O^+ measurements imply?

According to the limited cold ion observations in the magnetosphere to date, N^+ outflow from the Earth's ionosphere to the magnetosphere dramatically increases during periods of high geomagnetic activity (Figure 1.1, left panels). Specifically, the N^+/O^+ ratio increases from < 0.1 during geomagnetic quiet periods to 0.5~1.0 during geomagnetic active periods (Yau and Whalen, 1992). Thus the behavior of N^+ and O^+ are apparently different, and independent measurements of N^+ and O^+ escapes are needed to understand this. This difference partly comes from the difference in the initial speed or energy at the topside of the

ionosphere between N^+ and O^+, as was reported with cold ion measurements by Chappell et al. (1982). Molecular nitrogen ions, which are considered to be the mother ions for producing atomic nitrogen ions, also escape but the amount of N_2^+ escape is less than N^+ escape (Yau et al., 1993). The N_2^+/N^+ ratio is < 0.1 during geomagnetic active periods, and no N_2^+ outflow has been observed during quiet periods. Furthermore, O^+ loss is primarily driven by polar outflows but only 11% of these outflows escape the magnetosphere before return into the plasmaspheric and ionospheric ion populations (Seki et al. 2001), while N ion loss and return processes are relatively unquantified and unknown.

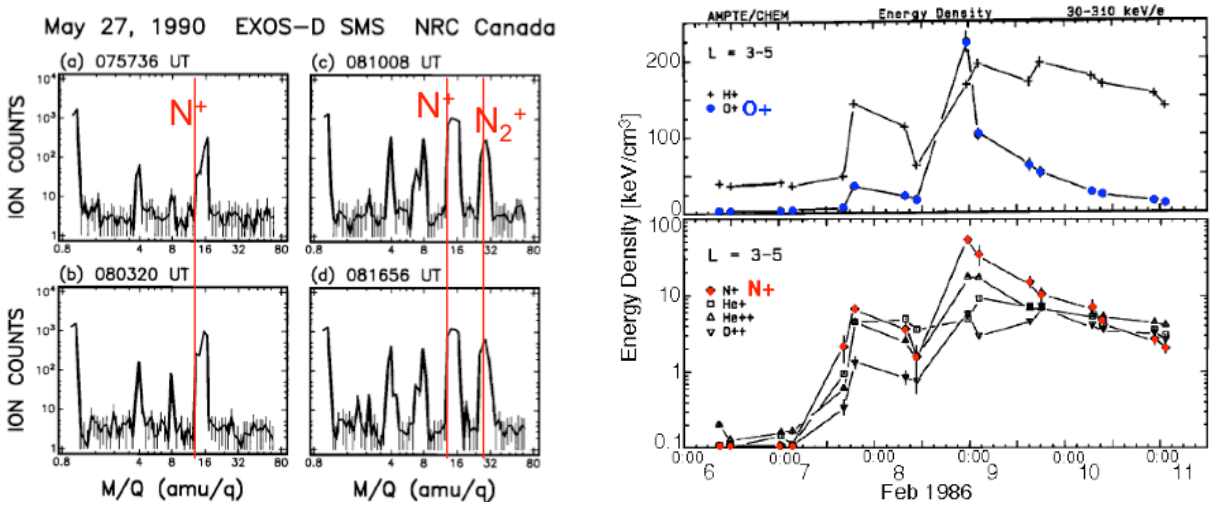

Figure 1.1: Akebono observations of cold ions at < 20 eV (left, SMS instrument, Yau et al., 1993) and AMPTE observation of energetic ions at > 30 keV (right, CHEM instrument, Hamilton et al., 1988): The broadening of M/q=16 in Akebono data is combination of N^+ and O^+, while no O_2^+, is detected in the N_2^+ channel. Both data sets indicate more dynamic change of N^+ compared to O^+.

The strong dependence of the N^+ outflow on geomagnetic activity is also detected at > 30 keV according to AMPTE observations. Figure 1.1 (right panels) shows the data acquired in the ring current during a magnetic storm, during which the enhancement of N^+ is the second strongest, after O+, and that of H^+ is the weakest among all species (Hamilton et al, 1988). The response of the two species to solar UV is also different. Surprisingly, the energetic N^+/O^+ ratio in the outer magnetosphere is a factor of two higher at solar minimum than at solar maximum (Christon et al. 2002, Mall et al. 2002). This is likely related to the effects of solar UV on the top-side ionosphere, but this overall dependence on solar UV is not understood.

In fact, the number flux of outflowing ionospheric ions from the ionosphere depends strongly on geomagnetic and solar activity, ranging between 0.03 - 0.15 kg/s for cold H^+ and 0.3 - 5 kg/s for cold heavy ions (O^+ and N^+) in the polar region (Cully et al., 2003). During geomagnetic activity, the inner magnetosphere becomes increasingly populated by the hot (0.01-10 keV) heavy ions ($O^+ + N^+$) that are traditionally tagged as O^+, consistent with the expected dependence of cold ion outflow on geomagnetic activity. Thus, the N^+/O^+ ratio, as well as the O^+/H^+ ratio or N^+/H^+ ratio, will be strongly dependent on external forcing, the degree of which cannot be determined without good observations separating O^+ and N^+. This information is essential in estimating the evolution of the atmosphere (particularly nitrogen) and its oxidation state on a geological scale for all planets, because geomagnetic and solar activities are expected to have been higher 4 billion years ago from Sun-in-Time studies on young G-type stars (Ayres, 1997, Yamauchi and Wahlund, 2007, Airapetian et al. 2014).

To understand the evolution of atmosphere through outflow, it is important to examine the outflow behavior at Earth now, during the relatively rare intervals of high geomagnetic activity, and then to treat these measurements as proxies for the past. We note here that the escape energy is around 10 eV for nitrogen (~5 km/s or ~2 eV for Mars and ~11 km/s or ~9 eV for Earth/Venus) and that ions are often accelerated to very high energies within a limited region. Furthermore, a magnetized planet has a magnetotail where cold ions can undergo cycles of adiabatic energization to one keV range (Yamauchi et al., 2009). Therefore, we need to measure N^+ (separate from O^+) over a much wider energy range below and above the escape velocity.

Fortunately, the mass-resolving ability of ion instruments has improved, and it has become possible to distinguish N^+ and O^+ within the 10 eV - few keV range, as demonstrated by the Japanese Kaguya mission in

which the single ion mass analyzer (MSA) succeeded in separating N^+ and N_2^+ from the other species at around 1 keV, although the geometric factor for N^+ and N_2^+ was much lower than that for O^+ and H^+ (Saito et al., 2014). Such a capability also opens up a possibility to investigate fundamental issues regarding the geospace environment with many unanswered questions as summarized in §1.2-1.7. For these questions, we can concentrate on the merit of distinguishing N^+ and O^+ rather than detailed studies of heavy ion dynamics (not distinguishing $C^+N^+O^+$).

All these observations indicate that N^+ and O^+ behave differently, particularly in their dependence on the solar radiation, solar wind, and geomagnetic activities. In other words, just studying the behavior of nitrogen ions (N^+ and N_2^+) as compared to oxygen ions (O^+) can contribute in answering fundamental questions in different scientific disciplines as described below (subsections §1.2, §1.3, and §1.4). In addition, such novel observations of nitrogen (N^+ and N_2^+) dynamics separated from O^+ dynamics naturally contribute to answering outstanding questions on plasma dynamics in space (subsections §1.5, §1.6, and §1.7).

1.2. Origin of Life: Chemical State of Ancient Earth

The nitrogen budget under different solar conditions is important from the astrobiology point of view, because nitrogen is a key element for pre-biotic molecules such as amino acids. Laboratory experiments (Figure 1.2) indicate that the formation of pre-biotic molecules is most likely related to both the amount and the oxidation state of the nitrogen (reduced form like NH_3, neutral form like N_2, and oxidized form like NO_x) near the surface in the ancient Earth (Miller and Urey, 1959). Without knowing the nitrogen abundance as compared to oxygen and hydrogen (for oxidation state of nitrogen), one cannot tackle the questions related to pre-biotic molecules and the origin of life.

Unfortunately, the relative abundance of nitrogen, oxygen, or hydrogen is expected to be quite different between the present value and the ancient value 4 billion years ago, because ion observations in space have detected massive escape of the CNO group ions from the ionosphere (Chappell et al., 1982, Nilsson 2011), and the relative amount of escaping N^+ and O^+ changes dynamically for energetic (>50 keV) ions and cold (< 20 eV) ions according to AMPTE and Akebono observations (Hamilton et al., 1987; Yau et al, 1993). In order to estimate the nitrogen abundance and its oxidation state 4 billion years ago, we need good estimates of the escape history on geological time scales,as done already for the water content on Mars using the O^+ escape measurements (Lammer et al., 2011).

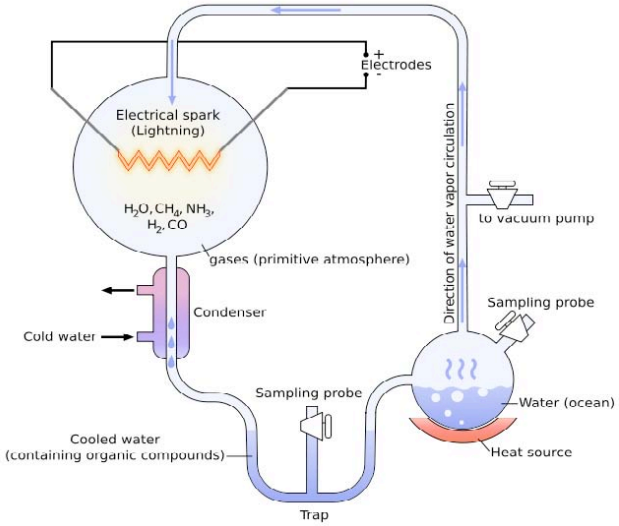

Figure 1.2: Miller's experiment to produce amino acid from modeled pre-biotic atmosphere. They imposed a discharge on the mixture of molecular gasses, simulating lighting on ancient atmosphere. After a series of experiments using different types of atmosphere, they found that (1) a reduced type atmosphere (NH_3) easily produces amino acids, (2) a neutral atmosphere (N^2) requires special conditions to produce amino acids, and (3) amino acids could not be produced from an oxidized atmosphere (NOx). Thus, low oxidation states of N (or relative amount N and O) are more important for non-biotic amino acid formation.

Since the ancient Sun had one to two orders of magnitude higher UV irradiance than at present (Ayres, 1997, Wood, 2006), even a small dependence on the solar, or stellar wind conditions would have led to large differences in ionic abundances. If the oxygen loss was about the same order as the nitrogen loss during extreme solar conditions, the ancient Earth should have had a neutral or weakly oxidized atmosphere. However, if the nitrogen loss was two orders of magnitude higher than the oxygen loss during high UV and active solar wind conditions, we would have lost significantly more nitrogen leading to a reduced atmosphere. The cold ion result cannot tell which is the case.

Faster solar rotation of the early Sun implies that there was a stronger solar dynamo, and hence a stronger and more variable interplanetary magnetic field (IMF). For the same reason, solar flares and

coronal mass ejections were most likely more active and larger in the past, resulting in more frequent and more dynamic atmospheric heating and geomagnetic storms than today. The solar energetic particles (SEP), constituted of MeV protons and higher energy electrons, are also expected to have been more frequent, causing increase of another type of atmospheric escape in the ion forms (Futaana et al., 2008). The elevated levels of solar FUV flux are thought to have resulted in a significantly more expanded ionosphere than we see today (Yamauchi and Wahlund, 2007), reaching altitudes even above the magnetosphere, perhaps to the degree that the early Earth should be considered as non-magnetized for the purposes of studying ion escape. Such conditions would appear to favor non-thermal loss mechanisms such as photo-chemical escape through the expanded exosphere and ionosphere.

Thus, the history of the average solar activity (SEP and solar UV flux) and solar wind activity can be estimated. Since average solar and resultant geomagnetic activities are likely the dominant external parameters affecting the amount and composition of the ion escape from the Earth (Peterson et al., 2006, Curry et al., 2003; Moore et al., 1999), we should be able to estimate the history of the average escape on a geological scale if we experimentally measure the different dependences of nitrogen and oxygen escapes on these parameters.

Estimation of the ancient atmospheric composition (the abundance of nitrogen and its oxidation state) then requires at least a zero-order estimate of the escape history of nitrogen compared with oxygen and hydrogen (eventually protons) on a geological scale. Fortunately the solar irradiance and solar wind conditions on a geological scale can, in the zero-order estimate, be represented by various solar, solar wind, and geomagnetic conditions as proxy. At the moment, we even lack this information, due to the absence of minimum observations of N^+ and N_2^+ in the magnetosphere: no observation for 90 eV - 30 keV up to now, and very limited observations at < 50 eV and > 30 keV from the 1980's and 1990's available. Therefore, systematic observations of N^+ and N_2^+ compared to O^+ and H^+ in the magnetosphere are mandatory pre-requisites for the study of origin of life formation on the ancient Earth.

By knowing the N^+/O^+ ratio of the escaping ions (for magnetospheric heavy ions at energies above the escape velocity, about 10 eV) for different conditions of solar activity (FUV flux and SEP), solar wind, and geomagnetic activity, we can also estimate the oxidation state of the ancient Earth. Since the O/H ratio of the observed non-thermal escape depends non-linearly on the solar parameters, with a high O/H ratio for a high solar input (Yamauchi and Wahlund, 2007), the ancient Earth must have had a much higher O/H ratio of atmospheric escape than at present. If N^+ escape is more sensitive to the solar input than O^+ escape, the N/O ratio (where O was most likely in the form of CO or CO_2) of the ancient atmosphere might have been much higher than at present, allowing a more reduced form of nitrogen to exist in the ancient atmosphere. Here, we should note the fact that the outflow fluxes do not depend in a simple way on any established activity indices. Therefore, obtaining even a generic response would be a big advancement.

Atmospheric nitrogen is essential for life development for one more reason: representing 78% of the Earth's atmosphere, it is a climate regulator through the pressure broadening effect (Goody and Yung, 1989). Although nitrogen is not a greenhouse gas, it plays a critical role in amplifying the greenhouse effect through the broadening of the infrared absorption lines of these greenhouse gases by collisional interaction with these molecules. In other words, if the total atmospheric pressure was lower, the climate forcing of greenhouse gases would be smaller, the magnitude of the greenhouse effect would be less, and the global mean temperature would drop (Li et al., 2009). Nitrogen also interacts with carbon, oxygen, and other atmospheric elements through bacterial fixation and denitrification at the Earth's surface.

1.3. Planetary Evolution: Mars Nitrogen Mystery

The study of nitrogen escape is crucial for comparative planetology. Nitrogen is abundant on the Earth (mainly in the atmosphere but also in minor amounts in the soil, crust, and oceans). It comprises 78% of the atmospheric pressure, or three quarter of total atmospheric mass of about $5 \cdot 10^{18}$ kg[1]. The amount of nitrogen in the Earth's soil, crust, and oceans is small compared to the amount in the atmosphere. Venus also has

[1] Since the atmospheric pressure (P_{tot}) is determined by the column mass above the measurement point, the column mass is estimated as P_{tot}/g, where g is the gravity, and the atmospheric total mass is calculated as $4\pi R^2 P_{tot}/g$, where $4\pi R^2$ [m] is the surface area of the planet/moon. This is about $5 \cdot 10^{18}$ kg for the Earth ($R_E = 6.4 \cdot 10^6$m, $P = 1.01 \cdot 10^5$Pa, $g = 9.8 ms^{-2}$). The total mass for species k is obtained by multiplying $(P_k/P_{tot}) \cdot (m_k/m_a)$ to this total mass, i.e., as $(4\pi R^2/g) \cdot P_k \cdot (m_k/m_a)$, where P_k/P_{tot} is the fraction of species k (78% for N_2 at the Earth), m_k is atomic mass [$kg \cdot kmol^{-1}$] for species k, e.g., 28 for N_2, 32 for O_2 and 44 for CO_2., and m_a is average atomic mass of the atmosphere [$kg \cdot kmol^{-1}$], i.e., 28.9 for the Earth.

abundant nitrogen with a total mass 2.5 times as much as that on the Earth[2]. However, Mars has only very little nitrogen, compared to the other planets, with only about 0.01% as much as on the Earth[3] (or 0.1% when comparing the ratio of nitrogen mass to planetary mass). The fact that Mars is colder and smaller than the Earth or Venus might be the cause, but Saturn's moon Titan, which is colder and smaller than Mars, has a very significant nitrogen atmosphere (>95%) resulting in more total nitrogen than on the Earth. Recent comet observations seems indicate N_2 existence even on comets, although confirmation is needed.

In contrast, the oxygen abundance is much more similar at Earth, Venus and Mars. Although the oxygen content in the Martian atmosphere (in the form of CO_2) is not very high today, significant amounts of oxygen are believed to exist in the Martian crust in the form of oxidized soil because the observed escape rate indicates the total oxygen loss of 1 bar, i.e., 10 m equivalent layer of water in thickness (Lammer et al., 2003; Barabash et al., 2007). Thus, the N/O ratio of Mars is three orders of magnitude less than those of the Earth, Venus, and Titan, that is called as the "Mars Nitrogen Mystery".

If the initial compositions of these planets were similar to each other, since they formed within the same vicinity in the protoplanetary nebula, the difference must be a result of nitrogen loss from the Martian atmosphere. The $^{15}N/^{14}N$ ratio also indicates extraordinary escape on Mars: this ratio ^{15}N is enriched in the Martian atmosphere compared to Venus and the Earth. In this case, Mars has retained oxygen (mass 16) but not nitrogen (mass 14) despite their similar atomic masses. At present, we do not know how the nitrogen could be lost only from Mars while it survived at Venus and Earth. None of the current known major escape mechanisms (a)-(g), particularly the thermal ones, can reasonably explain the extreme nitrogen loss on Mars:

(a) Jeans escape + momentum exchange for neutrals (thermal): Thermal tail exceeds the escape velocity and collisional transmission of momentum from escaping light molecules to heavier molecules.
(b) Photochemical heating for both ions and neutrals (thermo-chemical): Release of energy in the excited state, e.g., through recombination, gives escape velocity to the atom.
(c) Hydrodynamic blow off for both ions and neutrals (thermal): Same as the solar wind formation mechanism (might work under extreme radiation conditions during early Sun or Star conditions).
(d) Ion pickup and sputtering of neutrals by these ions (thermal and non-thermal combined): Ions that are newly exposed to solar wind start moving according to the electromagnetic force of the solar wind.
(e) Ion energization by electromagnetic energy (non-thermal): Solar wind energy impeded locally to low altitudes forms waves and field-aligned potentials that energize ionospheric and plasmaspheric ions.
(f) Large-scale momentum transfer for ions, e.g., instability-related transfer and reconnection (non-thermal): The solar wind dynamic pressure and electromagnetic forces push the planetary plasma anti-sunward at the boundary region of the magnetosphere.
(g) Adiabatic energization of ions (non-thermal): Small disturbances are enhanced through magnetospheric convection and finally escape, e.g., plasmaspheric plumes.

The Jeans escape and hydrodynamic escape are expected to be small for nitrogen on Mars. The photochemical escape is sufficient from some Mars model but the same model does not explain Venus very well. On the other hand, large uncertainty is expected for the non-thermal escape of N^+, because we do not have a good quantitative model of non-thermal escape against the external forcing that drastically changed during the past 4 billion years.

Although the triple-bond nitrogen molecules are generally more difficult to dissociate and ionize than double-bond oxygen molecules, this situation might be changed if the oxygen is protected by stronger binding, such as in the soil or in the form of CO_2. In such cases, it is unclear whether the nitrogen loss occurred while oxygen was tied up in the soil or while both species were similarly abundant in the atmosphere. If the early Martian atmosphere was more oxygen-rich, e.g., due to early lose of water-origin hydrogen, this might also account for the difference. Another possibility is that non-thermal escape did not contribute at all, and the ancient ionospheric conditions of an expanded ionosphere (Yamauchi and Wahlund, 2007) allowed an extremely strong photochemical escape. It is also possible that nitrogen ion formation drastically increases with increasing solar activity and solar wind activity. Thus we have at least three

---

[2] Partial pressure of N_2 at the Venus surface (3.5% of 92 atm) is about 4 times that of the Earth, surface area and gravity are both 0.9 times those of the Earth, and $m_{N2}/m_a = 0.64$, yielding to 2.5 (or 3) times the Earth for total amount (or ratio to planetary mass). (nssdc.gsfc.nasa.gov/planetary/planetfact.html)

[3] Partial pressure of N_2 at the Martian surface (2.7% of 0.0064 atm) is about 0.02 % of that of the Earth, surface area gravity are 0.28 times and 0.38 times those of the Earth, respectively, and $m_{N2}/m_a = 0.65$, yielding to about 0.01 % of the Earth for total amount.

possibilities, and cannot investigate this problem without actual observation of nitrogen ion dynamics in space.

Such a fundamental study can and must be done at the Earth first. Determining the non-thermal nitrogen energization mechanism(s) and amount of outflow, compared to oxygen in the Earth's ionosphere-magnetosphere system, is mandatory as the reference before we can investigate the Mars Nitrogen Mystery. The current data on the Earth's ionospheric nitrogen outflow is far from sufficient to understand the escape problem because most of the measured ions are cold, well under the escape energy.

Even ions that escaped from the ionosphere sometimes return back to the Earth (Ejiri et al., 1978; Yamauchi et al., 2009; Haaland et al., 2012). Such a return takes place also on Mars (Hara et al., 2013). In-situ observations in the magnetosphere are mandatory in order to observe the full nitrogen acceleration and transport. Remote sensing methods can also detect nitrogen column density, but do not measure the energy very well. Ideal observations should combination both, as illustrated in Figure 1.3.

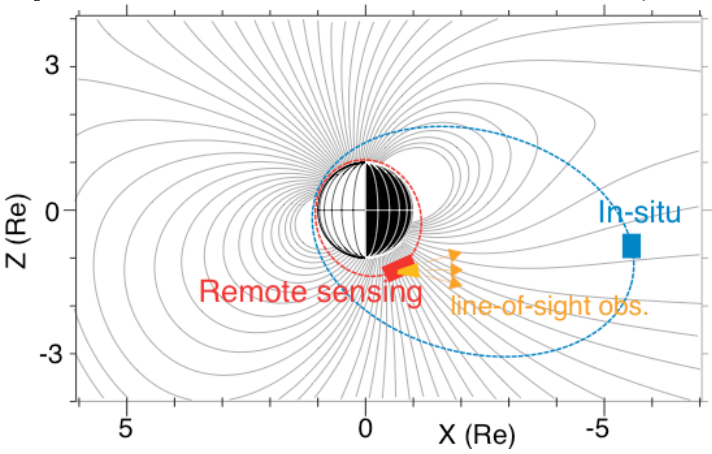

Figure 1.3: Illustration of observation region. The mandatory in-situ observations (blue) must include the inner magnetosphere, whereas it would be ideal to also monitor above the ionosphere, from which additional remote sensing of nitrogen column density (red) is possible. The exact orbit and instrumentation is given later.

1.4. Terrestrial Exosphere: First Direct Measurements at 1500-2400 km

We have very little knowledge of the terrestrial exosphere, and particularly of ion formation in the exosphere and non-thermal escape in neutral forms from the exosphere. The importance of the exosphere was recognized after Venus and Mars observations in the late 1980's found massive pickup ions of exospheric origin, because this ion pickup process turned out to be a significant atmospheric loss mechanism when the exosphere is exposed to the solar wind (including magnetosheath). However, with the large stand-off distance of the magnetopause due to Earth's dipole field, Earth's gravity is strong enough that the exosphere is very tenuous at the magnetopause. This is one of the reasons why the exosphere has not really been measured at high-altitudes, except through Lyman alpha (hydrogen) information and large-scale imaging information from FUV and EUV cameras (Bailey et al, 2011; Zoennchen et al., 2010, 2013). We have no direct measurement of the neutral exosphere above 1500 km, and even the UV measurements are limited to hydrogen. So far we know that the exobase is low during solar minimum (300-500 km) and high (1000 km) during solar maximum.

The lack of exospheric knowledge hinders the understanding of the upper ionosphere, because the exosphere is the ionization source. This is particularly important for nitrogen (N_2) because its ionization altitude is expected to be very high (note that photo ionization of N_2 causes N^+ and N directly). Since electron data from past missions at altitudes less than 1500 km show a photoelectron line for nitrogen at about 24-30 eV, the existence of N_2 in the exosphere and even N in the exosphere as the by-product of the N_2 -> N^+ + N reaction is evident, but we do not know how it works and varies. This means that to understand the source mechanism that produces cold (pre-accelerated) nitrogen ions in the upper ionosphere, direct detection of the nitrogen exosphere for both neutral and ionized nitrogen above 1000 km (in comparison to other exospheric constituents) is essential. The required measurement is somewhat different from that for the above two topics, but it is possible to make such a measurements with the observations proposed in Figure 1.3, and therefore it is worth having both observations.

1.5. Ionosphere: Dynamics, Chemistry, and Coupling with Exosphere

Since the exosphere-ionosphere coupling is relatively unknown at altitudes > 1500 km (and vaguely known > 1000 km), the dynamics of the source region where N^+ and N_2^+ are produced are also not well understood. Inversely, ionospheric dynamics, both internally excited and externally driven, is poorly understood at altitudes above 1000 km. Here external means both from space (including the Solar UV and radio bursts) and from the lower ionosphere or thermosphere.

From chemical theory as well as past observations below 1500 km, the ionization height of oxygen is lower than that of nitrogen (N^+). If the O^+ distribution shows any anomaly in the upper ionosphere compared to N^+, it is most likely rooted to either lower ionospheric convection of O^+ or production of N^+, depending on whether the anomaly is more on the O^+ distribution or on the N^+ distribution, respectively. This is already a strong clue in understanding the upper ionospheric dynamics compared to middle ionospheric dynamics.

One of the unknown but important dynamics is latitudinal transport. The N^+/O^+ ratio in the ion outflow above the ionosphere observed by Akebono indicates that N^+ ions are generally much less abundant than O^+ and the N^+/O^+ ratio increases only during large magnetic storms. The N^+ production most likely increases with increased input energy, and hence it is much larger in the auroral regions than in the sub-auroral regions. If a significant amount of N^+ is observed in the subauroral region, it indicates that either N^+ is transported to lower latitudes (which provides new information on the upper ionospheric dynamics) or there is increased production of N^+. Then O^+ data gives additional information on whether latitudinal transport is likely or not. This observation is not limited to the topside of the ionosphere but also applies to the magnetosphere, because escaped ions from the subauroral region are expected to stay trapped inside the inner magnetosphere. In this case, N^+ should be detected by both the in-situ SC and the remote sensing SC in Figure 1.3.

The ionization response time to the input conditions (both auroral and F10.7) is also an unsolved issue. At present, we know that the reaction time in the ionosphere is very quick (the chemical reactions take less than 1 s) for both N^+ and O^+. The transport to the higher altitude where energization starts is also quick for O^+, but this does not apply to N^+ because N^+ can be re-combined before reaching high altitudes. The overall response of N^+ to the input energy could well be slow, if we consider the time until actual energization and subsequent acceleration. Although the remote sensing SC passes above the source region too quickly to detect this response time, the in-situ SC is able to monitor the time scale to detect substantial response time differences between N^+ and O^+.

Another missing piece of information is the level of N^+ anomaly compared to the background level. At present we simply assume that the ionospheric composition for cold ions is uniform for the same solar zenith angle as the ground state without auroral precipitation. However, this is a simple assumption and, like in the stratosphere and mesosphere, local anomalies in the chemical conditions may exist, as often seen in the ionospheric temperature. Such a local anomaly is likely to influence N^+ much more than O^+ or H^+, because of the difficulty in the production. Similarly, the source latitudes of O^+ and N^+ are not necessarily constant because ionospheric convection might move the latitude of O^+ from where it is formed to where N^+ is formed. Generally speaking, N^+, N_2^+, and O^+ are expected to have different source locations and energies, and so they will end up having different circulation trajectories. This difference should be enhanced in the magnetosphere if the different source location is mapped along the geomagnetic field. One can shed light on all these problems by separating N^+ and O^+.

1.6. Inner Magnetosphere: Dynamics and Coupling with Ionosphere-Exosphere System

Since the required observations to address the nitrogen escape problem include in-situ ion measurements in the magnetosphere, we can also address some unanswered problems in magnetospheric dynamics. As illustrated in Figure 1.4, some of the ions flowing inside the polar cap will escape, while others will be recirculated to the inner magnetosphere. Whether or not the ions escape or recirculate, depends on the ion energy, pitch-angle, location, interplanetary magnetic field conditions and the energization during the stay in the inner magnetosphere. Understanding the role of the inner magnetosphere is crucical in studies of the escape processes for any ion species. The present knowledge on oxygen ion escape simply "assumes" that a certain percentage of ions leaving the ionosphere escapes. Therefore, the inner magnetosphere and the polar cap are regions to consider.

The inner magnetosphere has three major roles: (i) as the location of unique ion dynamics and energization processes; (ii) as a buffer for the energy transfer from the solar wind or magnetotail to the Earth; and (iii) as a destination of the planetary ions that once flowed out from the high-latitude ionosphere. The majority of the ions that enter the inner magnetosphere start drifting perpendicular to the geomagnetic dipole axis while bouncing between north and south in the magnetic bottle configuration that is inherent to the dipole geomagnetic field. This is quite different from the polar cap where ions simply flow along the field line to or from the ionosphere.

This difference between the inner magnetosphere and polar cap makes the inner magnetospheric ion dynamics much more complex than those of the polar cap, because it is not simple to de-convolve the complicated mixture of different ion populations from different pathways (mass-dependent) with different

energization processes (Figure 1.5). To distinguish those, we traditionally use four species: H^+ (comes from everywhere), He^{++} (ultimately from the solar wind), He^+ (from the plasmasphere), and heavy ions, O^+ and N^+ (from the ionosphere). For example, the continuous change of He^{++}/H^+ ratio from the exterior cusp to the plasma mantle or low-latitude boundary layer, and finally to the plasma sheet in the magnetotail, is considered to be a signature of how the solar wind is injected into the magnetotail.

However, compared to the polar cap or magnetotail, the observed ion morphology is far more complicated than can be handled only with this traditional "four-species method" in estimating the dynamics. The problem is that both pathways and local energizations are some time mass dependent and sometimes mass independent, depending on the types of transport processes, energization processes, and source regions (the ionosphere, plasmasphere, plasma sheet and the solar wind) in multiple regions.

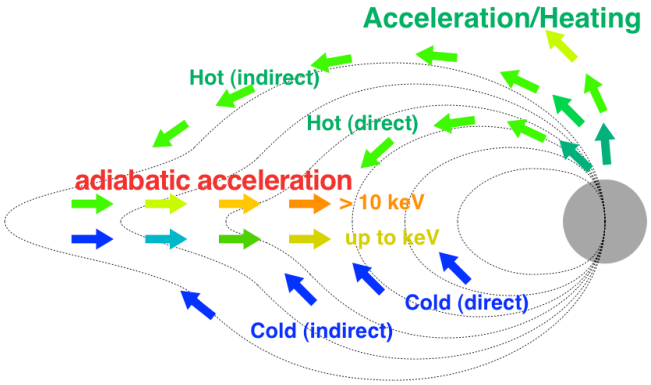

Figure 1.4: Filling of the inner magnetosphere by ionospheric ions through different pathways: directly, through the plasmasphere, and via magnetotail. The hot ions can also enter the inner magnetosphere either directly as bouncing ions or via the magnetotail. Ions that return from the magnetotail are energized during the sunward convection (Ejiri et al., 1978).

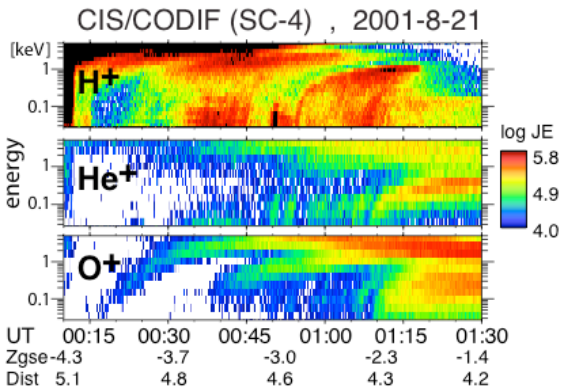

Figure 1.5: Cluster observation (energy flux density) of different energization between H^+, He^+, and O^+ in the inner magnetosphere (Yamauchi et al., 2014). Units are keV cm^{-2} s^{-1} str^{-1} keV^{-1}.

For example, Figure 1.5 includes local energization signature of He^+ at around 01:00 UT, whereas sudden switching of correlated H^+/O^+ pattern and anti-correlated H^+/O^+ pattern at around 00:50 UT and 01:10 UT. Ion heating mechanisms should not distinguish ion species unless some unknown mechanism creates very narrow band wave relevant to specific ion species, and the same energy-latitude or energy-time pattern between different species is expected from ion drift theory if the ions start drifting from the same location. One possible explanation is that different species followed different trajectories (e.g., location of direct filling to the plasma sheet), and such difference caused difference in the local energization. This is just a speculation, and even the pitch angle information is helpless because it is impossible to distinguish between field-aligned ions and bouncing ions at low mirror altitude when the observed pitch angles near the equator are very low.

However, additional information about N^+ ions would ease these problems because the initial energy of N^+ (M/q=14) is closer to that of He^+ (M/q=4) than to O^+ (M/q=16) due to its chemical property: O^+ is already pre-accelerated or pre-heated when it reaches the altitude where cold N^+ or cold He^+ are newly formed. Since the geomagnetic field is curved, and the impeding electric or electromagnetic force is time varying, ions with different initial velocities end up at different final locations and sometimes energies. We then expect that pathway-dependent energization (e.g., adiabatic acceleration from the plasma sheet) appears as a difference between O^+ and the N^+-He^+ group, and mass dependent local energization appears as a difference between He^+ and the N^+-O^+ group. Furthermore, the direct supply from the ionosphere would cause a time delay between the arrival of N^+ and O^+ ions, and hence, a measurable shift of the energy-latitude pattern between N^+ and O^+.

Simple comparison of N^+/O^+ and N_2^+/O^+ ratios between the topside ionosphere and the magnetosphere (between two spacecraft in Figure 1.3) is also needed because the N^+/O^+ and N_2^+/O^+ ratios in the ionosphere vary depending on the ionospheric temperature and on the solar F10.7 flux (e.g., Yau et al., 1993, and references therein). Comparing this ratio at time resolution of a few minutes hints at the pathways of both species. Even before making this comparison, we have to test whether the N^+/O^+ flux ratio for escaping ions directly reflects the N^+/O^+ ratio at the topside of ionosphere, and varies in the same way in response to

changing ionospheric conditions. Thus, using the additional tracer, N^+, as well as the traditional tracer, O^+, helps in separating the starting location and/or the acting mechanisms.

To study any mechanism in the inner magnetosphere, it is almost always necessary to correlate the geomagnetic conditions such as substorms. Normally, the geomagnetic indices (Kp, Dst, and AE) are used, but it would be valuable to be able to remotely monitor the ion injections from the plasma sheet. While geosynchronous satellites can provide a good monitor of substorm injections, ENAs (energetic neutral atoms) from charge exchanged BBFs (bursty bulk flow) are in principle possible to be detected because the exosphere, albeit very diffusely, exists even at 10 R_E (Fuselier et al., 2010), and this is worth testing.

1.7. Space Plasma Physics: Energization in the Polar Cap and Inner Magnetosphere

The ability to separately measure N^+ and O^+ will also provide new ways to distinguish between energization and transport mechanisms. Magnetospheric processes such as resonance with ion-cyclotron waves (André, 1997) can barely be distinguished between O^+ and N^+ ions, due to their similar masses. This implies that the differences between two species, observed in the magnetosphere, can be attributed to the initial energies at the topside ionosphere, not to the mass-dependent magnetospheric processes.

For example, (i) the effectiveness of centrifugal acceleration at high altitudes compared to parallel potential acceleration or ponderomotive acceleration at low altitudes, (ii) the different energization by different wave modes in the magnetosphere (e.g., near each resonant frequency or wide-band below proton cyclotron frequency (Yau and André, 1997)), and (iii) the energy conversion between the waves and the ions can be examined by studying the energy difference between N^+ and O^+, because virtually identical effects are expected from the wave-particle interaction scenario with only difference in the initial energy. The final energy of N^+ and O^+ will only reflect the initial energy, and the velocity-filter effect in the poleward convection will cause N^+ and O^+ to be observed at nearly the same energy at all times, until N^+ disappears if it has a lower initial energy compared to O^+. In other words, N^+ disappearance at a specific cut-off energy would characterize the low-altitude acceleration and indicate its relative contribution.

We can also estimate the timing of ionospheric outflow events, using (also for the first time) the small difference in TOF (time-of-flight) between N^+ and O^+ when no extra acceleration is expected, e.g., for the cases of direct supply from the ionosphere to the magnetosphere as shown in Figure 1.4. In the figure, ion data show sudden escape from the ionosphere, with TOF about 20 min assuming O^+. If we can separate N^+ from O^+, and if we can assume no extra energization between the ionosphere (or low-altitude acceleration region) and the spacecraft position, we expect a delay in time and location between these two species for the same energy. The resultant difference in the energy-time dispersion between N^+ and O^+ will give more precise information about the ejection time. Note that this signature is convoluted with a drifting component in the H^+ channel. This type of estimate is more powerful when ions have bounced between both hemisphere more than once. A separation between N^+ and O^+ will give a clue to how many times the ions have bounced, and therefore allows determination of the elapsed time. The estimated start time of the outflow can be directly compared with substorm injections monitored by ENA imaging.

1.8. Summary of Scientific Objectives related to N^+ and N_2^+ separation

Separating N^+ and N_2^+ from O^+ in space has multi-disciplinary objectives:

* Ancient Earth (amino acid formation depends on relative abundance of atmospheric N, O, & H).
* Planetary Evolution (why N/O ratio on Mars is only 0.1% of Earth, Venus, or Titan).
* Exospheric Morphology (we have little knowledge of the exosphere above 1500 km).
* Ionospheric Physics (ionization at the topside ionosphere under different external conditions determines ion escape and ionosphere-exosphere-magnetosphere coupling).
* Magnetospheric Dynamics (ion dynamics and circulation of ionospheric origin and the dependency of N-O-H ratio on solar and solar wind conditions are not well understood).
* Space Plasma Physics (tracing ions with similar masses but different initial topside ionosphere velocities gives extra information on energization mechanisms in space).

The science targets described for each science field (§1.2-§1.7) are summarized as (A)-(F) for primary questions and (V)-(Z) for optional questions (cf. Table 1.2):

(A) Amount of nitrogen escaping the ionosphere at different outflow regions.
(B) Amount, conditions and pathway of nitrogen outflow that finally enters the inner magnetosphere where some part is returning as compared to oxygen or hydrogen.
(C) Location and degree of ion energization of N^+, N_2^+ and O^+, along these ion outflow pathways.
(D) Altitude distribution of different exospheric neutrals > 1500 km where no in-situ measurements exist.

(E) Production of upper ionospheric N^+, N_2^+ and O^+ through the upper exosphere-ionosphere interaction.
(F) Degree of different responses between N^+, N_2^+, O^+, and H^+ to various external energy inputs.
(V) Re-distribution of incident energy to the ionosphere and exosphere toward lower latitudes, and its consequent impact on N_2^+ production.
(W) Role of electric and electromagnetic fields for the initial energization of ions above the ionosphere
(X) Fate of returned heavy ions.
(Y) Impact of substorms on ion escape.
(Z) Cause of ion structure formation in the inner magnetosphere.
All questions include dependencies on different external conditions such as solar UV, solar wind and interplanetary magnetic field, and particle and electromagnetic forms of external energy input.

Table 1.2: Specific science questions on each science field

Science Discipline	Primary questions	Secondary Questions	Relevant Themes
§1.2. Ancient Earth	(A), (B), (F)		CV1.3*
§1.3. Mars Mystery	(A), (F)		CV1.3
§1.4 Exosphere	(D), (E), (F)		CV2.1**
§1.5. Ionosphere:	(B), (E), (F)	(V), (W), (X), (Y)	CV2.1
§1.6 Magnetosphere	(A),(B), (C), (F)	(X), (Y), (Z)	CV2.1
§1.7. Energization	(C), (F)	(Y), (Z)	CV2.1

* Cosmic Vision sub-theme #1.3 "Life and habitability in the Solar System" under the theme "What are the conditions for planet formation and the emergence of life?"
** Cosmic Vision sub-theme #2.1 "From the Sun to the edge of the Solar System" under the theme "How does the Solar System work?"

2. Summary of Measurement Requirements to achieve Scientific Objectives (5.5 pages)

To answer the scientific questions (A)-(F) and (V)-(Z) in §1.8, the most essential information is (1) density and (2) energy distribution at each observation point in the magnetosphere, for N^+ and N_2^+ as compared to the "traditional" four species (O^+, H^+, He^+, He^{++}). For energy distributions, we need at least three components, i.e., three pitch angle directions: field-aligned, oblique, and perpendicular direction to the geomagnetic field. These observations, particularly the N/O/H ratios (both density and energy) must be compared with the solar wind parameters and geomagnetic indices. (3) For the source region above the ionosphere at around 2000 km, most ions of ionospheric/exospheric origin are less than 10 eV and at most 100 eV. Therefore, the mandatory information is density of ions and of neutrals. In addition to these essential measurements, we need (4) physical quantities that significantly control the ion energization and escape, e.g., ion cyclotron waves and lower hybrid waves that are the major cause of the local energization. Finally, (5) some extra measurements that take advantage of basic spacecraft configurations would lead to unique science results. This is optional, but worth pursuing if the budget allows.

Table 2.1: Required or recommended observations for I each science target

Questions	**two spacecraft**		**one spacecraft**	
key science	**essential**	**useful**	**essential**	**useful**
(A) Escape and budget	1a, 2a	1b, 1c, 3a, 3b, 5b	1a, 2a, 6a	1b, 1c
(B) Ion pathway	1c, 2a, 2b, 3d	1a ,1b	1c, 2a, 2b, 6a	1a, 1b
(C) Various energization	1c, 2a, 3d, 4a	2b	1c, 2a, 4a	2b
(D) Distribution in the exosphere	3a	3b	6a	
(E) Source ion production	3a, 3c	3b, 5a		
(F) Ion response difference	1a, 2a, 3b, 4a	1b, 1c, 3a, 3c, 3d	1a, 2a, 4a	1b, 1c
additional science	**essential**	**useful**	**essential**	**useful**
(V) Re-distribution in ionosphere	3b	3a, 3c		
(W) Initial energization of ions	3c, 5a	3b, 3d		
(X) Return to the ionosphere	5c	2a		2a
(Y) Impact of substorm injection	2a, 5b	1a, 1c, 2b, 4a	2a, 5b	1a, 1c, 2b, 4a
(Z) Ion structure formation	1c, 2a	1a, 5b	1c, 2b	1a, 5b

note: (3c), (5a)-(5c) are optional measurements, and (6a) is for the case when the UV/Visible telescopes are placed on the in-situ SC.

2.1. Required observations

Detailed descriptions of both the essential and useful measurement targets under (1)-(5) are summarized in Table 2.1 and following explanations.

(1a) Average 3D magnetospheric distribution and its orbit-to-orbit variation:

This information is essential in addressing the science targets on (A) nitrogen escape and budget, (F) different ionospheric response between different species, and is important on (B) ion pathway, (Y) impact of substorm injection, and (Z) ion structure formation.

The main measurement method is by in-situ ion detection at all the relevant energies and of all relevant species. The magnetosphere has multiple populations covering a broad energy range: cold (< 20 eV), hot (10 eV-10 keV) and energetic (10-220 keV), as classified by the detection methods. Only the energy range of 1 keV to 20 keV is relatively empty most of the time in the inner magnetosphere. Since the observations are only along the spacecraft trajectory, the orbit parameters should be defined to cover the entire inner magnetosphere during the three-year mission.

The other promising method to separate nitrogen ions from oxygen ions is to measure the line-of-sight integrated fluorescent emission from ions at UV/Visible range (N^+ at 91nm and 108nm, N_2^+ at 391nm and 428nm, O^+ at 83nm and 732-733 nm). Emissions from the upper ionosphere (> 1700 km) and magnetosphere are actually detected by the Hisaki spacecraft (Hisaki workshop, 2014). The challenge with this method is the difficultly in de-convolution of the line-of-sight integrated values.

(1b) Identification of regions in the magnetosphere:

In addition to the ion measurements in (1a), the spacecraft location need to be identified in terms of physically defined regions, e.g., polar cap, lobe, boundary layer, plasma sheet, ring current and other regions in the inner magnetosphere, because the magnetospheric regions dynamically vary over several degrees in geomagnetic latitude. This is particularly important for the investigation of (A) escape and budget, (B) ion pathway, (F) ion response difference, and requires hot electron measurements (10 eV–10 keV) and magnetic field. In addition, photoelectrons of ionospheric nitrogen ions at 24eV, 25 eV, 26 eV and 30 eV provide the connectivity to the ionosphere along the geomagnetic field.

(1c) Spatial and temporal variability of imaged line-of-site column density:

By combining the line-of-sight integrated UV/Visible emission method with the in-situ measurements, so that the line-of-sight includes the other spacecraft's in-situ observations (cf. Figure 1.3), one can obtain a better "guess" of the distribution along the line-of-sight, much better than the traditional "assumption" method, particularly in assessing the spatial variability and error range. If we scan the line-of-sight direction nearly along the trajectory, comparison with the temporal variations of the in-situ measurements leads to a direct separation in the spatial-temporal structure.

Such a separation is essential in understanding the science targets on (B) ion pathway, (C) various energization, and (Z) ion structure formation and is also important on (A) escape and budget, (F) ion response difference, (Y) impact of substorm injection,

(2a) Energy distribution (degree of energization and its direction) of ions in the magnetosphere:

This can be done only with in-situ ion detection with supplemental electron measurements as described in (1a). In addition, we need information on pitch angles in at least three directions (parallel, oblique and perpendicular to the geomagnetic field).

Knowing the energy distribution is quite essential in understanding (A) escape and budget, (B) ion pathway, (C) various energization, (F) ion response difference, (Y) impact of substorm injection, and (Z) ion structure formation, while it gives support information on (X) return flow to ionosphere,

(2b) Time delay between direct low-energy filling and convective high-energy filling:

This is essential in identifying (B) ion pathway. Since different pathway means different history of energization, it is also important in searching (C) various energization and (Y) impact of substorm injection. The required measurement is the same as (2a) with time resolution of substorm injections.

(3a) Average altitude distribution of source neutrals (exosphere) and ions (ionosphere):

This is the baseline source information for the nitrogen outflow, the exospheric science, and ionosphere-exosphere interaction, i.e., essential for (D) distribution in the exosphere and (E) source ion production, and important for (A) escape and budget, (F) ion response difference, and (V) re-distribution in the ionosphere.

The observation method is the same as (1a), but the measurement does not have to cover all energy ranges. The mandatory direct measurement is only cold (superthermal) ions and neutrals, because they are cold at the altitude we consider (< 2400 km). The line-of-sight integration of UV/Visible emissions can also be targeted toward the limb direction to obtain the altitude distribution of ions.

(3b) Spatial and temporal variability of source neutrals (exosphere) and ions (ionosphere):

This is the ionospheric/exospheric counterpart of (1c), and is essential in understanding (F) ion response difference and (V) re-distribution in the ionosphere, and important for (A) escape and budget, (D) distribution in the exosphere, (E) source ion production, and (W) initial energization of ions. The difference from (1c) is that we combine the line-of-sight integrated value of the UV/visible measurements with the local density at the low-Earth orbit instead of the magnetosphere (cf. Figure 1.3). An auroral camera is also helpful in understanding the general ionospheric conditions.

(3c) Degree of energization of ions in the ionosphere:

Although the ions are expected to be cold (< 20 eV) at the topside of the ionosphere, it is useful to measure hot ions up to 100 eV just above the ionosphere up to about 2000 km in case of the ionospheric disturbances, because the energization of enhances N^+ may already take place (at a different level from O^+, though) in such a condition. Therefore, this optional information is essential on (W) initial energization of ions and (E) source ion production, and very useful for (F) ion response difference and (V) re-distribution in the ionosphere.

(3d) Relation between the ionospheric/exospheric source density and magnetospheric density/energy:

The simultaneous comparison of conditions between the source region and the near-conjugate region provides essential information on (B) ion pathway, (C) various energization, and important information on (F) ion response difference and (W) initial energization of ions. This measurement can be obtained by either two-point measurements of ions with two spacecraft (in-situ ion detection) and/or remote sensing (line-of-sight observations) of UV-visible emission lines mentioned above. Therefore, the measurement method is the same as combination of (1a) and (3a).

(4a) Correlation between wave mode and ion velocity distributions of N, O, and H in the magnetosphere:

When discussing the energization mechanism of the ions, we need wave, field, and electron data to examine the wave-particle interaction that is a key driver of ion energization. Therefore, the wave data are essential in investigating (C) various energization and (F) ion response difference, and is useful for (Y) impact of substorm injection. The required measurements, in addition to the ion measurements, are the wave package including even DC field measurements and electron measurements.

(5a) Correlation between wave mode and the ion energy of N, O, and H in the ionosphere:

This optional measurement is the counterpart of (4a) in the ionosphere, which is important for ionosphere-exosphere coupling and pre-heating of ions rather than for the energization in the magnetosphere, i.e., for (E) source ion production and (W) initial energization of ions.

(5b) Relation between sunward return flow and ion dynamics in the magnetosphere:

If one can obtain this information, it would contribute all studies related to (Y) impact of substorm injection, which also contribute in understanding (A) escape and budget and (Z) ion structure formation. The energy range of ENA must cover 4-6 keV, the typical peak energy of burst bulk flows (Cao et al., 2013). Since this is a new trial without guarantee, this measurement is ranked as optional.

(5c) Heavy ion precipitation flux above the ionosphere:

Heavy ions entering to the inner magnetosphere, either directly from the ionosphere or returning from the magnetotail, are expected to precipitate after the majority are either neutralized through charge-exchange or drifting beyond the magnetopause. To measure these ions we need a mass-separating (N^+ and O^+) ion instrument that covers 0.1-50 keV. This measurement is ranked as optional.

(6a) Line-of-sight integrated fluorescent emission observation from in-situ SC:

This is the reference possibility in case of having only one spacecraft (in-situ SC in Figure 1.3) instead of two spacecraft. In this case, the UV/Visible telescope would be placed on this in-situ SC instead of the remote sensing low-Earth spacecraft. The detail is discussed in the next subsection.

Table 2.2 summarizes measurements target described above. The second column lists the actual measurement methods, and the last two columns list the relevant science questions in Table 2.1 and the previous section. The actual measurement methods are magnetospheric hot light ions (10eV-10 keV, M/q<20), magnetospheric hot heavy ions (10 eV-10 keV, M/q>10), magnetospheric cold ions (< 20 eV), magnetospheric energetic ions (10-220 keV), magnetic field, spacecraft potential, high-frequency waves, low frequency waves, magnetospheric electrons, energetic neutral atoms (ENA), ultraviolet (UV) emissions (N+ at 91nm and 108nm), visible emissions (N2+ at 391nm and 428nm), ionospheric cold ions (< 20 eV), exospheric neutrals, auroral images, ionospheric hot ions (< 100 eV), and precipitating hot ions to the ionosphere.

Table 2.2: Available observation method for each measurement (1a)-(5c)

measurement	measurement method	corresponding science target	
Magnetosphere		**essential**	**useful**
(1a) Ion density distribution	ion, emission	**A, F**	(**B**), (Y), (Z)
(1b) Region identification	electron		(**A**), (**B**), (**F**)
(1c) Variability of density	emission, ion	**B, C,** Z,	(**A**), (**F**), (Y)
(2a) Energy distribution	ion, magnetic field	**A, B, C, F,** Y, Z	(X)
(2b) Energy-time structure	ion, magnetic field	**B**	(**C**), (Y)
(4a) Wave-ion relation	ion, wave and field, electron	**C, F**	(Y)
(5b) Sunward return flow	ion, ENA	Y	(**A**), (Z)
Ionosphere/exosphere			
(3a) Neutral/ion distribution	ion, neutral, emission	**D, E**	(**A**), (**F**), (V)
(3b) Variability of distribution	emission, ion, neutral	**F,** V	(**A**), (**D**), (**E**), (W)
(3c) Energy distribution	ion	**E,** W	(**F**), (V)
(5a) Wave-ion relation	ion, wave and field, electron	W	(**E**)
(5c) Ion precipitation	precipitating ions	X	
Ionosphere & Magnetosphere			
(3d) Relation between the ionosphere/exosphere and the magnetosphere	ion (both), exospheric neutral, magnetospheric emission	**B, C**	(**F**), (W)

2.2. Why do we need two spacecraft?

We may perform a large part of the measurement targets listed above (1a, 1b, 2a, 2b, 4a, 5b, and 6a) with only the in-situ SC, if the UV/Visible telescope is placed there, and therefore, may conduct a large amount of science with one spacecraft. For example, large parts of (A), (B), (C) (F), (Y), (Z) could be fully explored with a single magnetospheric spacecraft, and in this sense the single spacecraft has by itself a strong science return. However, as summarized in the right column in Table 2.1, this would not reveal the dynamic changes on the time scale of tens of minutes to tens of hours, because of the lack of source information above the ionosphere. To obtain a comprehensive understanding, adding the second spacecraft gives a high added value. The telescopes can also provide temporal variation and context information for what the in-situ SC observes, because the spacecraft scans several times the region including the orbit plane. This would be extremely difficult, if at all possible, with a single spacecraft.

2.3. Requirements and constraints on the two spacecraft configuration

Since this is the first ever mission with a low-altitude spacecraft looking at a high-altitude spacecraft, we need special consideration on how these two spacecraft are placed and controlled.

2.3.1. In-situ SC:

This must have a high-inclination elliptic orbit to cover the inner magnetosphere and the polar cap at different radial distances for each latitude during the 3-year drift of perigee latitude. The apogee altitude should be below 35000 km from the requirement to avoid space debris near the geosynchronous orbit, while the apogee must be high enough to limit the total radiation dose < 50 krad behind reasonable shielding (5-6 mm), such that ordinary space-proved electric components (100 krad at Radiation Design Factor (RDF) = 2) can be used.

2.3.2. Remote sensing SC:

The emissions from ionospheric ions will dominate over the magnetospheric emissions below 1800 km. Therefore, the line-of-sight observations by the UV/Visible telescope to look towards the in-situ SC should be limited to > 1800 km. Furthermore, the UV telescope is sensitive to the background contamination from the radiation belts. Therefore, its observations will be limited to polar region (|Inv| > 60°). At the same time, the remote sensing SC should scan the exosphere between 1000 km to more than 2000 km, requiring an elliptic orbit, while keeping the radiation dose level acceptable.

2.3.3. Enough visibility from the remote sensing SC to the in-situ SC:

This requires the same longitudinal drifting speed of the perigee longitude. This means that two spacecraft should have different inclinations. The same drift velocity (maximum 20° in three years) should be achieved even when the actual inclination is off from the targeted inclination within the accuracy of the launch vehicle (0.15° for VEGA launcher).

2.4. What are the required resolution and sensitivity?

Temporal resolution (all sensors): As shown in Figure 1.5., the majority of the heavy ion events last more than ten minutes, and even short bursts last more than a few minutes. We are also not targeting fine spatial structures (less than 3° or 350 km in latitude at the spacecraft orbit) such as boundary processes in this large-scale circulation and distribution science. Therefore, we require 2-min resolution for the particle (ion, electron, and ENA) measurements on board the in-situ SC (the instruments will be turned off at < 2000 km altitude where the remote sensing SC covers) as well as the line-of-sight UV/visible measurements from the remote sensing SC, and 30 sec resolution for plasma measurements on board the remote sensing SC. If the spin rate of the in-situ SC is 20-30 sec, we can integrate the data over 4-6 spins to minimize the telemetry if necessary.

On the other hand, field measurements need higher resolution. The spacecraft potential measurement that is needed to correct ion data as well as to feedback to spacecraft potential control needs a fraction of spacecraft spin period (22-26 s) as the temporal resolution. DC magnetic field measurements should cover the ion cyclotron frequency of N^+, O^+, or N_2^+ in the in-situ SC, indicating 0.05 sec resolution.

Mass separation for ion measurements: The mission should be able to separate N^+ and N_2^+ from the traditional four species (H^+, He^{++}, He^+, and O^+), particularly from O^+ ($M/\Delta M>8$) in the magnetosphere. However, we do not need to measure N^{++}, O^{++}, or O_2^+ because the past data (Akebono and DE-1) showed $O_2^+ << N_2^+$ and $N^{++}/O^{++} \approx N^+/O^+$ for the cold ions and the ionospheric model. Separation of these ions are then a bonus of the mission, if it is feasible. For cold ions (that constitute the majority of the density), we further require the accuracy of N^+/O^+ ratio detection at 10% level or more for both spacecraft, and therefore need 3-4 mass channels between N^+ and O^+ ($M/\Delta M > 30$). We also require two independent measurements for hot ions, one including H^+ and the other excluding H^+, because the high H^+ fluxes could eventually "bury" the signal from minority species such as N^+. For the remote sensing SC, we do not need to measure H^+ or He^{++} because H^+ exists everywhere and most He^{++} (and many H^+) in the magnetosphere are of solar wind origin.

Energy range for ion/electron measurements: From past observations, heavy ions exist from cold (< 1 eV) up to energetic (> 100 keV) at altitudes covered by the in-situ SC and from cold to about 100 eV for the altitude covered by the remote sensing SC. Since the detection method is different between different energies (cold < 20 eV, hot = 10 eV - 10 keV, and energetic > 30 keV), we need at least three ion instruments for the in-situ SC and two ion instruments for the remote sensing SC. The energy coverage reaches to significantly higher energies than the minimum energy needed for gravitational escape (11 km/s implies ~9 eV for Earth) because ion acceleration processes such as those in the auroral acceleration region or the magnetotail are known to be capable of accelerating ions to keV energies (cf. Figure 1.4). For electrons, we need a standard coverage of 10 eV to 10 keV for the identification of different regions and energy.

Energy resolution for hot ions and electrons: Since the energy difference between N^+ and O^+ gives essential information in identifying the energization mechanism within the magnetosphere, i.e., at low energy < 1 keV, the hot ion instruments must be able to distinguish the energy difference between N^+ and O^+ (12% difference if the velocity is the same) for 10 eV - 1 keV ions (majority of the heavy ions). This means two steps for 12% increases, i.e., 6% stepping with energy band of $\Delta E/E<8\%$ (40 steps for a factor of 10 increase) for both spacecraft. A sparse resolution is acceptable for ions > 1 keV. A similar requirement applies to electron measurements: we need 1 eV accuracy between 20 eV to 35 eV where photoelectron lines for nitrogen lies (24 eV, 25 eV, 26 eV, 30 eV), while a sparse resolution (e.g., 30-50%) is permissible outside this energy range.

For low energy ions of <100 eV, the spacecraft potential may change the ion energy when it enters the instruments. Therefore, accuracy of the potential measurement is 1 V.

Angular coverage and resolution for hot ions: For the in-situ SC, we need approximate pitch angle directions (// , oblique and perpendicular directions to the geomagnetic filed). Converting to all directions of the magnetic field, we need about 22.5° x 45° resolution. For the remote sensing SC, we monitor outflowing heavy ions, and a single pixel that contains the geomagnetic nadir (in the moving spacecraft frame) is the minimum requirement. Since the inclination is nearly 90° and spacecraft faces the ram and the nadir directions, the geomagnetic nadir oscillates to the left and right against the ram direction by about 10°, whereas there are more than 10 traversals every day. This means that a long field-of-view (FOV) is the slid it narrow (e.g., 8° x 60°) is the minimum requirement while a wider FOV (e.g., 30° x 60°) is ideal.

Dynamic range and sensitivity (all instruments): For cold ions, in-situ measurements should be able to detect the density of 1 -1000 cm^{-3} (with 10% accuracy for > 10 cm^{-3}) in the magnetosphere and 1 -10000 cm^{-3} (with 10% accuracy for > 10 cm^{-3}) above the ionosphere. The sensitivity for hot N^+ should be the same as

for hot O^+, when its flux is enhanced, i.e., should be able to detect when the energy flux is > $5 \cdot 10^5$ keV cm^{-2} s^{-1} str^{-1} keV^{-1} (or G-factor >10^{-4} cm^2 str keV/keV for all angle without efficiency if integration time is 20 ms). Dynamic range of N^+ count (differential energy flux) should be >1000. This applies to both spacecraft. For higher fluxes of electrons, we need only G>10^{-7} cm^2 str keV/keV. For optical detection, the total column density of O^+ in the magnetosphere is estimated ~10^9 and ~10^{11} cm^{-2} in the magnetosphere including and excluding plasmasphere, respectively, and N^+ must be detected when it is comparable to this baseline value (>10^{10} cm^{-22}). For the two-minute duty cycle, optical telescopes need sensitivity of >0.1 count $s^{-1}R^{-1}$, whereas auroral and airglow detection requires lower sensitivity >0.01 count $s^{-1}R^{-1}$.

The magnetic field strength is expected to be between -5000 nT and 5000 nT, and 10% accuracy is sufficient for the absolute direction, while it would be valuable if the electric current can be derived from the variation of the magnetic field with 5 nT accuracy. The wave instruments also need a good frequency resolution near frequencies that are associated with ions (not electrons) at around 1-100 Hz. The required dynamic range is four orders of magnitude in the spectra power density.

2.5. Need for two hot ion instruments

The success of the mission strongly relies on the ability to separate the masses of heavy hot ions (N^+, O^+ and N_2^+) at 0.05-5 keV in the magnetosphere where there are no past observations. We should particularly consider the fact that all past hot ion instruments on magnetospheric missions, at the energy range 0.1-10 keV with a theoretical resolution of m/Δm>8, did not produce reliable data for N^+ and N_2^+ separated from both H^+ and O^+ in the magnetospheric environment. However, recent technology developments of hot ion instruments significantly improved the mass separation capability. For example, the Kaguya moon mission actually succeeded in separating hot N^+ and hot N_2^+ from the other species. Possible reasons can be related to lack of ideal start mechanism in the time-of-flight (TOF) method for this energy range: (1) energy loss using carbon foil and (2) dissociation N_2^+ into N^+ and N or at least deceleration of N_2^+ during the start timing detection.

To avoid these problems, the best method is to have two separate instruments, one without start-timing interaction (e.g., magnetic method or shutter method) to target heavy mass only (m/q=10-40), i.e., without covering H^+ and even He^+, and the other concentrated on atomic ions (m/q=1-20). By overlapping m/q=10-20 by both instruments, we have a smooth mass coverage. In other words, we abandon the traditional concept of "one instrument measures everything" concept in this specialized mission. In addition, we have to cover different energies (which was possible with one instrument each).

For the remote sensing SC, we need two hot plasma instruments (one is optional) because the spacecraft must be three-axis stabilized: looking toward nadir and zenith. Figure 2.1 summarizes the mass/energy coverage of particle measurements.

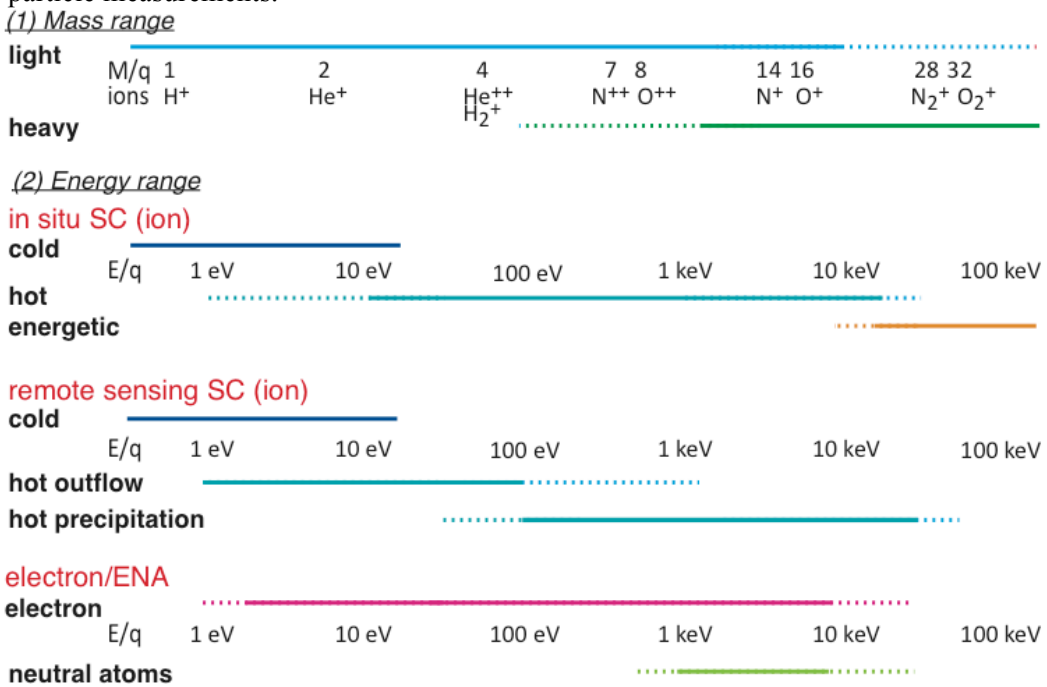

Figure 2.1: Required mass and energy ranges for ion and electron instruments.

3. Proposed Scientific Instruments (15 pages)

Table 3.1a: Scientific payloads for in-situ spacecraft (red=core, orange=baseline, green=optional)

Measurement / in-situ SC	Required ability to measure	SI (PI institute)	Heritage TRL level	Minimum information to get. () is per spin=24s instead of 2min	extra information data rate	allocated telemetry
(a) light hot ions:	H^+, He^{++}, He^+, O^{++}, N^+, O^+ (10 eV - 20 keV), dE/E≤8% for < 1 keV/q, > $5 \cdot 10^5$ keV cm^{-2} s^{-1} str^{-1} keV^{-1}	**MIMS (IRAP)**	new **TRL=5-6**	32 mass x 96 energy x 8x8 dir x 16 bit / 2 min = 26 kbps (130 kbps)	TOF data compressed: 8 kbps	8 kbps
(b) heavy hot ions:	N^+, O^+, N_2^+ (10 eV - 20 keV/q), dE/E≤8% at < 1 keV/q, > $5 \cdot 10^5$ keV cm^{-2} s^{-1} str^{-1} keV^{-1}	**NOID (IRF)**	MEX (2003) **TRL=7**	32 mass x 96 energy x 8x8 dir x 16 bit / 2 min = 26 kbps (130 kbps)	compressed: 8 kbps	8 kbps
(c) cold ions:	H^+, He^{++}, He^+, N^{++}, O^{++}, N^+, O^+, N_2^+, O_2^+ (< 10 eV), 1 - 1000 /cc	**NIMS (UBern)**	Rosetta (2004) **TRL=7-8**	800 mass line x 8 dir x 16x8 bit / 2min = 7 kbps (42 kbps)	TOF data processed: 7 kbps	7 kbps
(d) energetic ions:	H^+, He^{++}, He^+, O^{++}, N^+, O^+ (20-200 keV/q), dE/E ~3% > $5 \cdot 10^5$ keV cm^{-2} s^{-1} str^{-1} keV^{-1}	**CHEMS (UNH)**	Cassini (1997) **TRL=7-8**	8 mass x 24 energy x 16x6 dirs x 16 bit/2 min = 2.4 kbps (12 kbps)	pulse-height TOF data compressed: 3 kbps	3 kbps
(e1) SC potential:	1 V accuracy every spin	**SLP-IS (BIRA-IASB)**	PICASSO **TRL=4-5**	2 sensor x 100 Hz x 8 dir x 16 bit / 2 min = 2 kbps (10 kbps)	electric current raw: < 3.5 kbps	2 kbps
(f) magnetic field:	-5000 - +5000 nT dB<5 nT, 10% accuracy in direction	**MAG (IWF)**	VEX (2005) MMS (2015) **TRL=8**	2 sensor x 3 component x 20 Hz x 16 bit = 2 kbps (10 kbps)	compressed: 1 kbps	1 kbps
(g) wave analyser	10 Hz – 1 KHz df/f < 10% for < 20 Hz	**WAVES (ASCR/IAP)**	Solar orbitor TARANIS **TRL=5**	256 frequency x 16 bit x 6 component x 8 dir / 2 min = 2 kbps (10 kbps)	wave forms raw: 200 kbps	10 kbps
(h) waves detector	together with WAVES	**SCM (LPC2E)**	Solar Orbiter TARANIS **TRL=7**	together with WAVES	together with WAVES	n/a
(i) electrons:	(10 eV - 10 keV), dE<1 eV for 20-30 eV > 10^8 eV cm^{-2} s^{-1} str^{-1} eV^{-1}	**PEACE (MSSL)**	Cluster (2000) **TRL=7-8**	2x64 energy x 8x8 dir x 16 bit / 2 min = 1 kbps (6 kbps)	raw: 12 kbps	2 kbps
(j=optional) ENA	4 - 20 keV	**STEIN (UCB/SSL)**	Stereo (2006) **TRL=6**	16 energy x 8x4 dir x 16 bit / 2 min = 0.1 kbps (1 kbps)	raw: < 7 kbps	1 kbps
(x) SC potential control:	activate for > 1 V keep SC potential < 5 V	**ASPOC (ESA)**	Cluster (2000) **TRL=7-8**	**house keeping only**		< 0.1 kbps
(y) SC DPU + radiation belt detection	10 GByte memory + radiation belt warning	**subsystem (ESA) + UAthens**	**many + new**	**~ house keeping level**		< 0.1 kbps

Table 3.1b: Scientific payloads for remote sensing spacecraft (red=core, orange=baseline, green=optional)

Measurement / remote sensing	Required ability to measure	SI (PI institute)	Heritage	Minimum information to get. () is per spin=24s instead of 2min	extra information data rate	allocated telemetry
(k) UV/visible line-of-sight emission:	91 nm (N^+), 108 nm (N^+), 391 nm (N_2^+), 428 nm (N_2^+) > 0.5 count $s^{-1}R^{-1}$	**(k) NUVO (LATMOS)**	Hisaki (2013) BepiColomb **TRL=6-7**	32 kbit / Spectrum x 120 scanning angle / 2 min = 32 kbps	raw:100 kbps	33-100 kbps
(l) cold ions and neutrals:	H^+, He^{++}, He^+, N^{++}, O^{++}, N^+, O^+, N_2^+, O_2^+, N, O 1 - 10000 /cc	**(l) CINMS (NASA/ GSFC)**	MMS (2014) Exocube (2015) **TRL=7**	200 mass x (1/0.2) resolution x 2 component x 16 bit / 30 sec = 1 kbps	TOF data raw: 18 kbps compressed: 2 kbps	4 kbps
(m) airglow & auroral emission:	two of auroral emission > 0.05 count $s^{-1}R^{-1}$	**(m) CAAC (TohokuU)**	Reimei (2005) IMAP (2012) **TRL=7-8**	2 imags x 128x128 pixel x 16 bit / 30 sec = 18 kbps	raw: 72 kbps	10-50 kbps
(b2) heavy outflowing ions:	N^+, O^+ (1 - 100 eV) dE/E≤8% at10-100 eV > $5{\cdot}10^5$ keV cm^{-2} s^{-1} str^{-1} keV^{-1}	**(b2) NOID-RS** (same as in-situ)	same as in-situ	32 mass x 64 energy x 8 dir x 16 bit / 30 sec = 9 kbps	compressed: 4 kbps	4 kbps
(e2) SC potential:	same as in-situ	**(f2) SLP-RS** (same as in-situ)	same as in-situ	2 sensor x 100 Hz x 16 bit / 30 sec = 0.1 kbps	raw < 3.5 kbps	2 kbps
(n=optional) precipitating heavy ions:	N^+, O^+ (100 eV - 30 keV) dE/E≤12% at < 1 keV > $5{\cdot}10^5$ keV cm^{-2} s^{-1} str^{-1} keV^{-1}	**MSA (ISAS)**	Kaguya (2007) BepiColombo **TRL=7-8**	32 mass x 96 energy x 8 dir x 16 bit / 30 sec = 13 kbps	TOF data raw: 13 kbps	6 kbps
(f=optional) magnetic field:	same as in-situ	**MAG** (same as in-situ)	same as in-situ	2 sensor x 3 component x 20 Hz x 16 = 2 kbps	compressed: 1 kbps	1 kbps
(g=optional) wave analyser	same as in-situ	**WAVES** (same as in-situ)	same as in-situ	256 frequency x 16 bit x 6 component / 30 sec = 1 kbps	raw: < 200 kbps	3 kbps
(h=optional) wave detector	same as in-situ	**SCM** (same as in-situ)	same as in-situ	included in above		
(i=optional) electrons:	same as in-situ	**PEACE** (same as in-situ)	same as in-situ	2x64 energy x 8 dir x 4 dir x 16 bit / 30 sec = 2 kbps	raw: 12 kbps	2 kbps
(y2) SC DPU	10 GByte memory	**subsystem (ESA)**	same as in-situ	**house keeping only**		
(z) scanner for NUVO	270° mobility 90° in 2 min	**SC subsystem (ESA)**	VEX (2005) **TRL=6-7**	**house keeping only**		

Table 3.2: Size, mass, and power of scientific payloads (Total values is with ASPOC for in-situ SC)

Instruments	Size	Weight / Power (inc DPU/power supply)	Maturity Margin
(a) MIMS	Ø35x24 cm inc DPU/Power	4 kg + shield* = **6 kg** **6.0 W** @ 28 V	+15% +15%
(b) NOID	Ø19x30 cm + 15x16x6 cm	5 kg + shield* = **8 kg** **7-8 W** variable @ 28 V	+10% +10%
(c) NIMS	36x18x19 cm inc DPU/Power	3.5 kg + shield* = **5.3 kg** **23 W**	+20% +10%
(d) CHEMS	40x15x20 cm + 11x11x11 cm	7.7 kg + shield* = **9.7 kg** **7.1 W**	+20% +10%
(e1) SLP-IS	Ø5 cm probe@ 1.5-2 m boom + 15x15×10 cm	0.4 kg (sensor) + 0.4kg (Ebox)+shield* = **2.5 kg** (exc. boom) **7.5 W** (peak **25 W** optional) @28V/12 V	+10% +10%
(e2) SLP-RS	Ø5 cm probe@ 1.5-2 m boom + 15x15×10 cm	0.2 kg (sensor) + 0.3kg (Ebox)+shield* = **2.2 kg** (exc. boom) **5 W** (peak **25 W** optional) @28/12 V	+10% +10%
(f) MAG	8x8x5cm@End & 2/3 of boom + 16x17x12cm	0.4 kg +harness 7m = **0.9 kg** (exc. boom) Ebox:1 kg+shield*= **1.8 kg** 2.0 W + 1.5 W = **3.5 W**	+20% +5%
(g) WAVES	15x20×15 cm inc DPU/Power	2.5 kg + shield* = **5 kg** (exc. boom) **8.4 W**	+20% +10%
(h) SCM	Ø11x14 cm	**0.6 kg** without shielding* (exc. boom) **0.2W** (0.13W@±12V)	+20% +5%
(i) PEACE	20x14x12 cm + 12x12x8 cm	5 kg + shield* = **7 kg** **7.8 W** (sensor)	+20% +10%
(j) STEIN	8x12x10 cm inc DPU/Power	1.2 kg + shield* = **2 kg** **2-2.1 W**	+20% +10%
(k) NUVO	31x25x16 cm + 28x28x75 cm	5 kg + shield* = **9 kg** **20 W** (operation) / 5 W (stand-by)	+10% +10%
(l) CINMS	Ø20x47 cm + 24x20 cm	3.8 kg+shield* = **5.8 kg** **3.5 W**	+20% +10%
(m) CAAC	20x15x30 cm inc DPU/Power	3.5 kg + shield* = **6 kg** **12 W**	+20% +15%
(n) MSA	40x29x38 cm inc DPU/Power	6.6 kg + shield* = **9.7 kg** **11.2 W**	+10% +10%
(x) ASPOC **(ESA)**	2 x (Ø6x6cm) + 20x12x10cm	2x160g + 1.7kg (EBox) +shield* =**3.5 kg** **3.7 W**	+10% +10%
Total (+optional)	**50.3 kg** (52.3 kg) for in-situ / **31.0 kg** (56.0 kg) for remote-sensing* **75.2 W** (77.3 W) for in-situ / **48.5 W** (79.6 W) for remote-sensing*		56.1 kg / 33.5 kg 85.4 W / 54.0 W

* Value includes even SLP-RS as the first priority optional instrument.

Based on the observation requirements summarized in Table 2.1 and Table 2.2, the NITRO scientific instruments (SIs) are as listed in Table 3.1. This table also briefly summarizes the required measurement capability or range in the third column, heritage (if the instrument is small modification of existing instrument in the current or past missions) or TRL level (if it is new development or large modification of their heritage) in the fourth column. Nearly all SIs have achieved the required TRL level (>5-6) in its functionality by the PI institutes (SLP and Wave Power converter is TRL=4-5) and most of them have even achieved the required TRL level in its sensitivity, dynamic range, and resolution.

The rest of Table 3.1 (Columns 5-7) summarizes the data rate from each SI. Since the required temporal and spatial resolutions are only 2 min for the in-situ SC and 30 sec for the remote sensing SC, the required amount of data (fifth column) is much lower than the data production rate from each SI, and therefore, most SIs have to process data (e.g., integrating over time) before finally compressing the data.

The last column lists the allocated data rate for each SI after considering the data processing and compression (all SIs have DPU subunits). Note that some instruments have to downlink extra information (e.g., time-of flight (TOF) or pulse-height distribution) to obtain the required output as noted in the sixth column, and such data have to be downloaded quite often.

The payload is classified into four categories: core scientific instruments (SIs); supporting baseline SIs; supporting spacecraft subsystems; and optional SIs. The core SIs directly measure magnetospheric nitrogen ions (cold, hot, and energetic), upper ionospheric cold ions, and exospheric neutral nitrogen, by directly detecting ions and neutrals ((a) MIMS, (b) NOID, (c) NIMS, (d) CHEMS, (l) CINMS) or indirectly through nitrogen emission lines (UV 91 nm, 108 nm, 123-139 nm, visible 391 nm, 428 nm for (k) NUVO). The core SIs are marked by red colors in Table 3.1.

Supporting SIs are required (technically or scientifically) for understanding the nitrogen measurements, and therefore, are also considered as part of the baseline payload. For the in-situ SC, we need Langmuir probes ((e1) SLP-IS) for the spacecraft potential with 1 V accuracy, magnetometers ((f) MAG) for approximate pitch angle information and for determining the existence of O^+/N^+ cyclotron waves, electron analyser ((i) PEACE) for the identification of the spacecraft location in terms of the magnetospheric regions and the connectivity to the ionosphere through the photoelectrons (25-30 eV), and wave measurements ((g) WAVES, (h) SCM) for understanding local energization mechanisms of ions. For the remote sensing SC, supporting SIs include a CCD camera ((m) CAAC) that monitors the ionospheric airglow and auroral conditions, and a low-energy ion analyser ((b2) NOID-RS) for the pre-acceleration level of the source ions as well as for the spacecraft potential, provided that the instrument measures both the ram ions and the upgoing ions (this is possible by placing the tophat viewing plane along the ram-nadir direction, but for better measurement, (e2) SLP-RS is ideal). The supporting SIs are marked by orange colors in Table 3.1.

The supporting non-scientific payloads for the in-situ spacecraft (ESA's responsibility) include active spacecraft potential control ((x) ASPOC) to keep the spacecraft potential less than 5 V and the (y) spacecraft DPU that handles telemetry, as well as issuing automatic commands to warn of an unexpected high radiation dose. The spacecraft subsystems also include a (z) scanner for NUVO and booms for the magnetometers, wave measurements, and Langmuir probes. These subsystems are marked by red or orange colors in Table 3.1, depending on the target they support .

Finally, the optional SIs, which corresponds to (5a)-(5c) in Table 2.2, take advantage of the unique orbital configuration of the 2-spacecraft mission. They include an ENA instrument ((j) STEIN) on board the in-situ SC, and precipitating ions, electrons, magnetic field and waves instruments ((n) MSA, (i) PEACE, (e2) SLP-RS, (f) MAG, (g) WAVES, (h) SCM) on board the remote sensing SC. These are marked by green colors.

Table 3.2 summarizes the size of each subunit (second column), mass, and power (third column), and Table 3.3 summarizes the field-of-view (FOV) requirements of ion and electron instruments. The detailed description of each scientific payload is found in §3.1-3.3, whereas the photos and illustrations of these instruments are shown in the appendix. The shielding mass from the radiation dose for radiation-sensitive subunits is obtained by assuming 5.5 mm and 5 mm aluminum shielding (spot shielding) for the payload on board the in-situ SC and remote sensing SC, respectively. Such a shielding brings the three-year total radiation dose to less than 50 krad, half of the normal specification for space-qualified electric components.

Tabe 3.3: Accommodation requirements for ion and electron instruments in the in-situ spacecraft.

type of FOV	SI	where	how
Tophat (360° x ~10°):	MIMS, NOID	entrance must stick out from rim & FOV is not blocked by solar panels or booms	symmetry axis is perpendicular to the spin axis
Half-tophat (180° x ~10°)	CHEMS, PEACE		symmetry axis is perpendicular to spin axis
Mouth (60° x ~10°)	NIMS		entrance better faces spin's ram direction

3.1. Baseline payload (Core SIs and Support SIs): red and orange colors in Table 3.1/3.2

(a) Light hot ions: MCP Ion Mass Spectrometer (MIMS)

Instrument design principle: The MIMS instrument is a time-of-flight (TOF) ion mass spectrometer, capable of obtaining full three-dimensional ion distributions (about 1 eV to 40 keV) within one spacecraft spin (~24 sec) and with a high-resolution mass-per-charge composition determination. Ions are selected as a function of their E/q (energy per charge) ratio, by sweeping the high voltage applied between the two hemispheres of an electrostatic analyser (360° x 5° FOV). Then they go through a ~5 kV post-acceleration and they next

enter into theTOF section, where their velocity is measured, allowing the calculation of their m/q (mass per charge) ratio.
MIMS is internally divided into two sub-instruments, using the same electrostatic analyser, post-acceleration and TOF section, each one corresponding to a ~180° x 5° instantaneous FOV:
• One sub-instrument using a specially designed thin microchannel plate (MCP) as conversion surface for the production the "start" TOF signal secondary electrons (Fig. 3.1). This technique takes advantage of the processes occurring during the scattering of the particles off a surface, i.e. kinetic electron emission. The energy loss of an incoming ion as it is scattered through a channel of this thin MCP is minimized, which minimizes the uncertainty of the TOF signal, allowing a very good mass resolution ($m/\Delta m \geq 15$). This sub-instrument is based on the prototype developed and successfully tested at IRAP, Toulouse (Devoto et al. 2008; Cadu et al., 2012) and it is optimized for the study of low to medium energy (1 eV to 20 keV) ions (Fig. 3.1).
• One sub-instrument using a thin (1 µg/cm^2) carbon foil for the production of TOF start signal secondary electrons. This sub-instrument is optimized for the study of medium to high energy (10 keV to 40 keV) ions, and it is based on the same principle as the successful CODIF instrument onboard the Cluster spacecraft (Rème et al., 2001), but with thinner carbon foils for improved mass resolution ($m/\Delta m \geq 10$).

Subsequent detection of the ions ("stop" TOF signal) and of the secondary electrons ("start" TOF signal), for both sub-instruments, is performed by MCP detectors. There are 7 x 22.5° discrete detection sectors for each sub-instrument, whereas the remaining two 22.5° sectors are "blind" and serve to provide a clear separation of the detection areas of the two sub-instruments, minimizing any potential cross-talk between them. The two sub-instruments operate in parallel, and the 10-20 keV overlap in energy between them allows for a cross-calibration between the two sub-instruments.
Data handling: The MIMS instrument is controlled by FPGAs. It generates 3D distribution functions for typical ion species and detailed mass histograms (4096 TOF bins). These are then compressed, within the instrument digital board, to 64 ion species: The instrument provides packets with compressed data. The MIMS electrostatic analyser performs 16 full energy sweeps per spacecraft spin (22.5° angular resolution in azimuth). For a ~24 sec spin period this corresponds to ~1400 ms per energy sweep, each sweep consisting of typically 200 energy micro-steps. There are five main categories of telemetry products, sent in parallel: (1) Mass histogram arrays, compressed to 64 M (mass) x 6 angles x 5 E (energy) x 16 bits, per 24 sec, i.e., ~1.3 kbps. (2) 3D distribution functions for typical ion species: 16 x7 angles x 64 E x 8 M x 8 bits, per 24 sec, i.e., 20 kbps, subsequently compressed / binned to ~5 kbps. (3) Moments of the distribution functions for typical ion species: 13 moment components (N, V (3 comp.), P (6 comp.), H (3 comp.)) x 5 E x 8 m x 16 bits, per 24 sec, i.e., 0.4 kbps. (4) Energy spectra for typical ion species: 180 E x 8 m x 8 bits, per 24 sec, i.e., 0.5 kbps. (5) Auxiliary and diagnostic products, overhead: ~0.8 kbps. Thus total MIMS telemetry rate is ~8 kbps after compression.

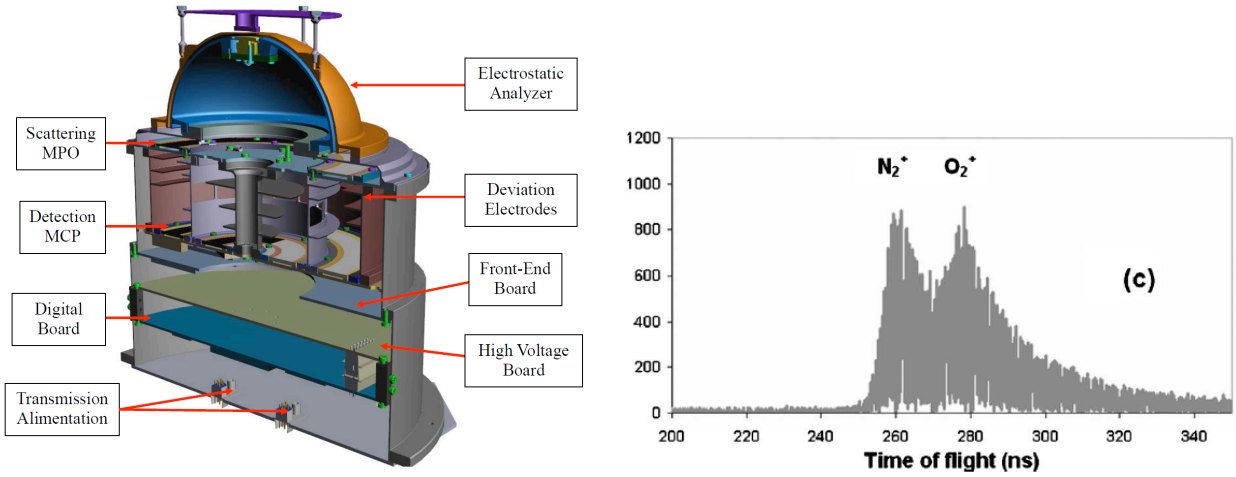

Figure 3.1: Left: Instrument system overview of MIMS. Sub-instrument uses a thin MCP as conversion surface for the production the "start" TOF signal. Right: Spectra of N_2^+ and O_2^+, acquired in the IRAP calibration facilities with an ion beam energy of 10 keV (Devoto et al., 2008). They reveal the capacity of the instrument to clearly separate closely spaced ions, and in particular to separate nitrogen from oxygen ions.

Operating modes: The MIMS instrument has a large amount of flexibility in the selection of the operational mode. These modes provide for the selection of different combinations of telemetry products and/or different energy/angular/mass/time resolution of the transmitted 3D distribution functions, allowing different schemes with respect to the above typical instrument telemetry products description.
TRL level: The MIMS sub-instrument with the thin MCP "start" conversion surface is based on the successfully tested prototype, developed at IRAP (Devoto et al. 2008; Cadu et al., 2012). The other sub-instrument, using a thin carbon foil for the "start" signal, is based on the CODIF instrument onboard the Cluster spacecraft, part of the CIS experiment operating since 2000 (Rème et al., 2001). There are actually about 1000 scientific publications based on the analysis of data provided by this experiment. The overall TRL of MIMS is 5 to 6.

(b) Heavy hot ions: Nitrogen-Oxygen Ion Detector (NOID)
Instrument design principle: The NOID instrument has a traditional top-hat design (16 sectors over 360° entrance) using a magnetic mass separation system as shown in Figure 3.2. Ions entering NOID first pass a semi spherical electrostatic energy analyzer, then a two-slit electrostatic lens, and finally the mass analyzer using 16 radially oriented permanent magnets, where light ions (H^+, H^{e++}, and He^+) are deflected completely away from the 100mm diameter MCP. The sampling time of each energy step is about 25 ms, covering 96 energy steps (from 10 eV to 10 kV or 1 eV to 1 keV) every 2.5 sec that correspond to 45° angles with 20 sec spin. After converting the electron shower from the MCPs to a raw count at each anode of the two-dimensional anode system (32 rings representing ion mass and 16 sector anodes, giving 640 kpbs), the data are processed to the required resolution (27 kbps), and after noise-reduction of isolated one-count events, compressed by a loss-less RICE compression method to about 6-8 kbps. In addition to data processing, the DPU also receives commands from the spacecraft, monitors voltages and temperatures, and sets the operation mode, including the energy table.
TRL level: NOID is as magnetic type mass-separating ion instrument, and is based on successful MEX/IMA (2003) and Rosetta/ICA (2004) that are built by IRF and are still in operation without instrument degradation. IMA and ICA are capable of separating molecular ions from atomic ions with a similar efficiency because the entered ions do not rely on grid or surface interactions with this method, and reached M/ΔM=4. They are designed for a 3-axis stabilized platform, which required an extra deflection system in the entrance to cover a third dimension, but this is not required for NOID, simplifying the design. The other alternation is increasing the diameter of the electrostatic energy analyser to extend it to 145° instead of 127° for IMA, and to use 40% larger magnets than IMA's magnet. This maintains the right angle trajectory to the MCP and more than doubles the mass resolution (this will give M/ΔM=8, that provides a redundancy to MIMS) whereas the required ability is to separate N_2^+ and O^+. Therefore, all overall TRL level is >6.

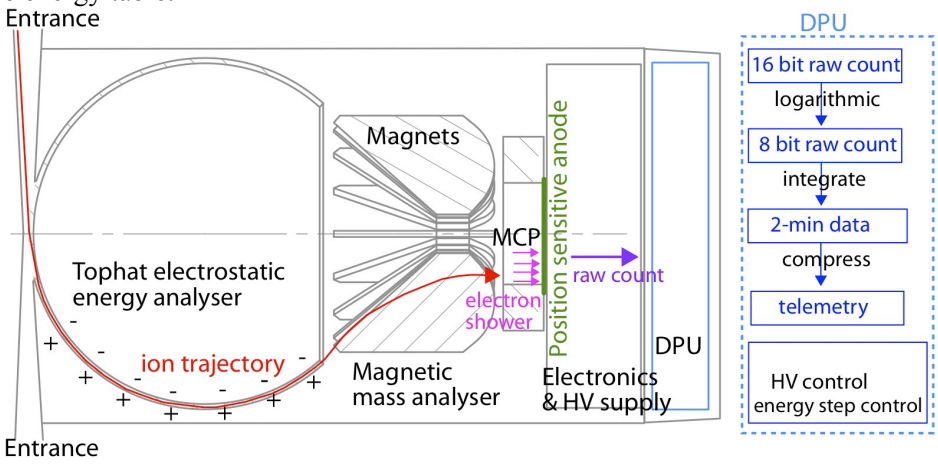

Figure 3.2: Instrument design and flow of ion count generation and its processing of NOID.

Operation: NOID operation modes mainly concern different energy stepping, because the 6% energy resolution and stepping can cover only a factor of 250 over 96 steps. Therefore, different stepping schemes must be used, depending on the region. Furthermore, we leave the possibility of choosing 3% stepping to cover a narrow energy range.
Calibration and accommodation: In-flight cross calibration with MIMS is needed. For accommodation to the remote sensing SC, FOV must include both ram and nadir directions.
Alternative for remote sensing SC: If NASA funds extra instruments (NASA normally funds two instruments that are reserved for CHEMS and CINMS), Southwest Research Institute is willing to provide an

instrument with similar mass (TRL=5-6) that covers a wider mass range for the remote sensing SC with a design similar to MIMS. While NOID satisfies this requirement, a wider international participation would benefit this ESA-led mission. In that case, power is 2 W more.

(c) Cold ions: Neutral and Ion Mass Spectrometer (NIMS)

Instrument design principle: NIMS is a TOF coincidence mass spectrometer with M/ΔM = 1100 resolution over a mass range of M/q = 1-1000. The ambient ions entering within the FOV are extracted into the acceleration region by a high-voltage, high-rate (10kHz) pulsed potential. Then each ion packet is shaped and accelerated inside the ions source by a series of acceleration electrodes towards the grid-less ion mirror (reflectron). After passing the first leg of a field-free drift path, ion packets are reflected by the reflectron (potentials up to 5 kV), which allows energy and spatial focusing (time domain focusing), and are then directed onto a fast micro-channel plate detector. During their TOF the initial ion packet separates into several ion packets according to mass-per-charge. The ions are recorded on a detector, with 2 MCPs in the chevron configuration and an impedance-matched anode (Wurz and Gubler, 1994, 1996). The resulting charge pulse on the anode is registered by a fast analog-to-digit converter (ADC) system with 2 Gs/s sampling rate and 8 bit vertical resolution (Luna-Glob heritage). The sequence of charge pulses, the TOF spectrum, is converted into a mass spectrum in a straightforward manner.

Operation: TOF spectra are recorded continuously and accumulated typically for 5 seconds to achieve a dynamic range of at least 6 decades in an accumulated spectrum. Accumulation time can be set via command between 1 to 300 s to accommodate different operation scenarios. Ion density of about 10^{-3} to 10^{3} cm^{-3} (six orders of magnitude) can be measured every 5 sec.

TRL level: NIMS has heritage from Rosetta/RTOF (Scherer et al., 2006) and is significantly reduced in size already for JUICE/PEP, for which the prototype has been verified (Wurz et al., 2012). Radiation shielding is already fitted to high radiation environment of Jupiter. The TRL level of NIMS is 6-7.

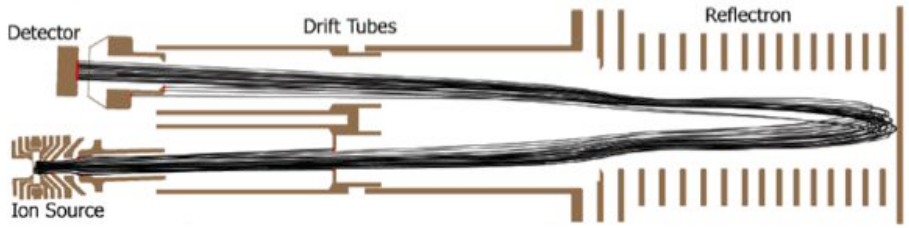

Figure 3.3: Ion-optical design drawing of NIMS sensor, with the ion source and the detector at the left side, and the ion mirror on the right.

(d) Energetic ions: Charge-Energy-Mass Spectrometer (CHEMS)

Instrument design principle: The Charge Energy Mass Spectrometer (CHEMS) instrument combines an energy per charge selection with a time-of-flight and energy measurement to determine mass and mass-per-charge over the energy range 10 keV/e to 220 keV/e. The design is closely based on the CASSINI/CHEMS instrument (Krimigis et al., 2004). A schematic of the sensor and dataflow is shown in Figure 1. The entrance system is a toroidal section electrostatic analyzer (ESA) that selects ions by energy per charge. The ion passes through the ESA, and then through a thin (~ 1 µg/cm2) carbon foil. Electrons knocked off the carbon foil are steered to MCP to give the start signal. The ion travels across a 10 cm flight path and hits the solid state detector (SSD). Electrons emitted from the SSD are steered to a second MCP which gives the stop signal. The time of flight is determined from the difference between start and stop. The combination of the time-of-flight and the energy per charge from the analyzer gives the mass per charge of the ion. Combining the time-of-flight with the energy from the SSD allows the mass and charge state to be determined separately.

TRL Level: The sensor configuration is based on the CASSINI/CHEMS instrument, which was designed and built at the University of Maryland, with the design led by NITRO Co-I Dr. D.C. Hamilton. The principle of the instrument (combination of electrostatic analyzer, time-of-flight and energy measurement) is the same as the STEREO/PLASTIC instrument, which was designed and built at the University of New Hampshire, led by NITRO Co-I Dr. A. Galvin, and the Heavy Ion Sensor (HIS) for Solar Orbiter, for which UNH is building the mechanical time-of-flight system, the MCP power supplies, and the anode boards. For NITRO, the instrument will be built predominantly at the University of New Hampshire based on the CHEMS optical design, using subsystem elements based on those designed for STEREO PLASTIC and Solar Orbiter HIS. Thus the instrument is at TRL>6.

Operating modes: The CHEMS electrostatic analyzer performs 16 energy sweeps per spacecraft spin (22.5° angular resolution in azimuth). Each sweep covers 12 energy steps. The stepping sequence alternates between a high energy spin and a low energy spin, so that the full range is covered in two spins. The data will be summed over 6 spins to give 2 minute time resolution.

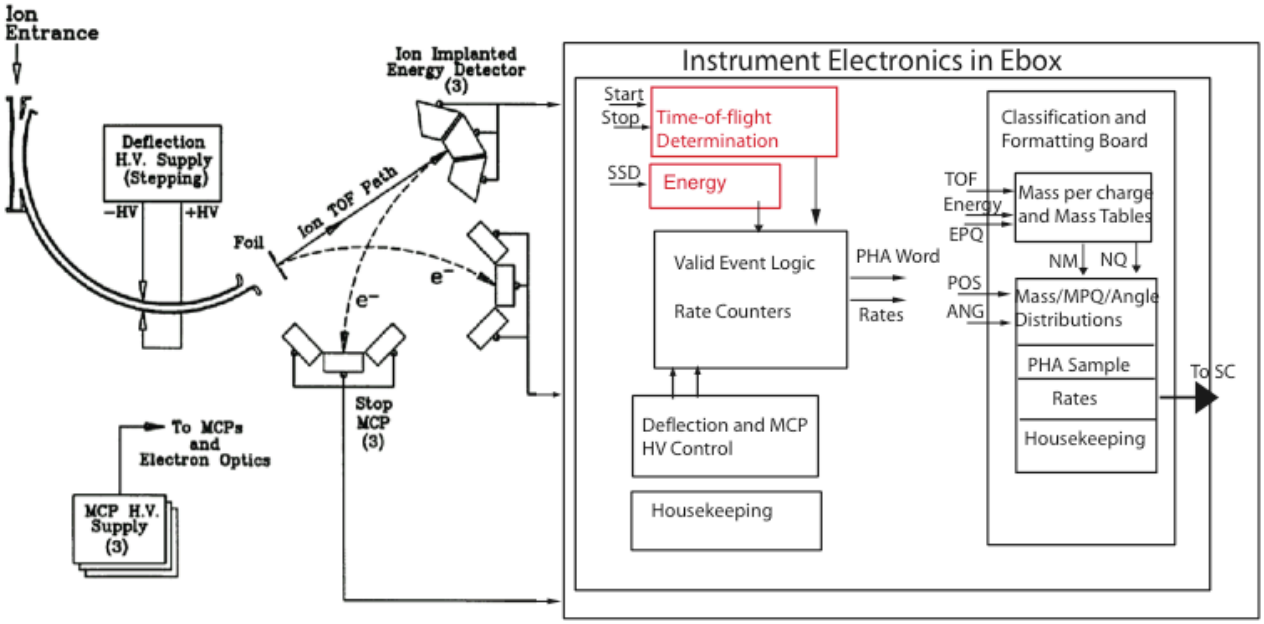

Figure 3.4: The CHEMS instrument design and data flow (modified from Krimigis et al., 2004)

(e) Spacecraft potential: Sweeping Langmuir Probe (SLP)

Instrument design principle: The Sweeping Langmuir Probe (SLP) instrument uses spherical Langmuir probes mounted on booms. Two probes are present on the in situ spacecraft (SLP-IS1 and SLP-IS2) and one on the remote sensing spacecraft (SLP-RS). The main goals of the instruments are to measure 1) the spacecraft potential, the plasma density and electron temperature (on both spacecraft) and 2) the DC electric field, by combining SLP-IS1 and SLP-IS2 (on the in situ spacecraft only).

Measurement in Langmuir probe mode consists of setting the probe potential and measuring the collected current to establish the current-voltage relation (I-V curve) from which spacecraft potential, electron density and electron temperature are derived. Measurement in electric field mode is based on a differential measurement to infer the electric field from the floating potentials of both probes. The maximum measurement rates are 20 I-V curves / s and 20 Hz for the Langmuir probe mode and electric field mode, respectively.

Accommodation on NITRO: On both spacecraft the probes are mounted on deployable booms (provided as spacecraft subsystems) that are at least 1.75 m long to be outside the spacecraft sheath. For SLP-IS, the booms have to be positioned opposite to each other with respect to the spin axis to maximize the tip-to-tip distance. With a distance of ~5-6 m one can achieve a reasonable precision on the spin-plane DC electric field components (on the order of 2 mV/m), which are useful for providing context. Alternatively, if the technology is available, wire booms can be used to achieve tip-to-tip distances of 50 m or more, yielding a scientifically more interesting result.

Data handling: The instrument is fully controlled by an FPGA, which is also used as DPU. The instrument provides data packets without compression. There is a specific output for the spacecraft potential every 4 seconds to the spacecraft bus to steer the ion emitter. A second specific output is towards the wave instrument.

Operating modes: Basic modes are (a) Langmuir probe mode with transmitting the full I-V curve every time, (b) Langmuir probe mode with transmission of one full I-V curve plus a number of onboard derived potentials, densities, and temperatures at higher time resolution, (c) electric field mode, and (d) instrument housekeeping mode.

TRL level: The SLP instrument heritage is from the PICASSO SLP cylindrical probe instrument. The TRL is 4-5 presently, but will increase rapidly with the implementation of ESA's PICASSO in orbit demonstrator.

(f) Magnetic field: Magnetometer (MAG)

Instrument design principle: The DC magnetometer is a dual-sensor fluxgate magnetometer for measuring the ambient magnetic field. The design of the magnetometer consists of two triaxial sensors and the related magnetometer electronics, digital processing unit, power supply, and electronics box.

Each sensor consists of two entwined ring-cores to measure the magnetic field in three directions and is housed in a 8x8x5 cm package. One sensor is placed at the end of a solid boom and the second at an intermediate distance along the boom to enable reliable subtraction of any residual spacecraft magnetic field. The magnetometer electronics are based on the MMS/FIELDS suite and employ the same Magnetometer Front-end ASIC (MFA-3). This provides major improvements in miniaturization, mass and power, and provides 300 krad TID radiation hardness. The core of the electronics is the MFA-3, a third-generation magnetometer front-end ASIC developed at IWF. The digital processing unit of MAG will be based on the design of the BepiColombo MPO magnetometer.

TRL level: The fluxgate type is a matured instrument has a high TRL(8). IWF led the fluxgate magnetometer for Venus Express and is leading the digital fluxgate magnetometer (DFG) onboard MMS, planned to be launched in March 2015.

Noise level and EMC requirement: The DC magnetometer will return magnetic field vectors (low range of ±500 nT to high-range or ±8000 nT) at up to 128 sps with > 20 bits digital resolution and with a noise floor less than 0.006 nT/√(Hz) at 1 Hz. An appropriate magnetic cleanliness plan such as implemented on previous space missions is required for the magnetometer measurement.

(g) Waves signal processing (WAVES)

Instrument design principle: The WAVES instruments processes the electric signal from SLP and the magnetic signal from the search coil magnetometer (SCM) in the frequency range up to 20 kHz. WAVES is composed of a wave analyzer board (LFR) responsible for digitization and processing of signals from SLP and SCM (search coilmagnetometer) in the frequency range up to 20 kHz, a Digital Processing Unit (DPU), a power converter, and an electronic box. Three institutions are directly involved in the instrument realization. The data digitized by LFR are processed by integrated digital logic implemented in an FPGA, performing filtering, decimation and spectral analysis of the signals. This on-board pre-processed digital data from WAVES and SLP units are transmitted to the DPU for formatting and compressing before transmitting to the spacecraft. DPU software will also perform numerical calculations such as producing the wave properties from the complex spectral matrices.

The IAP-ASCR takes care of the LFR (four DPU units, two per each spacecraft) and the DPU hardware, the University of Sheffield of the DPU software and the SRC-PAS of the power converter and the electronic box. The DPU is common for SLP and WAVES.

TRL level: IAP has significant heritage in the development of wave analyzers for recent missions (Solar Orbiter, TARANIS, JUICE etc.). IAP will be responsible for the delivery of two complete LFR boards (all required models), including FPGA firmware and Ground Support Equipment. IAP has also a strong heritage in the DPU hardware, and therefore TRL>=5.

Data products: WAVES can capable of producing four different products. (1) The magnetic waveform at a 122Hz cadence. (2) The magnetic spectral matrices that are also produced continuously at a 1s resolution with 200 bins in frequency. The bin widths are distributed following a logarithmic scale. (3) The full 2s waveform snapshot of a 4 components (including one electric field component from the Langmuir probe), one snapshot per minute, to study the electrostatic emissions, and generally, the electric component of the emissions. (4) With only one electric component, it is still possible to get the Poynting flux orientation. Total of all products occupies 140 kbps after compression with 20 bit/data. Since the mission requires much lower resolution data, WAVES will actually produce only 10-20 kbps after compression.

(h) Search Coil Magnetometer for wave detection (SCM)

Instrument design principle: The search coil unit SCM is a magnetic sensor of inductive type. This is the sensor intended to measure the three components of the magnetic field from near DC (5 Hz) to about 20 KHz. It is composed of 3 ELF-VLF magnetic antennas (search coils) made of a ferrite core with a primary coil of 16000 turns. A secondary coil is used as a flux feedback, to create a flat frequency response on a bandwidth centered on the resonance frequency of the main coil. This active part is potted inside an epoxy tube (104 mm long, external diameter 20 mm). The magnetic antennas are assembled orthogonally in the most compact way possible by the body of the sensor. This mechanical support is made in a nonmagnetic

material (PEEK KETRON) and stands for the interface with the satellite. Illustration is found in Figure 3.5, and photos are found in Annex.

The amplification electronic circuit is made using 3D technology. It is divided into several printed circuit boards (PCB), which are stacked and moulded in an epoxy resin. Tantalum layers are inserted between electronic boards to improve the radiation tolerance. They are composed of 3 ELF-VLF amplification channels, and 1 power supply regulation circuit. The 3D module will be boarded in the sensor's foot (close to the antennas) to reduce the signal-to-noise ratio. The sensitivity of SCM is 2.10^{-3} nT/(Hz)$^{1/2}$ at 10 Hz and 8.10^{-6} nT/(Hz)$^{1/2}$ at 2 kHz.

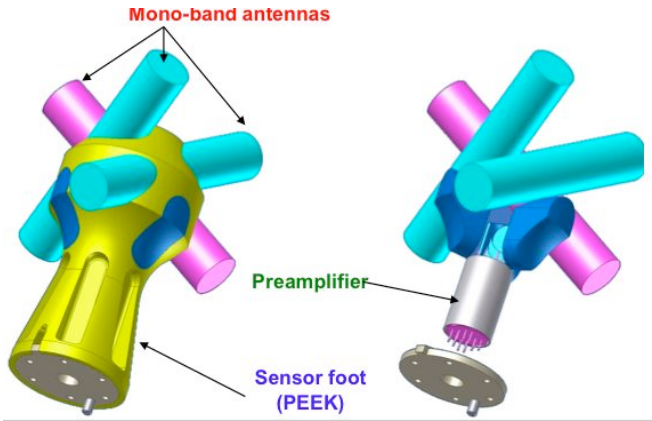

Figure 3.5: SCM design (photo is found in Annex)

(i) Electrons: Plasma Electron And Current Experiment (PEACE)

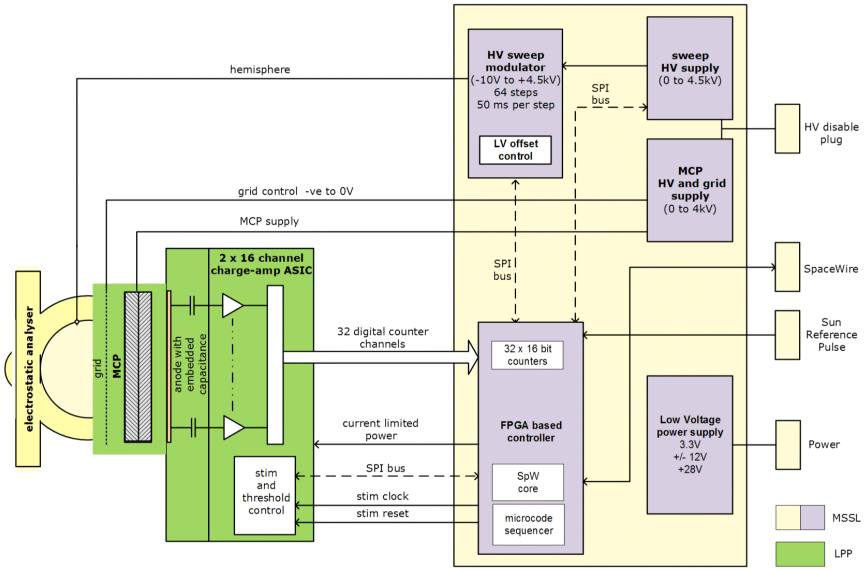

Figure 3.6: Instrument design and flow of ion count generation and its processing of PEACE

Instrument design principle: The NITRO PEACE instruments will use the classic top-hat electrostatic analyser design (two separate top hat analysers attached to a single sensor electronic unit) in which electrons are energy-selected using a swept high voltage applied between a pair of hemispheric electrodes and angle selected using a pixelated anode. For the in-situ SC, PEACE-IS, the second angular direction is sampled by performing multiple sweeps during the spacecraft spin and the spacecraft rotation will ensure that during every spin, PEACE-IS looks along themagnetic field direction where the ionospheric photoelectrons (IP) are expected to be seen. PEACE-IS is required to measure the IP population in the energy range 20 - 35 eV with an energy resolution of ~ 1 eV at 2 min resolution, which is done by $\Delta E/E \sim 3\%$ in the energy range 10 eV to 60 eV, with energy steps of < 1 eV below 35 eV. PEACE-IS-IP is also required to measure the magnetospheric electron (ME) population in the energy range ~10eV to ~10 keV with a coarser energy resolution of $\Delta E/E \sim 13\%$ up to 20 keV. and to provide these data at 2 min resolution. There will be an option to float the energy range coverage relative to the spacecraft potential information from SLP. The instrument will be closely based on the dual-analyser Solar Orbiter SWA-EAS, with the aperture deflection grids removed. Additionally, for PEACE-IS-IP the collimator will be adjusted to reduce $\Delta E/E$; the corresponding reduction in geometric factor will be compensated by longer accumulation times to ensure adequate count rates. A more elegant approach that will be explored is to use a single larger top hat analyser with an electrostatically variable energy resolution, as an adaptation of the "variable geometric factor system" on Solar Orbiter SWA-EAS. The stated mass and power budget is compatible with both these options. The operation of the instrument is controlled by an FPGA, synchronized to the spacecraft spin using

the sun pulse. Data will be collected during each spin, accumulated and compressed in the instrument to produce data at the required 2 min cadence, but the instrument can provide data at other cadences if required.

PEACE-RS on the 3 axis stabilized remote sensing spacecraft must observe the ionospheric photoelectrons at 30 s cadence. PEACE-RS will use an aperture deflection system (as on SWA-EAS) to track the magnetic field direction to see the ionospheric photoelectrons. It must be provided with a clear 360° field of view from zenith to nadir, taking account of a ±10° aperture deflection.

TRL level: Due to the heritage of Solar Orbiter SWA-EAS and Cluster PEACE, the TRL is considered to be >=6. The instrument has a science operation mode, a standby mode and an off mode. LPP (France) will provide the ASIC system.

(k) UV/visible line-of-sight emission: Nitro Ultraviolet Observer (NUVO)

Instrument design principle: NUVO (Nitro Ultraviolet Observer) is a Far-Ultraviolet spectrometer dedicated to the study of ultraviolet airglow emissions. The spectral range covers the 85nm-140nm bandwidth with two additional visible channels at 391 nm and 428 nm for observation of N2+ emission lines. The NUVO UV channel is an imaging spectrometer using a holographic diffraction grating. The optical scheme of the UV channel is shown on the left part of Figure 1. Its entrance pupil is defined by a baffle with a guard angle of 30°. The field of view is defined by a slit (2°x0.1°) placed between the primary mirror and the grating. The intensified detector is placed at the focal plane of the diffraction grating. Photon detection is obtained by combining Micro-Channel Plate based intensifiers with CsI photocathode. The read-out is made by a cross delay anode (provided by the University of Tokyo) with one axis for the spectral dimension and the second axis for spatial imaging along the long dimension of the slit. The visible channel is shown on the left part of Figure 3.7. It has a very similar concept using primary mirror, slit and grating. The main difference is that this channel uses dedicated detectors for each line of interest (391nm and 428nm). These detectors are Photomultiplier Tubes from Hammamatsu.

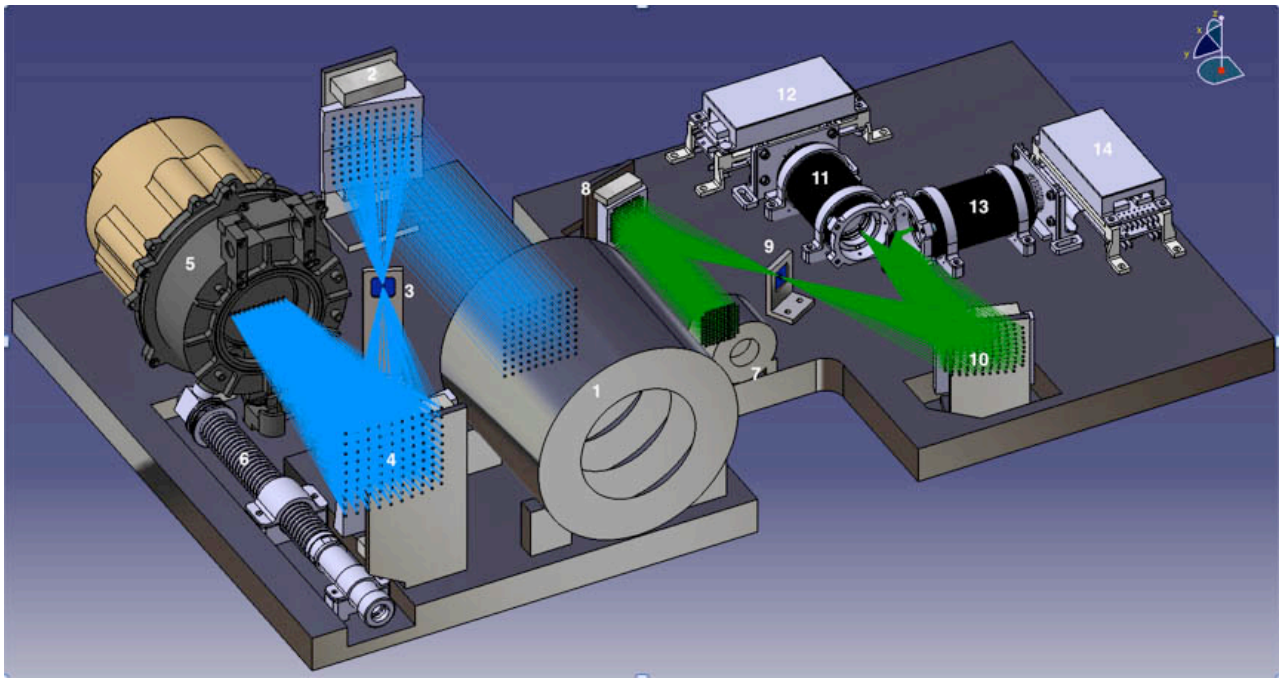

Figure 3.7: Optical concept of the UV (left) and visible (right) channels of NUVO.

TRL level: The NUVO concept is based on previous UV experiments designed and built at LATMOS (Guyancourt, University of Versailles Saint-Quentin) such as SPICAM on Mars-Express, SPICAV on Venus-Express and PHEBUS on Bepi-Colombo. The University of Tokyo detector is the same design as the one on PHEBUS-BepiColombo and the Hisaki mission. The Digital Processing Boards (not shown on the graph) will be a copy of the PHEBUS (Bepi-Colombo) boards. This ensures that all components of NUVO have a very high heritage from one of the previous instruments developed at LATMOS.

Operation: All operations consist of successive acquisitions of detector images made at different positions of the orbit and for various pointing of the scanning platform. The fastest sampling rate will be 2 sec. The acquisition time varies between 0.1 sec up to 100 sec depending on the line brightness.

Calibration and special request: NUVO is placed on a scanning platform provided by the spacecraft. The Field of View of NUVO should be free of any obstruction. Calibration will be monitored by looking at bright calibration stars on a weekly basis during the mission. These calibrations do not require special maneuvers. In the integration and pre-launch phase, the UV detector will be pumped at all times. For special periods, like vibration tests, the detector pumping can be stopped. Each period without pumping should be limited to two days.

(l) Cold ions and neutrals (< 10 eV): Cold Ion and Neutral Mass Spectrometer (CINMS)
Instrument design principle: The CINMS instrument, based on gated time of flight with pre-acceleration and reflectron, is shown in Figure 3.8. Cold ions entering the ion aperture from the ram direction, through a cylindrical wire mesh slightly biased to balance spacecraft potential, are radially pre-accelerated and focused through a circular electric gate structure, into a top hat electrostatic analyzer (ESA), focused into a reflectron, and finally hit an annular micro channel plate (MCP) with arrival times organized as $M/q= (2E/q)*(TOF/L)^2$, where E is the total energy, and L is the TOF path from the first gate (start) to the MCP (stop). The ESA, biased at a fixed potential, filters out of band particles and UV light, whereas the reflectron increases the mass resolution. A gating electronic duty cycle control (~ 20% -0.002%) allows optimum tradeoffs of sensitivity and dynamic range. The neutral side is identical except for annular thermionic ionizer, a larger aperture (~1cm^2 versus ~0.1cm^2 for ions), and positive bias of entrance grid to block the low energy ions. A delay line position sensitive anode with TOF ASIC / FPGA, are used for the read out, multi hit binning in 1000 bins of 5 ns intervals, and 30 sec integration in 9 angular sectors around the ram direction. With 30-bit counters per bin the data rate is 1kbps per sector or 18kbps for all ion and neutral sectors uncompressed, and to 1.8kbps after 90% lossless compression, rounded to 2kbps with housekeeping.
TRL level: CINMS draws heritage from similar ESA/Foil/TOF/MCP ion composition instruments in the energy range 0-30KeV/q, i.e., Cassini, Messenger, JUNO, MMS. However because of the much lower energies, the foils and ~20 kV HVPS are replaced with electric gating and much lower HVPS ~5KV. Figure 1b shows N+ and O+ measurements from the gated CINMS prototype with excellent mass separation. Additionally a miniature CINMS without the reflectron has also been developed for two Cubesat missions: Exocube scheduled to fly on 29 Jan 2015 and Dillinger in June 2016. The overall TRL of CINMS is >5-6.
Accommodation and Operation: A spacecraft turn- table is not required because of the wide FOV around the RAM direction. Operating modes include adjusting entrance grid potentials, electronic adjustments of gate duty cycle, ionization filament current adjustments, and data modes. In flight calibration will be required for ions and neutrals.

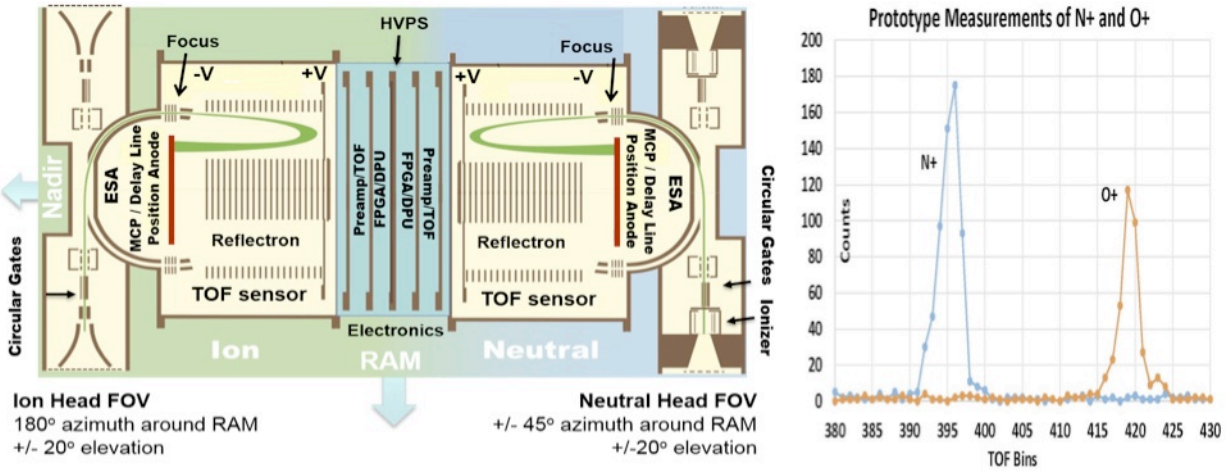

Figure 3.8: Schematic view of the CINMS with ion sensor (left), neutral sensor (right), and electronics in the middle. Particle trajectories are shown in green entering from ram direction; Fig 1b shows N+ and O+ measurements from the laboratory prototype with mass resolution of $M/\Delta M > 50$.

(m) Aurora/airglow camera: CCD Auroral and Airglow Camera (CAAC)
Instrument design principle: CAAC has two CCD cameras, each consists of an interference filter, objective lens, and CCD detector that is connected with a thermal path to a radiator. Two interference filters have center wavelengths that are optimized for measuring the auroral N2 first positive band at 670 nm (bandwidth 35 nm) and the auroral and airglow O2 A-band at 762 nm (bandwidth 2 nm), respectively. The objective

lenses have 10 degrees FOV, covering an squire area of 70-400 km at the auroral and airglow altitudes measured from 500 km to 2400 km spacecraft altitude. The CCD detector using fused silica for blocking radiation has an efficiency better than 0.7 when it is cooled to -10°C to -30C° to reduce thermal noise. Cooling is achieved by a peltier cooling thermal path connected to the radiator.
Data production: The CCD pixels of 1024x1024 are divided into 8x8 binning (for aurora) or 16x16-pixel binning (for airglow) because the mission does require high spatial resolution. The exposure time need a few seconds for faint airglow emissions. The estimated data rate will be 10 – 50 kbps.
TRL level: The auroral and airglow camera is based on the multi-spectral auroral camera (MAC) on the Reimei satellite (Sakanoi et al., 2003). The CCD detector is commercial-based front-illuminated interline type which is relatively resistant to radiation. The digital and analog electric boards are also commercial-based which contribute to quick manufacturing. On the other hand, objective lens and cooling unit are custom made to obtain sufficient performance in space.The optical and electrical systems were tested and established in the development of Reimei/MAC and IMAP/VISI on the international space station (Sakanoi et al., 2011).
Accommodation: The FOV cameras of CAAC does not have to be in the nadir direction but rather obliquely placed (e.g., 45° to nadir direction as shown in Figure 3.9) to maximize the change to direct the foot point of the magnetic field. This slant angle will be optimized in the future with precise designing.

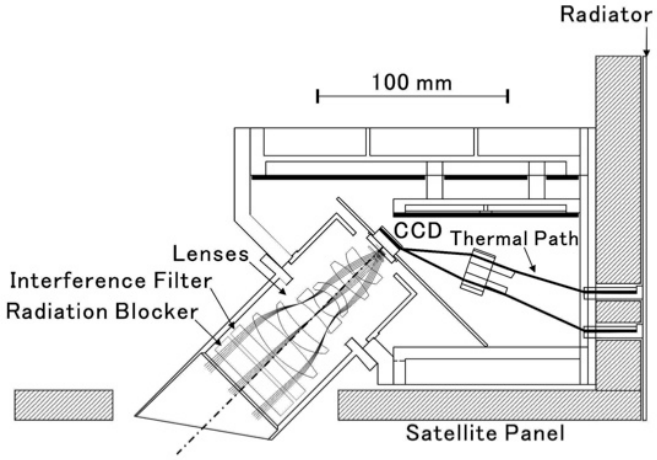

Figure 3.9: Schematic of CAAC and its accommodation.

3.2. Optional payload (for optional science in Table 2.1): green color in Table 3.1/3.2
(j) energetic neutral atoms: SupraThermal Electrons, Ions, & Neutrals (STEIN)

Instrument design principle: The STEIN instrument was developed at the University of California Berkeley Space Sciences Lab as an extension of the STEREO STE instrument (Lin et al., 2008) with the addition of electrostatic deflection for sorting neutrals from ions and electrons. It uses the same thin window pixelated silicon as STE allowing it to go to ion and neutral energies of ~4 keV, but with an ASIC to expand the number of pixels (now 32) while reducing power and mass requirements to ~1kg and ~800 mW. The STEIN detector has been delivered for use on several cubesats which failed before turning on their detectors and has been adapted with different post-ASIC readout electronics for the Solar Orbiter STEP instrument. It has been thoroughly tested in measurement chambers with several mechanical variants similar to the planned NITRO version.

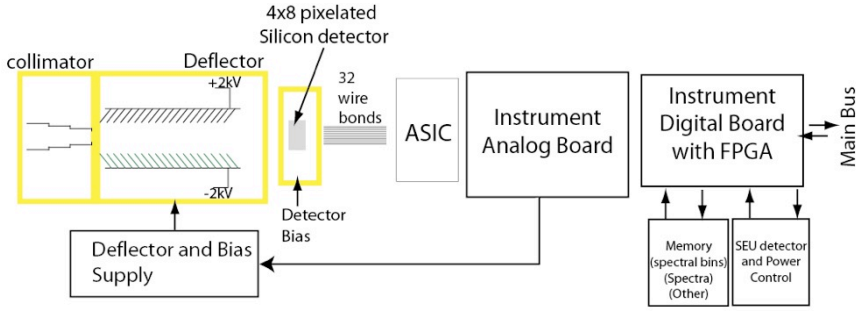

Figure 3.10: Schematic diagram of STEIN.

Particles enter the front aperture with passive collimation to obtain the desired angular field of view. They then pass through an electrostatic deflection region with knife edge plates that carry a settable (or swept) applied potential of ±2 kV. The potential sorts ions from neutrals uniquely up to 30 keV, while higher energy particles are not sufficiently deflected to uniquely identify. Each event is pulse height analyzed and recorded with a time tag by an in-instrument FPGA that allows for tailoring the data stream (and volume) and interface to the science and spacecraft requirements.
TRL level: UCB-SSL has significant heritage in providing instrumentation for a wide range of NASA and ESA missions. STEIN for NITRO is at TRL 6 with close mechanical and electrical analogues to the instrument having been flight qualified. The STEIN FPGA allows for easy interface to the rest of the NITRO payload.

Operation: STEIN's normal operating mode allows for choice of a set deflection voltage or a stepped scheme. For ENA focused operations, a steady ±2 kV maximum deflection voltage is the most common.
Calibration and special request: Routine self-calibration as requested, for accurate energy determination the 16 bit energy calibration data can be read out at low cadence.

(n) heavy precipitating ions: Mass Spectrum Analyser (MSA)
Instrument design principle: MSA consists of an energy analyzer (FOVdeflectors at the entrance and spherical electrodes inside) and an LEF (Linear Electric Field) TOF ion mass analyzer (McComas and Nordholt 1990; Yokota and Saito 2005a; Yokota et al. 2005b). The FOV is electrically scanned between ±45° around the center of the FOV, which is 45° inclined from the axis of symmetry. The ions transmitted through the energy analyzer of MSA are post accelerated to -15 kV and enter into the LEF TOF mass analyzer part. For the ions, the TOF section of MSA acts as a so-called "isochronous time-of-flight" to first order of energy deviation. The raw data rate of MSA is 16 Mbps (4 polar x 16 azimuth x 96 energy x 1024 TOF x 16bits / 6 sec) that is reduced to 13kbps (32 mass x 96 energy x 8 dir x 16 bit / 30 sec) by using TOF-mass mapping table and FOV sector - dir mapping table. The 13 kbps data will be compressed to ~6kbps by DPU.
TRL level: MSA is almost the same as Ion Mass Analyzer (IMA) on Japanese Moon Orbiter Kaguya. To reduce the blind sectors in IMA's FOV, the structure of the entrance part will be slightly modified. Another point that is different from IMA is its charge detection anode and front-end electronics. To reduce the blind sectors and dead time, a delay-line type MCP anode will be used instead of resistive MCP anode. The frontend electronics is also changed from charge amplifier + Analog to Digital converter to fast timing amplifiers + Time to Digital converter. This detection system has already been used for Mass Spectrum Analyzer (MSA) on BepiColombo/MMO. Therefore all the components of MSA have already reached TRL 6.
Operation: MSA has multiple operating modes where energy stepping modes are different. The 4 pre-defined energy stepping modes can be selected by commanding. The energy level can be changed by rewriting energy stepping tables stored in EEPROM.
Calibration and special request: The FOV should not be blocked by booms or solar panels. In-flight cross calibration with other ion sensors with the similar energy rage is necessary

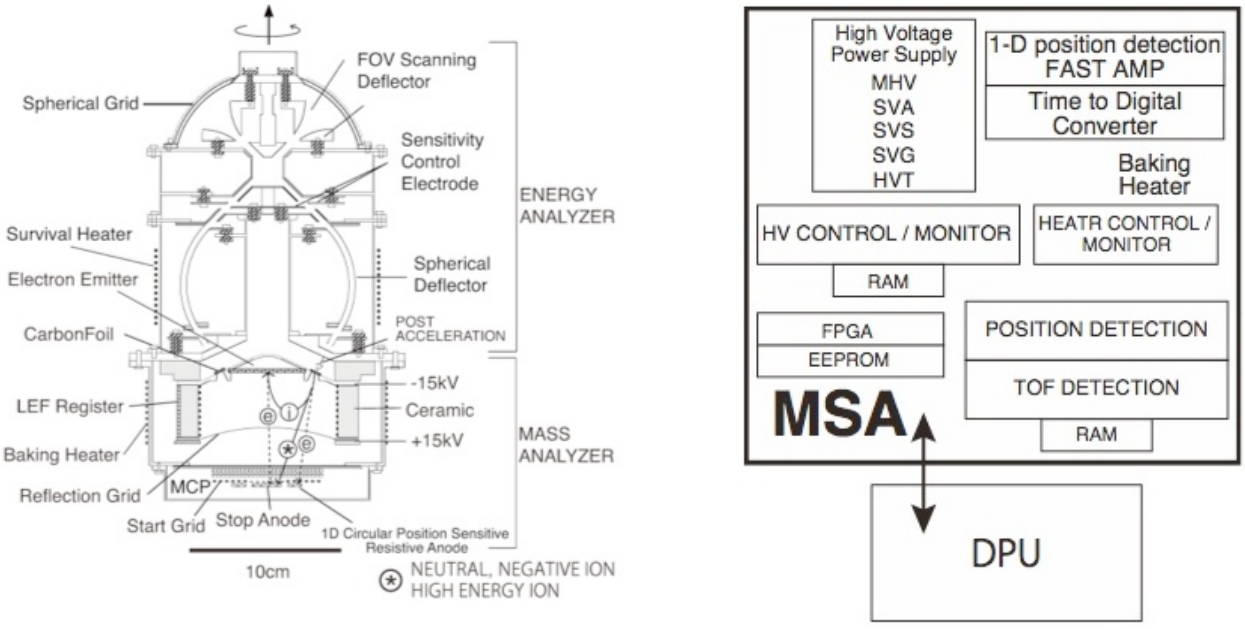

Figure 3.11: Instrument design and functional block diagram of MSA

3.3. Mandatory support spacecraft subsystem (needed to understand data from core instruments)
(x) Active spacecraft potential control: (ASPOC)

By emitting indium ions of 4 to about 10 keV energy, to compensate for the photo-electron emission, ASPOC reduces the positive spacecraft potential to less than 5 V when the spacecraft surface is conductive

(activated when more than 1 V), allowing for much more accurate plasma measurements at energies less than 50 eV. Form this reason, ASPOC should be located on the shadow side of the in-situ SC. ASPOC contains a pair of ion emitter units, each connected to a dedicated high voltage supply. The number of emitters (four for Cluster case) is determined based on lifetime and redundancy reasons (MMS emitters have lifetimes of > 9000 hours, i.e., 1 full year). Since ASPOC was successfully used on Cluster, TRL level is 8 (IWF has know-how, but we consider this as an ESA's instrument or spacecraft subsystem because it is a supporting device for the core instruments).

(y) Spacecraft DPU and a "virtual instrument"

Modern spacecraft include a spacecraft DPU that buffers and compresses telemetry data as well as distributing uplink commands. Since the downlink capacity will be about 1 GB/day for the in-situ SC and 5 GB/day for the remote sensing SC, we plan to have 10 GB buffering ability in the spacecraft DPU. In addition, the spacecraft DPU on the in-situ SC would include a digital processing board to process the HK package related to the energetic particles for a real-time etimate of the on-board radiation belt flux. This kind of information is relevant to spacecraft health, and therefore, this "virtual instrument" function should be placed in the spacecraft DPU. While ESA provides the DPU hardware, the software will be developed by the University of Athens.

The virtual instrument program will need information of (1) total counts of energetic particles and in addition counts of energetic ions in a representative energy channel of CHEMS, (2) readouts of start and stops signals from the time-of-flight system and , double coincidence rates observed by CHEMS and/or MIMS (for redundancy). Therefore, CHEMS and MIMS will include these data in their HK package. From this information, the virtual instrument program issues alerts of different levels within the spacecraft DPU, adding extra commands for "emergency sleep" or "safe mode" to relevant SIs. Such on-board analyses of the radiation belt should also be transmitted to the ground as a data product, because the information is precious both for operations (sensitive instrument protection) and for studying the dynamics of the radiation belts in a handy format, although the latter information can also be obtained from CHEMS.

(z) Scanner for NUVO

The scanner design described here is based on a successful scanner used for the Mars Express ASPERA-3 experiment (Barabash et al., 2006). The scanner consists of the 0°-180° rotating platform, a high voltage power supply, and housekeeping and DC/DC boards. Rotation is accomplished by the use of a worm gear mechanism. A large diameter worm wheel on the rotating platform is rotated by a stepper motor via a co-axial worm screw. The worm wheel is fixed to the structure with a large diameter angular contact ball bearing. The position of the movable parts relative to the scanner is given by three magnetic sensors. No mechanical contact exists with the sensors. In addition to a worm gear type of mechanism that provides a self-locking behavior without electrical power, a launch lock mechanism was introduced for extra stability during high vibration conditions. The locking mechanism consists of a wire that ties together two small levers, locking the square-shaped worm screw axis.

The motor electronics provides motor control and driving. By command, the axis is unlocked by applying a voltage to a resistor that burns the wire and then the levers are forced to move apart by the actions of a spring. The stepper motor is driven by a classical H-bridge drive system with a motor current control system. The following modes of the scanner operation are possible: (1) continuous scanning back-and-forth between both ends, (2) continuous back-and-forth scans in steps of predefined degrees and predefined sampling times for each step, (3) positioning to any position. The parameters can be changed by command. The angular positioning accuracy of the scanner pointing direction is 0.2.

booms + deployment mechanism

The booms are mandatory for a spacecraft with electric and/or magnetic field observations. For the in-situ spacecraft, they must be placed symmetrically within the spin plane for the in-situ SC to maintain stability. To avoid blocking the FOV of the particle instruments, the ideal solution is to place two long booms (MAG and SCM) along the solar panels, as done on Astrid-2 (1999), but the other two short booms (SLP) should be away from the solar panels, as they produce interference. Optimally, they can be placed 30° off, and at different layer of the spacecraft from the solar panels. The booms on the remote sensing SC are optional, with one SLP boom a higher priority than the others. The optional MAG booms for the remote sensing SC can also be shortened because of higher background magnetic field (magnetic cleanness requirement is lower).

4. Mission Configuration and Profile (11.5 pages):

4.1. Orbit design

4.1.1. Requirement for orbit

To fulfill the unique observation conditions as described in section 2.3, the following conditions are required for the orbit and attitude of the spacecraft:

* The 3-year radiation dose for each SC shall not require a higher level of shielding than 6 mm (in-situ SC) or 5 mm (remote sensing SC) to reach <50 krad on EEE level), i.e., a low altitude for the remote sensing SC (below inner radiation belt) while maintaining the visibility requirement.
* Orbital parameters must be designed to require as few maneuvers as possible (e.g., free drift).
* The in-situ SC must slowly cover the inner magnetosphere three dimensionally at different altitudes (20000km-32000km), latitudes (0°-45°) and longitudes (0°-360°) within 3 years. The best solution is an elliptic orbit with latitudinal drift velocity of the apogee-perigee axis of about ±2°, in which the orbit slowly covers the inner magnetosphere both in latitude and in equatorial L-values (altitude).
* The in-situ SC must not enter the geostationary ring during the operational phase; i.e., considering the latitudinal drift of the orbit parameter, apogee should be placed < 35000 km altitude.
* The remote sensing SC must cover the exosphere of 1000-2000 km at different altitudes and solar zenith angles (longitude); i.e., the orbit must be elliptic.
* The line-of-sight observation to the in-situ SC is possible for at least 100 hours / 2 months from the remote sensing SC at invariant latitude >+60° or < -60° (from outside the inner radiation belts) and altitude > 1800 km (above the topside ionosphere).
* The longitudinal drift rates of ascension (RAAN drift rate) of both SC must be the same within < ±5°/year accuracy, which is guaranteed by VEGA launches.
* At mission completion, each SC can be de-orbited.

The two spacecraft do not have to be geomagnetically conjugate to detect the same ion population at both SC because ions that once enter the inner magnetosphere start drifting in the longitudinal direction due to the magnetic and ExB drift. The in-situ SC covers a longitudinal range of more than 20° if the ions are bouncing between both hemispheres, and thus we can make semi-conjugate observations of the outflowing ions.

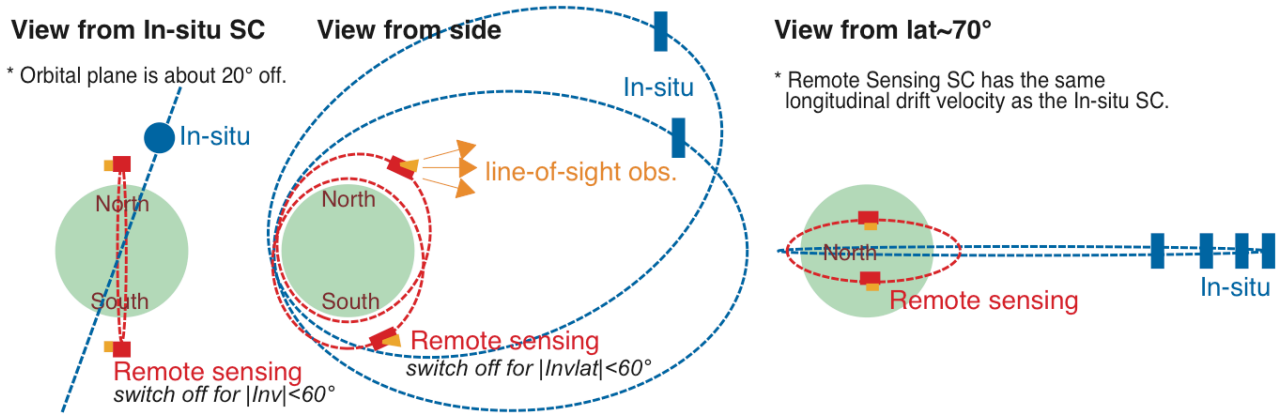

Figure 4.1: Relative locations of the in-situ SC orbit (blue dashed lines) and remote sensing SC orbit (red dashed lines). While longitudinal drift velocity is the same between both SC, latitudinal drifts are quite different.

4.1.2. Proposed orbits

Within the above requirements, the following orbits are considered close to optimal:
(1) 800 km x 33000 km altitude with 68.5° inclination for in-situ SC (Ω-start =180° and ω-start = 200°)
(2) 500 km x 2400 km altitude with 88.35° inclination for the remote sensing SC (Ω-start=180° long. and ω-start = 270° lat.)

These orbital elements make the RAAN (longitudinal) drift rates about -53°/year (413°/year with respect to the Sun) for both SC with <5°/year separation assuming maximum error in the orbit insertion by VEGA launcher (0.15° in inclination). The initial arguments of the in-situ SC (200°) are determined to cover a latitude range from about +20° to about -50° (perigee from -20° to +50°), with minimal risk of the instruments being adversely affected by the radiation belt (total dose is < 50 krad after 5.5 mm aluminum).

The drift of the argument of perigee of the remote sensing SC is about 75°/month and thus much higher than that of the in-situ SC. By locking the RAAN drifts in combination with the high 2400 km apogee of the remote sensing SC, it is still possible to acquire ~850 hours/year imaging of the in-situ SC (by the NUVO instrument), taking into account that we limit science operations of the remote sensing SC to occur only in the polar region outside the inner radiation belt (> +60° Inv or < -60°) and above the topside ionosphere (> 1800 km altitude). The elliptic orbit of the remote-sensing SC also allows in-situ measurements of ion and neutral populations at and above the upper ionosphere and in the exosphere at different altitudes.

Table 4.1: Orbital parameters for different options for the remote sensing SC

Orbit	Orbital period	Latitudinal drift (ω)	Longitudinal drift (Ω)	Visibility of in-situ*1	Radiation Shielding*2
800 x 33000 km i=68.5° (in-situ)	**589 min**	**-0.0647°/day (-23.63°/yr)**	**-0.1445°/day (-52.74°/yr)**	**target**	**5.3 mm**
500 x 2400 km (remote sensing) i=88.35° i=88.5° i=88.2°	**115 min**	**-2.495°/day**	**-0.1443°/day** **(-52.71°/yr)** -47.92°/yr -57.49°/yr	**> 800 hr/yr**	**4.5 mm**
500 x 2000 km i=88.5°	111 min	-2.7059°/day (-988°/yr)	-0.14215°/day (-51.88°/yr)	~ 500 hr/yr (too little)	3.2 mm
500 x 3000 km i=88.1°	122 min	-2.22°/day (-810°/yr)	-0.1483°/day (-54.13°/yr)	> 800 hr/yr	6.6 mm (too much)
2000 km circular i=87.8°	127 min	- -	-0.1472°/day (-53.73°/yr)	> 2000 hr	6.6 mm (too much)
1800 km circular i=88.5°	123 min	- -	-0.1457°/day (-53.18°/yr)	-	4.8 mm

*1 Only when the remote sensing SC is above 1800 km and invariant latitude > 60° or <-60°.
*2 Aluminum equivalent thickness that keeps total dose < 50 krad during the 3 year mission

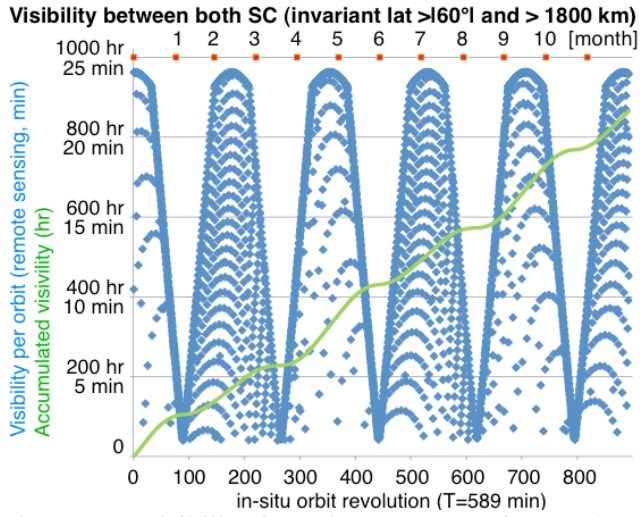

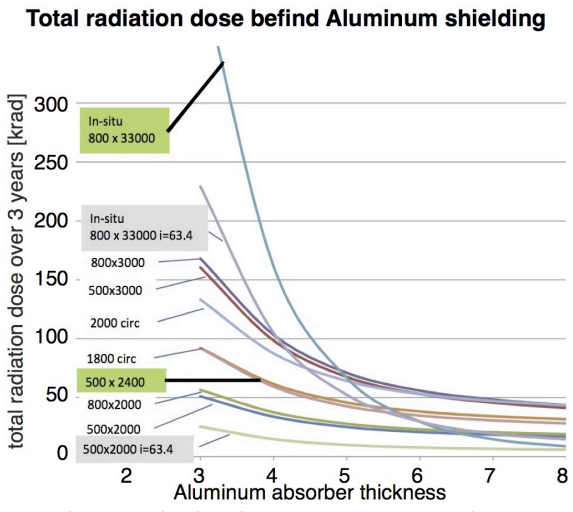

Figure 4.2: Visibility from the remote sensing SC (500x2400 km) to the in-situ SC (800x33000 km)
Figure 4.3: Mission radiation doses for candidate Nitro orbits

A small increase in the inclination of the in-situ SC increases the RAAN drift rate, resulting in a higher inclination for the remote sensing SC, and a much faster latitudinal drift rate of the argument of perigee. Inversely, to limit the latitudinal drift rate of perigee of the remote sensing SC to between 60°-90°/month (apogee returns to polar region every 2-3 months) as well as to cover at least 0°-45° in latitude by the in-situ SC, we have to keep the inclination for the in-situ SC about 68-69°.

Table 4.1 summarizes the RAAN drift rates (dΩ/dt) and arguments of perigee (dω/dt), as well as the radiation dose (necessary thickness for shielding) and the visibility from the remote sensing SC to the in-situ SC. The initial RAAN (180°) has been selected to minimize the maximum eclipse durations for the in-situ

SC (max eclipse duration of 1.91 hours over the 3-year mission). The initial argument of perigee for the in-situ SC (200°) places the apogee 20° above the equator (moves to about -50° in three years).

Figure 4.2 shows "conjugate" times during which the in-situ SC is visible from the remote sensing SC when located above 1800 km and at higher invariant latitude than ±60°. For reference, we examined the conjugate times for different orbits for the remote sensing SC. Longer contact time from the remote sensing SC is expected for higher apogee altitudes, but with an undesirable increase in the radiation dose rate. For reference, Table 4.1 compares "conjugate" time and radiation dose for different apogee altitudes. The table indicates that the 500 km x 2400 km orbit is an optimal one.

The proposed orbits for the remote sensing SC are also optimized for radiation dose. In Figure 4.3, the mission-averaged radiation levels have been calculated for both SC. The target is to select a shielding thickness that limits the total dose to 50 kRad over the mission duration. With a safety factor of two, this allows the use of 100 kRad EEE components as baseline.

4.2. Requirements for spacecraft designs (inc. attitude control and payload accommodation)

4.2.1. Common requirements for both SC

* The instruments must be placed such that there is minimum blockage by spacecraft appendages.
* The spacecraft must be designed for compatibility with VEGA launchers.
* The spacecraft should be as clean as possible from N^+ contamination from propulsion, i.e., propellants used for the attitude control during the operational phase must be nitrogen-free (no maneuver in our orbit plan).
* Real-time attitude accuracy of < 2° (with 100 acr-sec in the data).
* An external conductive surfaces, linear regulated power system, and distributed single-point-ground (DSPG) power system for basic EM cleanliness.
* 10 GByte onboard memory.
* The power and telemetry supported by the spacecraft must allow continuous operation of all experiments.
* No constraint on the Sun aspect angle.
* Spacecraft must keep operational temperature for SIs when all instruments are on.

4.2.2. Requirements for in-situ SC

* A spin-stabilized configuration should be selected in order to maximize instrument FOV coverage.
* Spin-stabilized with spin period of 22-26 sec. This is defined from the energy sweeping time scale and required angular resolution (about 3 sec full energy sweep and 8 azimuthal sectors).
* The spin period is long enough to cover the full energy sweep (96 to 128 steps) within 45° spin angle, and therefore should be 22-26 sec.
* Sun-pointing spin axis (like Freja) is preferred baseline, but north-pointing spin axis (like Cluster) is another possible option.
* FOV of all ion/electron instruments on board the in-situ SC must cover the largest possible solid angle.
* The spacecraft must be dynamically balanced both in the fully stowed configuration and in the fully deployed operational configuration. For dynamic stability, the MoI of the spin axis shall be ≥1.1 x transverse MoI both in the stowed and in the deployed configurations.
* The FOVs of the particle instruments are not blocked by booms, panels, or by the spacecraft structure.
* Moderate magnetic cleanliness (10 nT at magnetometer sensor locations on a boom at 5 m and 3 m).
* Minimum EMC cleanliness (only 1-10 Hz and three times easier than Cluster)
* Average scientific data rate of ≥ 60 kbps.
* Processing of some HK from instruments in the spacecraft DPU (including in-flight patches) should be possible, in order to issue radiation warnings to instruments, allowing them to be switched OFF.

4.2.3. Requirements for remote sensing SC

* A three-axis stabilized attitude should be selected in order to provide good line-of site observations from the remote sensing SC toward the in-situ SC with the NUVO instrument.
* This line-of-sight observation must be possible with a single-axis scanning mechanism within the orbital plane, instead of a two-axis mechanism, in order to minimize the risk of mechanical failure.
* One axis (Z) must face nadir direction.
* One axis (X) keeps as much ram direction as possible keeping the above conditions.
* The real-time pointing accuracy does not require more than 1° because our target is less than 10 R_E away, and NUVO has 2° wide FOV that scans over 45° with scanner.
* Average scientific data rate of ≥ 80 kbps.

4.3. Proposed spacecraft designs (inc. attitude control and payload accommodation)

4.3.1. Proposed design for the in-situ SC

We propose a sun-pointing SC with a platform diameter of 1800 mm, and solar panel dimensions of 1000 x 1000 mm. Figures 4.4 and 4.5 illustrate CAD designs and accommodation (schematics) of the proposed in-situ SC. The CAD does not include optional instruments such as STEIN (enhanced option) and NUVO (one-spacecraft option) or some of baseline payload that the accommodation location is not critical (e.g., spacecraft DPU).

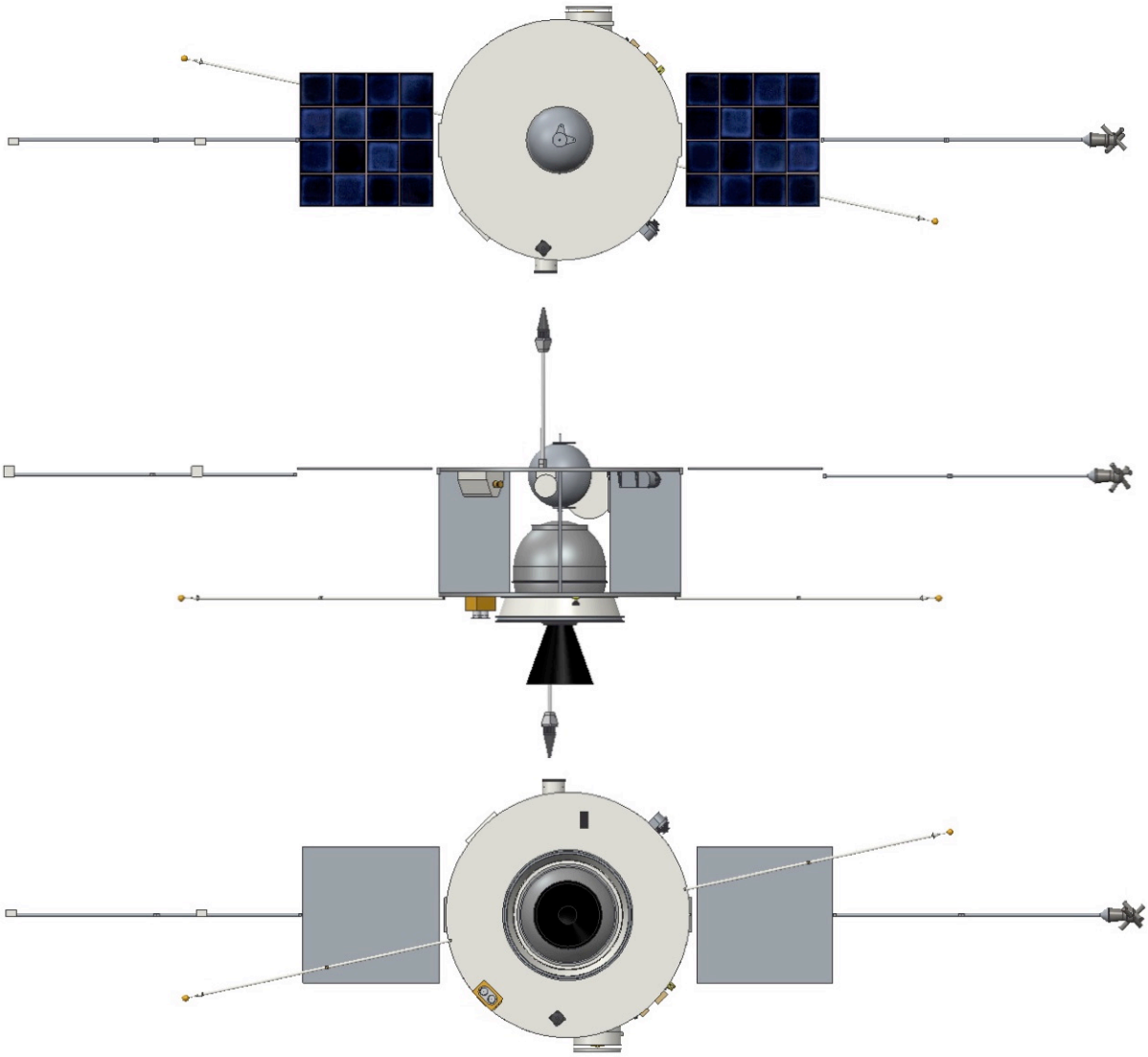

Figure 4.4: In-situ satellite top (CAD) view (top), side view (middle), and bottom view (bottom).

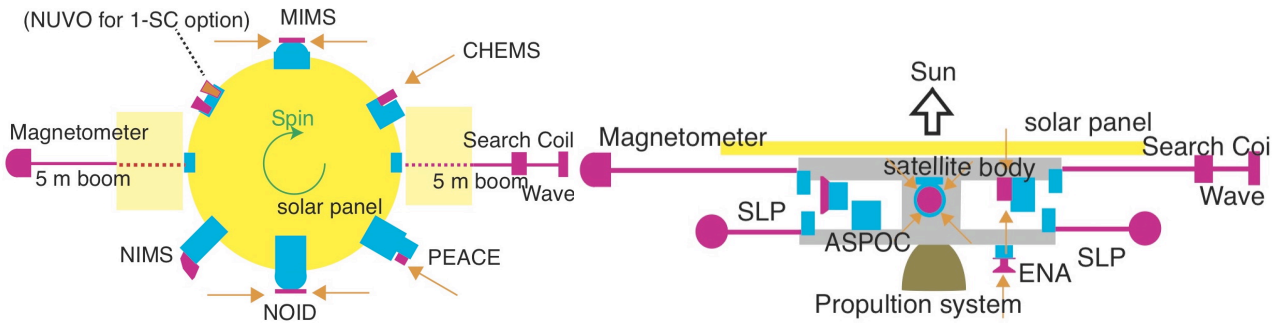

Figure 4.5: Illustration of accommodation of SIs on the in-situ SC (correct geometry is Figure 4.4). The orange allows indicate entrance direction of particles.

Table 4.2: Comparison of propellant alternatives for in-situ SC (operational phase)

	lsp (s)	desired thrust (N) & gms/s	Δenthalpy kJ/kg (180>10 bar)	W	density at 180 bar, 20° C	Itot (Ns)	mprop	Tank Ø (m)	Max p*3 (bar)	approx. tank mass (kg)	Total tank + propellant (kg)
C_3H_8*1	**61**	**1 & 1.7**	**327**	**546**	**484**	**8303**	**13.9**	**0.41**	**20**	**0.9**	**14.8**
Kr	37	1 & 2.8	36	99	805	8303	22.9	0.38	360	15.6	38.4
Xe	25	1 & 4.1	56	229	2065	8303	33.9	0.32	360	9.2	43.1
N_2*2	73	1 & 1.4	29	41	200	8303	11.6	0.48	360	33.2	44.8
He	165	1 & 0.6	55	34	28	8303	5.1	0.71	360	106.4	111.5

*1 80% fill ratio of propane, 10 bar, heat of vaporization *2 Cannot be used for NITRO
*3 Maximum tank pressure = 2 x MEOP

Prior to the deployment of solar array and booms, a solid rocket motor is fired to increase the apogee of the VEGA injection (800 km x 2427 km) to 800 x 33000 km. A suitable candidate is the STAR27H, which is confirmed available at ATK and which was used by NASA's Interstellar Boundary Explorer (IBEX) mission in 2008. At the end of the mission, we propose the use of a small blow-down hydrazine system to provide the required Δv=80 m/s to de-orbit the satellite. This is done by consecutive retro-firings at apogee, lowering the perigee to ~60 km and allowing for an uncontrolled atmospheric re-entry.

During the operational phase, the spacecraft will require spin vector precession control and spin rate maintenance. Applying a 100% margin for precession control and spin-rate maintenance, including spin-up and spin-down to 60 rpm in connection with the SRM firing, a total impulse of around 8300 Ns will be required. Use of magnetic torquers is not desirable due to their interference with the magnetometer measurements, and propane (C_3H_8) is considered the best selection as the propellant for the operational phase, because the use of nitrogen-based propellants is not allowed due to their interference with the scientific objectives. A comparison of different cold gas alternatives is summarized in Table 4.2. The use of liquid propane providing a vapour pressure of around 10 bar at 30ºC results in a significantly lower tank mass than if high-pressurized gases were to be used.

Hydrazine, whether mono-propellant or bi-propellant, is the standard propulsion technology for missions of the NITRO type. However, this propellant enhances the spacecraft-induced nitrogen background. Before hydrazine propulsion is used, instrument entrance systems or full instruments will be shut down. We also need to monitor the decaying background level after instrument turn-on to assess whether nitrogen levels have returned to sufficiently low values so as not to compromise the measurements.

Akebono observations of superthermal N^+ (< 30 eV) outflow at around 2000 km altitude showed clear short-time variations (of about 5-30 min scale) in response to geomagnetic activity (Yau et al., 1993), and the NITRO mission objective is to examine these short timescale variations. Therefore, a slowly decaying background level does not harm our science objective. Furthermore, for the in-situ cold gas system (propane as baseline), adding an appropriate mix of noble gases (e.g. Kr and Xe) could actually facilitate the mass calibration of some of the instruments (e.g. NIMS).

4.3.2. Proposed design for the remote sensing SC

We propose a 3-axis stabilized SC to provide good line-of-sight observations with the NUVO instrument., as illustrated in Figure 4.6 (accommodation schematics and CAD). In CAD, optional SIs except SLP-RS are not included. The X-axis is pointed in the velocity direction (RAM direction) and the +Z axis is pointed towards nadir. This allows for the use of one-dimensional scanning mechanisms for the UV and visible telescopes (NUVO). Due to the varying local time of the orbit, a two-axis solar panel mechanism is also required, as illustrated in Figure 4.7 The baseline of the Attitude and Orbit Control Systems (AOCS) is an inertially referenced zero-momentum bias system using 4 reaction wheels as main actuators, three magnetic torquers for wheel un-loading and star trackers as main attitude sensors. In the next study phase, it can be investigated whether a simpler system using only an Earth sensor and a momentum wheel would be preferable.

The de-orbit of the satellite at the end of the mission is similar to the in-situ SC, i.e., a small blow-down hydrazine system is used to provide the required Δv=118 m/s. In addition, the hydrazine system will provide approximately Δv=21 m/s to remove the VEGA launch dispersion errors in the beginning of the mission. We need this initial Δv because the remote sensing SC will not use propulsion during the operational phase. However, in the next study phase it will be further verified that the atmospheric drag at 500 km perigee is

acceptable. Should this prove not to be the case, the perigee height can be increased to about 600 km (inclination is changed accordingly to keep the same RAAN velocity). In this case the de-orbit requirement would be ~143 m/s.

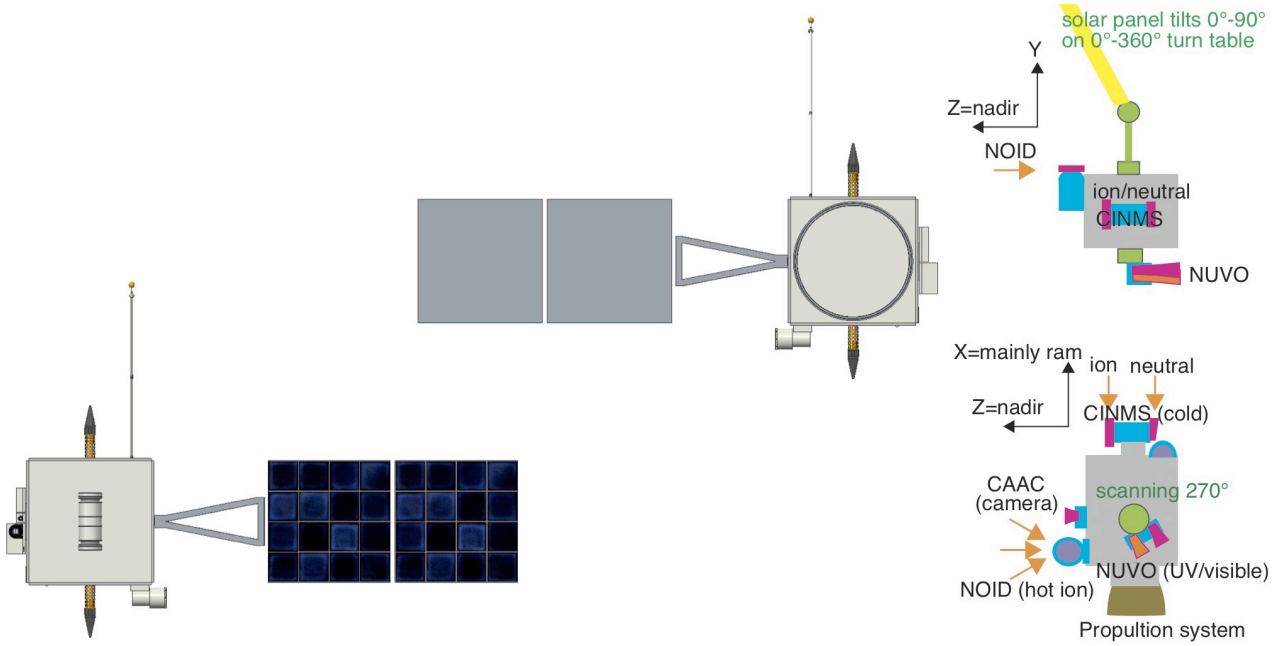

Figure 4.6: Remote sensing satellite CAD (left) and schematic accommodation of SIs (right). The orange allows indicate entrance direction of particles, and green circulars indicate rotating directions of 1-D scanner.

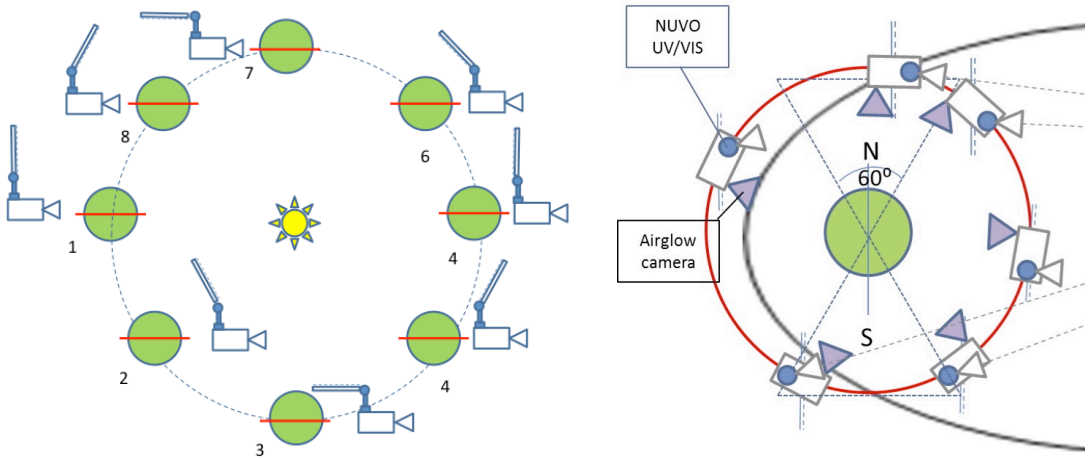

Figure 4.7: Left: Solar panel configuration. Right: scanner and camera directions for the remote sensing SC.

4.3.3 Common design elements / platforms

Concerning the fairly high radiation levels (TID doses) encountered on both satellites, one can consider two basic approaches for the procurement of platform equipment:

Use of telecom-standard hardware
- Typically 1553B standard I/F
- TID 15 yrs GEO ~120 kRad with 5 mm Aluminum shielding
- Recurring products typically available only for regulated power buses (50V, 100V, …)
- High non-recurring costs for design modifications

Use of LEO-standard hardware
- Typically RS-422 I/F or similar
- TID typically <10-20 kRad with 3 mm Aluminum shielding
- Typically designed for 28V±4V unregulated power buses
- Medium non-recurring costs for design modifications

Since non-switched spacecraft power supplies are preferred by the scientists, combined with the fact that large launch mass margins exist for both NITRO spacecraft, the LEO-standard equipment approach is

baselined. In practice, this means that an additional shielding allocation of 50% has been added for all electronic units.

To reduce platform costs, it is further suggested that equipment procurements (and delta-developments) are performed jointly as far as possible for both spacecraft. This is envisaged to e.g. include the following:

* Same solar panel design with electrically conductive coverslides.
* Same design of power system (linear regulated with distributed power dumps).
* Same SMU with integrated drive electronics e.g. for Star tracker, hydrazine thrusters, rate sensors etc).
* Same hydrazine blow-down system

4.3.4 Alternative options of the mission implementation and the spacecraft design:

As described in §2.3, there are one baseline and two alternative options for the mission implementation:

(A) The baseline as depicted above

* The two SC are equipped with the baseline instrumentation, but without the SIs that are listed as optional in Table 3.1.
* Each SC uses a dedicated VEGA launcher. In terms of payload mass, only half the capacity of each VEGA will be used.

(B) The enhanced option

* The baseline in-situ satellite is augmented with the optional STEIN instrument.
* The baseline remote sensing satellite is augmented with the optional six SIs in Table 3.1.
* Each SC uses a dedicated VEGA launcher.
* While the complexity of the remote sensing satellite increases mainly with the addition of the booms, it is still considered possible to fit the enhanced option within the total 450 MEur budget (see §6).

(C) The reduced, single-satellite option

* Only the in-situ SC is retained. While this means a loss of almost all studies related to the ionospheric source region, it is still possible to perform about 70% of the key science as summarized in Table 2.2.
* The baseline in-situ satellite is augmented with the optional STEIN plus the NUVO (moved from remote sensing SC). Since NUVO targets the magnetospheric region inside the in-situ orbit, it can be placed on the edge of spining platform looking out radially by empoying cart-wheel mode spining as, e.g., Viking.
* Only one VEGA launcher (plus SRM kick stage) is required in this case. The use of a dedicated Soyuz is however not considered cost-effective.

4.4. Budget summaries and TRL level of proposed designs (only Tables 4.3-4.5)

Table 4.3: Platform mass summary, in-situ and remote sensing (RS) satellites

	In-situ spacecraft				**RS spacecraft**			
	Mass (kg)	**DMM (%)**	**Shielding (kg)**	**Total (kg)**	**Mass (kg)**	**DMM (%)**	**Shielding (kg)**	**Total (kg)**
Structure	60	20%	0	72	49	20%	0	58.8
DHS	15	20%	5	23	15	20%	5	23
Thermal	8.4	20%	0	10.1	8.4	20%	0	10.10
Power	13.0	20%	5	20.6	35.2	20%	5	47.2
ACS	6.4	10%	2	9.0	32.2	10%	2	37.4
Propulsion	19.0	5%	0	20.0	17.8	5%	0	18.7
TT&C	16.1	10%	2	19.7	16.1	10%	2	19.7
Harness	17.7	20%	0	21.2	17.7	20%	0	21.2
NUVO mechanism	N/A				5	20%	0.5	6.5
CINMS mechanism*	N/A				(5)	(20%)	(0.5)	(6.5)
SA mech/HDRM	2	10%	0	2.2	6.2	20%	0.5	7.94
Booms	12	20%	0	14.4	1	20%	0	1.2
ASPOC	1.9	10%	0	2.09	N/A			
S/C DPU	10	20%	2	14	10	20%	2	14
Balance mass	5	20%	0	6	0			
Baseline Payload	33.0	Avg 17.5%	17.3	56.1	17.8	Avg 14%	13.2	33.5
Total	**219.5**		**33.3**	**290.4**	**236.3**		**30.7**	**305.8**

* At moment we do not need it but included it for safely in mass budget calculation.

Table 4.4. Platform power summary, in-situ and remote sensing (RS) satellites, incl DMM.

Unit	**TRL**	**Units ON**		**Ave.Duty Cycle**		**Ave. power (W)**	
		in-situ	**RS**	**in-situ**	**RS**	**in-situ**	**RS**
Data Handling System (DHS)		**4**	4				
Spacecraft Ctrl + MM	7-8	1	1	100%	100%	8.6	8.6
S/C DPU (for P/L processing and storage)	7	1	1	100%	100%	7.7	7.7
Telemetry/Telecommand unit	7-8	2	2	100%	100%	8.1	8.1
Attitude & Orbit Control (AOCS)		**16**	16				
Star Trackers	9	1	1	100%	100%	13.9	13.9
Sun sensors	9	3	3	100%	100%	0.0	0.0
SADM + NUVO mech + INRS mech avg	6	0	3	0%	75%	0.0	15.6
Rate sensor + RTU	9	1	1	100%	100%	8.9	8.9
Reaction wheels + RTU	8	0	3	0%	100%	0.0	12.9
Hydrazine thruster ctrl	8	1	1	1%	1%	0.5	0.5
Hydrazine Pressure Transducer + HTRTU	8	1	1	100%	100%	6.7	6.7
Propane thruster ctrl	8	1	0	1%	0%	0.5	0.0
Propane Pressure Transducer + HTRTU	8	1	0	100%	0%	6.7	0.0
Magnetic Torquers	9	0	3	0%	10%	0.0	0.5
Magnetometer (Safe Mode only)	9	0	1	0%	0%	0.0	0.0
Release Mechanisms		**1**	1				
Thermal Knife Ctrl	9	1	1	0%	100%	0.0	0.0
Pyro	9	1	1	0%	0%	0.0	0.0
TT&C		**3**	3				
Tx	8	1	1	100%	100%	27.5	11.0
Rx	8	2	2	100%	100%	14.2	14.2
Thermal Control System (TCS)							
Thermal Control TCRTU	7	**2**	2	100%	100%	9.4	9.4
Hydrazine thruster valve heaters	9	8	8	1%	1%	0.0	0.0
Hydrazine thruster feedline heaters	9	4	4	50%	50%	4.0	4.0
Hydrazine thruster catbed heaters	9	4	4	1%	1%	0.2	0.2
Hydrazine tank heater	9	2	2	1%	1%	0.1	0.1
Propane tank heaters	9	2	0	5%		0.6	
Propane feedline heaters	9	4	0	5%		0.5	
Spacecraft heaters							
Science Mode Eclipse		1	1	100%	100%	36.0	36.0
Science Mode SUN		1	1	30%	30%	10.8	10.8
ASPOC	8	1	0	100%	0%	2,8	0
Science instruments		**1**	1	100%	100%	85,4	54,0
Distribution losses							
Harness losses	7	1	1	100%	100%	2,4	2,1
PCDU losses	7	1	1	100%	100%	22,2	20,7
Total Power incl DMM (Sun)						**240,1**	**209,8**
Total Power incl DMM (Eclipse)						**266,8**	**235,0**

4.5. Launch and End-of-mission scenarios

The baseline mission uses two dedicated VEGA launchers. Our current understanding is that the Kourou launch site infrastructure will be able to manage the two consecutive Nitro VEGA launches within a month. Apart from this ground constraint, there will always be a daily launch window for the launch of each satellite. Note that an eventual delay in the launch of one of the two satellites would have no negative impact in the mission, because the in-orbit spacecraft could start its commissioning phase, and then start acquiring valuable data before the second launch.

Table 4.5: System budgets summary

Overall mass budget	**(kg)**	
	in-situ	**RS**
Platform mass incl DMM	234.3	272.3
Payload mass incl DMM	56.12	33.51
ESA system mass margin 20%	58	61
S/C dry mass	349	367
Propellant mass	20.1	24.6
Propellant margin (10%)	2.0	2.5
Propellant residuals (2%)	0.4	0.5
S/C wet mass	370.6	394.0
Perigee kick motor (STAR27H)	368.1	N/A
VEGA L/V Adapter	80	80
Launch mass	**818.8**	**474.0**
VEGA P/L capability (estimate)	**900**	**1100**
Margin on launcher capability (%)	**9.9%**	**132%**

Orbit parameter (km)	**in-situ**	**RS**
VEGA injection orbit perigee	800	500
VEGA injection orbit apogee	2427	2400
Apogee after PKM firing	33000	N/A

Overall Power Budget		
	in-situ	**RS**
S/C consumption in sunlight incl DMM (W)	240.1	209.8
S/C consumption in eclipse incl DMM (W)	267	235
ESA system power margin 20% (W)	53	47
Orbital period (hrs)	9.81	1.91
Max eclipse duration (hrs)	2	0.64
Average eclipse duration (hrs)	0.5	0.5
#eclipses over mission (3 yrs)	1220	9680
Max allowable battery DoD (W)	0.4	0.2
Max allowable charge rate (C/5) (W)	0.2	0.2
PCDU BDR eff (W)	0.9	0.9
PCDU BCR eff (W)	0.9	0.9
Depleted energy in max eclipse (Whrs)	711.5	200.5
Battery charge power in sunlight (W)	101.2	174.8
Required solar array power (W) EOL @ 1321 W/m2	394.7	431.6
BOL solar array power @ 1321 (W/m^2)	500.0	500.0
Installed battery capacity (Whrs)	1778.7	1002.6
Actual charge rate (W)	0.06	0.17
Max DoD (%)	40.0	20.0
Approximate battery mass (kg)	17.8	10.0

Propellant budget	**Δv (m/s)**		**mprop (kg)**	
	in-situ	**RS**	**in-situ**	**RS**
Correction L/V dispersion errors (m/s)	N/A	20.9		3.6[*1]
De-orbit (m/s)	80	120	14.2[*1]	21.0[*1]
Isp (s)			6.9[*2]	0

*1) Isp =220s (N_2H_4) *2) Isp=61 s (C_3H_8)

The exact performances of VEGA for the desired injection orbits of the NITRO satellites have not yet been confirmed by Arianespace. It is clear however that the RS satellite will consume a significantly lower part of the VEGA capacity than the in-situ spacecraft. A single shared launch carrying both spacecraft is not considered plausible even with Soyuz, given the non-standard inclinations of the two spacecraft.

Figure 4.8 depicts each satellite mounted on its 937 VEGA adapter. As can be seen, an interface ring of approximately 250 mm height is required to maintain the In-situ SRM nozzle above the -386 mm limit.

The inclinations of both orbits are selected to provide the same longitudinal drift rates. The VEGA launcher dispersion errors is dominated by the ±0.15° inclination error which mainly affects the longitudinal drift rate (RAAN drift) of the remote sensing satellite. If not corrected, this inclination would generate a separation between the two orbit planes of ~5°/year, which would be manageable, but not optimal. In the operational orbits, the RAAN drift rate sensitivity to inclination error is 13 times higher for the RS orbit than for the in-situ orbit. However, for the in-situ parking orbit (800x2427 km, i=68.5º) the RAAN drift rate is 2.4º/day which is 12 times higher than the operational drift rate of the RS satellite. This means that if there should occur an early in-situ spacecraft anomaly resulting in a delay of the SRM firing, significant relative RAAN errors could build up between the two satellites.

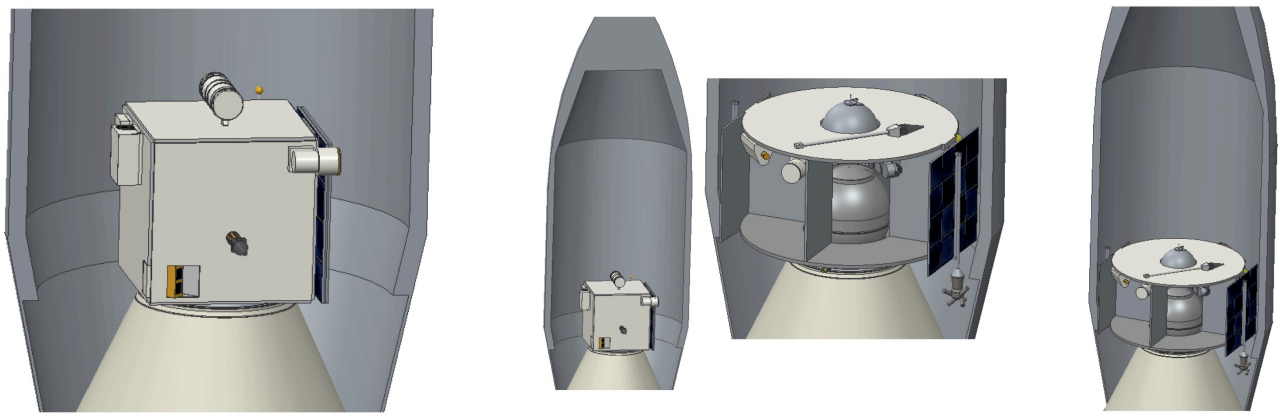

Figure 4.8: In-situ satellite (right) and remote sensing satellite (left) on the PLA 937 VG adapter

Table 4.6: The preliminary list of events from launch till commissioning is provided below.

Time	Event	Comment
T=0	VEGA #1 launch of in-situ satellite to 800 x 2427 km orbit, i=68.5°.	*1)
T=30 min	Star-tracker/accelerometer assisted nutation damping and re-orientation of spin-vector using AOCS thrusters (propane)	Re-orientation only in case of faulty separation attitude
T=24 hrs	Ground-based orbit determination and upload of AOCS commands and SRM firing commands.	
T=25 hrs	Reorientation of spin vector to AKM firing position. Spin-up of satellite to 60 rpm	Using solid spin-motors or propane AOCS thrusters
T=26 hrs	SRM firing at descending node, increasing apogee to ~33000 km.	
T=26.2 hrs	Spin-down to ~ 5 rpm and nutation damping	Using propane AOCS thrusters
T=27 hrs	Re-orientation of spin-axis towards Sun	
T=27.2 hrs	Deployment of solar arrays	
T=28 hrs	Increase spin-rate to ~10 rpm using propane AOCS thrusters	*2)
T=30 hrs	Deployment of magnetometer booms	
T=32 hrs	Deployment of SLP booms	
T=3-10 days	In-situ SC commissioning	
T=11-29 days	Preparation of remote sensing satellite and launch site for second launch.	
T=30 days	VEGA #2 launch of remote sensing satellite to 500 x 2400 km, i=88.35°.	2-3 AUM firings at perigee expected. 3-axis stabilized separation. Injection with inclination error ±0.15°.
dT=30 min	Autonomous spin-up of reaction wheels, attitude adjustment, deployment of solar array.	
T=31 days	Ground-based orbit determination and command upload for injection dispersion cancellation.	Using hydrazine thrusters. Expected Δv~21 m/s
T=32-40 days	Remote sensing SC commissioning	
…..	Start of operational phase	

*1) Spin-stabilized separation @ 5 rpm, pointing error ~6°. Sun perpendicular to spin vector (barbeque mode, 160W average S/A power). Apogee selection based on final launch mass and VEGA capabilities.
*2) Rate to be selected on the basis of required boom centrifugal deployment force and maximum boom base bending moment.

The preliminary strategy is therefore to launch the in-situ SC first, followed by the firing of its solid rocket motor to increase the apogee to approximately 33000 km. The 3-sigma variation on total impulse for the STAR27H SRM has been confirmed by ATK to be within ±0.6%, resulting in an apogee variation of

approximately ±700 km. The final selection of kick motor will be performed only after the VEGA launch capabilities have been confirmed.

Once the in-situ final orbit has been determined, the target inclination for the remote sensing satellite is frozen. Taking worst-case injection errors into account, it may be up to some tenths of a degree from the nominal value of 88.35°. The VEGA injection error for the remote sensing satellite is thereafter removed by its on-board hydrazine propulsion system (Δv~21 m/s). The end result is essentially zero relative drift in longitude between the two orbital planes. The possible effect of atmospheric drag at the RS perigee will be evaluated in the next study phase and may require a small amount of Δv over the mission duration. Table 4.6 summarize events from launch till commissioning.

De-orbiting of both SC is performed by reverse thrusting in the apogees of both satellite orbits, using the on-board hydrazine systems. The perigees will be lowered to ~60 km, resulting in uncontrolled atmospheric re-entries. The required delta-vs are reported in sections 4.3.1 and 4.3.2 above.

4.6. Ground segment

4.6.1. Commanding and Telemetry (TM)

For the remote sensing SC, a northern (or southern) station should be used for the telemetry. Examples of ESA stations are Svalbard or Kiruna. Using X-band, with a 2 W on-board transmitter and an LGA antenna (-1 dBi) and a 13-m dish on ground (G/T=35.6 dB/K), we could then have a 5 Mbps downlink for approximately 100 minutes per day, which means we can downlink around 4 GBytes per day. This means that the average telemetry rate would be about 350 kbps, which is higher than the required telemetry rate for the full option with all optional instruments. The individual passes are however quite short when the perigee is in the southern hemisphere. The worst case situation is provided, showing that average passes are around 9 minutes long or total only 200 MBytes. Therefore, we need a spacecraft-level DPU that can store the data (ideally up to 10 GBytes).

For the in-situ SC, we get the best performance if we use an equatorial station. We could then have contact times of e.g. 8 hours every 49 hours. Using X-band, with a 5 W on-board transmitter and an LGA antenna (-1 dBi) and a 15-m ESTRACK station (G/T=37.5 dB/K), we can downlink at a rate of 500 kbps. This means that for each ground station contact (8 hours, once per 49 hours) we can downlink approximately 1.8 GBytes of data, and the average telemetry rate is about 80 kbps. This is also sufficient telemetry for continuous operation for the baseline information. Since all instruments may have the possibility of generating a much larger amount of data, e.g., spin data instead of 2-min resolution data , a higher telemetry rate is preferred. The exact rate will depend on the data compression efficiency, and that can only be confirmed with actual data.

All data are processed first at ESOC where the level 0 (telemetry) data are unpacked and converted to level 1 (raw) data, and quick-look plots are produced before both the level 0 and level 1 data are distributed to each PI institute. Due to the non-criticality of the platform operation (no maneuver with ΔV is planned), weekly platform commands are uplinked from ESOC.

4.7. Operations

4.7.1. Science operation modes

The mission has five phases.

(1) Initial health check phase (From the launch until the end of the functional test of each instrument after sufficient outgassing of the spacecraft). During this time, we need real-time or semi-real-time operations and therefore the ground stations must provide good real-time contact. Since many SI uses HV supplies, we need to wait one month (outgassing) before the first instruments with HV supplies are turned on. We also need to examine the level of ion contamination from both maneuvers and attitude control. The data will be immediately compared between different ion instruments covering the same mass range and energy range. This will take about 2 months from the launch.

(2) Equatorial science phase (First two years): The in-situ SC apogee moves from about +25° to -20° during the first 20 months, and spends a large amount of time in the ring current near the equatorial region, just outside the outer radiation belt where many past observations by the geosynchronous satellites have been performed. This allows us to compare our high mass resolution results with ion measurements from geosynchronous satellites to cross check the energy and geometric factor (efficiency included). During this period, some instruments using MCP's may be turned off during high-fluxes of radiation belt particles to avoid the degradation of the MCP, while SIs with well planned shielding and use of double or triple coincidence (as with CHEMS) should be able to operate in the outer radiation belt.

(3) Mid-latitude science phase (Last one year): As the orbit axis of the in-situ SC moves from the equatorial region to a higher latitude region of the inner magnetosphere, the equatorial crossing of the in-situ SC moves inward, closer to the radiation belts. Thus, the in-situ SC explores a magnetospheric region with latitudinal scan (high inclination). To take advantage of the unique location, the threshold to turn off the SI using MCPs will be raised.
(4) Bonus phase (In case a 2-year extension is approved): The apogee of the in-situ SC (45-90°) will explore the mid to high-altitude lobe and even polar cap boundary even though the inclination is only 68.5°. Although we expect lower density there than in the inner magnetosphere, new data will help in understanding the relative importance of different energization mechanisms in the polar cap.
(5) End of mission phase (During deorbiting the spacecraft): We switch-on all instruments as far as the power budget and telemetry allows to take advantage of the unique orbit insertion into the atmosphere, because we expect unusual heavy ion formation. This could be used as a reference to meteor burning.

Although we have different mission phases, we will not impose any special campaign telemetry mode (e.g., burst mode) at the spacecraft level because the time resolution that is required from the mission science is as slow as 2 min for the in-situ SC and 30 sec for remote sensing SC. All commands, including the instrument on/off, will be performed by time-tagged command after the initial commanding period of first 2 months.

However, we still have different operation modes for each SC.
* For the remote sensing SC, the observation modes naturally changes depending on whether or not the in-situ SC is visible. During the period when the in-situ SC is not visible, the observations should concentrate more on the exosphere, e.g., rim observations or zenith observations by the NUVO instrument.
* For the in-situ SC, we switch on/off according to the spacecraft location in the radiation belt, as mentioned in (2) above. In addition to the modeled radiation belt that can easily be implemented by a spacecraft system level command to switch off the relevant SIs, we also introduce an automatic warning system of unexpected radiation belt encounters because their location can change dynamically. This is done by a program in the spacecraft DPU, using a small subset of the CHEMS and MIMS data, as described in §3.3.

4.7.2. Calibration

We will also have cross calibration between difference ion instruments, by comparing over the range where more than two instruments cover the same parameter (overlapping mass and energy for particle instruments, and overlapping frequency for MAG and SCM). This will be done at least every 6 months. We do not have to have a special campaign for such calibration but can just compare data taken in normal modes. However, as mentioned above, use of the cold gas propulsion (Propane) for the attitude control gives us the opportunity of mass calibration for the cold or low energy ion mass spectroscopy, and therefore, we will sometimes keep instruments on during (or immediately after) such attitude controls.

5. Management scheme (4.5 pages)

5.1. Organization and responsibility

During the pre-study phase until ESA appoints the Project Scientist(s) from ESA, the Science Working Team (SWT) that includes all PI teams and CoIs teams is led by three core teams: IRF (Yamauchi), IRAP (Dandouras), and UNH (Kistler). IRF is the single point contact, while the majority of physical representation (e.g., attendance to ESA, ESTEC, ESOC, and ESAC) will be performed by IRAP because of its travel convenience. UNH is the scientific contact point between ESA and NASA (through IRF). The scientific contact point to JAXA (ISAS is the actual manager) is IRF's role. We also introduce Interdisciplinary Analyses Coordinator to enhance the musti-disciplinary nature of the mission.

The Project Scientist(s) will chair the SWT and is responsible for all the above interfaces between ESA and PI/CoI teams. The SWT is responsible for (1) science planning including calibration and telemetry re-distribution, and (2) science operations planning. Based on the approved plans, each PI team creates data for data analysis and archives them for open use (see §5.4 in detail). It also creates an individual command plan, which is assembled by ESOC based on the operations plan. All the ESOC activities are ESA's responsibility.

Since the payload includes US instruments and Japanese instruments, the mission needs support from NASA and JAXA for the SI level. We do not expect those agencies to provide spacecraft support. All manufacturing and operation elements, except SIs, are ESA's responsibility. No other agncy is involved. However, ESA may negotiate support at more than the payload level because many US institutions showed

interest in providing instruments. An example of US platform support could be e.g. the provision of the STAR 27H SRM. The financial situation for the payload support is summarized in §6.2.

5.2. Tasks during mission implementation (Phase A-D)

Throught Phase A-D, SWT's tasks are, in addition to the tasks as SI preparation and manufacture:
* Keep update of SI's maturity margin.
* Review and approve proposals of new CoI on the hardware level.

5.2.1. Phase 0 / (pre-study)

This phase is led by ESA, and the SI teams are responsible for answering questions from ESA or implementing requests from ESA about the design of their instrument, e.g., power, telemetry, thermal design etc. The major tasks for ESA during this phase are as follows.
* Both technical TRL level (function of each component including payload) and scientific TRL level are examined. Although the majority of the SIs are simply copies or slight modifications of instruments that actually took data in the past or on on-going space missions, several SIs are newly developed (they reached TRL=5-6). All SI will be re-examined from the viewpoint of the purpose and area (relatively high radiation dose) of the mission, mainly through documentation, during this pre-study phase.
* Since this type of two-spacecraft configuration (looking at the high-altitude spacecraft from low-Earth orbit) is completely new, the optimum orbit and attitude control method will be tuned. Although we have done extensive analysis and found acceptable orbit parameters and attitude control methods as described in the previous section, for which OHB-Sweden found it is feasible to construct appropriate spacecraft, there may exist even better, or more cost-effective solutions.
* Which option to take must be determined. So far, we have three options: baseline (two spacecraft without optional SIs), enhanced (with optional SIs), and one-spacecraft (with NUVO transferred to the in-situ SC) options. According to our calculations (next section), the standard option is well within the 450 MEur ceiling, and even the enhanced option most likely meets this boundary. On the other hand, with the one-spacecraft option, 70% of the primary sciences can be achieved, and it is much less expensive (nearly half the price). This cost performance discussion is one of the most important tasks during this phase.
* Launch option and launch procedure must be examined.
* The attitude control system must be examined, e.g., type of cold gas for the in-situ SC and whether a simple system using only Earth sensor and momentum wheel is possible for the remote sensing SC.
* The final satellite platform including all platform equipment must be defined and designed through direct contact with all SI team because changing platform for one payload might interfere the other SI's observation.
* Downlink and uplink stations must be determined. We need as a minimum one low-latitude (equatorial) station for the in-situ SC and one (northern hemisphere) or two (northern and southern hemisphere) for the remote sensing SC. The latter might be important for the initial test-phase during 1-2 month after the launch when the real-time operation is needed.
* Verify if the atmospheric drag at 500 km perigee is acceptable for the remote sensing SC.

5.2.2. Phase A/B1 (Definition phase)

The NITRO implementation schedule is assumed to follow the ECSS phased approach. The definition phase (A/B1) ends with a Preliminary Design Review, after which it is expected that the M-class mission selection is concluded by ESA. This will be followed by the RFP & Tender Evaluation Process for the "System Prime Contractor".

5.2.3. Implementation Phase (B2/C/D)

It is foreseen that ESA is Mission Responsible and issues an overall industrial contract for the space segment to a "System Prime Contractor". Due to the "thin Prime approach" favored by ESA in the Science Programme (first used on SolO), and also governed by geographic return constraints, it is foreseen that the System Prime Contractor may subcontract the provision of the two spacecraft platforms to different suppliers. These platform suppliers may thereafter subtract provision of complete subsystems and/or procure directly on equipment level. To reduce overall cost, it is however proposed that certain equipment is jointly developed and procured for both spacecraft (e.g., §4.3.3).

The System Prime Contractor will be overall responsible for the integration of payload with the two platforms, and the overall System PFM Assembly, Integration, and Test (AIT) campaign. The in-situ solid

kick motor is procured as an off the shelf article for delivery and integration at the launch site. The System PFM AIT is followed by the Flight Acceptance Review, which gives the go-ahead for spacecraft shipment to the launch site. The successful FAR marks the formal delivery of the spacecraft to ESA.

ESA will rely on the national delegations for the funding and provision of the payloads, and provide these to the System Prime Contractor as Customer Furnished Equipment (CFE). Concerning the system interface to the PI's, it is proposed to be handled by a single contact point for each PI. It is further assumed that ESA has the responsibility for the procurement, preparation and execution of the launch and operations of both spacecraft.

The development and/or procurement of booms and payload mechanisms may be included as part of the System Prime Contractors tasks, or procured separately by ESA and provided to the System Prime Contractor as CFE. In the latter case, the specification and SoW for these items shall be jointly agreed by the concerned PIs, the System Prime Contractor, and ESA.

5.3. Tasks after launch (Phase E)

5.3.1. Launch and Early Orbit Phase (LEOP/Phase E1)

The launch campaign is proposed to be performed under overall ESA management, with full technical support provided by the System Prime Contactor. The LEOP and commissioning of the platforms are performed by ESOC with full support of the System Prime Contractor.

The commissioning and initial tests of the instruments will be performed after the commissioning of the platforms. During this period, all SI test different observation modes and parameter settings to determine the optimum configuration of their instruments. Some tuning must be possible during the ground testing. Since the instrument response should be observed as soon as the command is implemented, we need near real-time commanding, as was done for Cluster (Cluster was the latest mission with similar instrumentation to NITRO for such initial-phase test purpose). What we need to examine is:

* interference from other instruments
* cross calibration of energy ranges for ions to adjust the energy table (need re-programming ability)
* testing of on-board mass classifications for ions to adjust the mass tables.

The phase concludes with an ORR (Operational Readiness Review).

5.3.2. Operational Phase (Phase E2)

The operational phase is performed entirely by ESOC, with support provided by the System Prime contractor on a need-basis. The command lists to the SIs will be generated by the SOC (Science Operation Center), for checking and uplinking by the MOC (Missions Operations Centre). Spacecraft telemetry from the ground station will be provided as CCSDS Space Packets to MOC. The science data will be stored in a central data repository in the SOC from where it can be accessed by all PI's. All activities done by ESOC, SOC, and MOC are ESA's responsibility while the PI's activities are national funding agency's responsibility. ESA-lead SI (ASPOC and boom deployment) are also ESA's responsibility, but scanner planning should be performed by the NUVO team through their national funding agency.

ESOC also generates time-tagged commands for scientific instruments, which is an assembly of command requests from each PI. These will be uploaded to the spacecraft weekly. Since power and telemetry supported by the spacecraft allows continuous operation of all experiments, the nominal science operation plan can be closer to the nominal operation of Mars Express or Venus Express rather than Cluster (many special campaigns). However, ESOC will need at least one week to assemble them because the instrument team is large. ESOC also has to define the radiation belt timing to switch off the instruments and the visibility timing for line-of-sight operation by NUVO. On the other hand, we do not plan any major maneuvers with ΔV during the three-year mission, and therefore, the operation should be relatively simple compared to Cluster.

5.4. Science management

5.4.1. Data handling and archiving

The telemetry (Level 0) data that is received by ESOC will directly be uncompressed to produce raw data (this is level 1a data), and to produce quick-look plots (QL). The format of the QL is defned by the SWT. While keeping both level 0 and level 1a data, ESOC will directly distribute both (level 0 and 1a) data to each PI institute.

Each PI institute is responsible for examining the quality of the level 1a data and processing and cleaning them to produce a processed data set (level 2a data) for general analyses by Co-Is as well as all the

other PIs by request. The PI institutes are also responsible for producing final physical parameters (level 3 data) to store at ESA in a common format, like at the Cluster Science Archive (CSA) or Planetary Data Archive (PDA). Here we strongly recommend that this final format includes also raw count data that can easily be converted to physical parameters with a single calibration efficiency table, because this efficiency is one of the most important parameters that degrades in time and count rate directly gives uncertainty.

The level 1a and 2a data are produced for internal analyses within the PI-CoI teams to avoid mis-interpretation of noise and artificial signals, while the direct production of these level 1a and 2a data in the summary plot format (level 1b), or the ASCII CEF format with science quality data (level 2b) ready to be used in scientific papers, will be produced for everybody's use after 1 year (this can be shortened if EU policy of open data changes). The planned content of these open-access data are summarized in Table 5.1.

For the final archive, the CEF (Cluster Exchange Format) which has successfully been used for Cluster data exchange and archive, is machine-readable and human-readable, is self-descriptive, and a variety of software tools are available. The plots are normally produced immediately after the arrival of level 1a data for internal use and then will be open to the public after 1 year, but the detailed method will be determined by each PI. The open-access data do not have to be limited to key parameters, such as moment data for ions (density, velocity, and pressure), but could alternatively include differential energy flux (JE) or power spectrum density (PSD) that contains more information because these moment data are a "product under many assumptions" rather than the data itself.

Table 5.1: Open data format that should be open to outside the team

SI (in-situ)	**content**	**level 1b/2b data (within 1 year) low resolution**	**level 3 data (final archive) full resolution**
(a) MIMS	hot ion	E-t spectrograms, ion moments	JE(E, p/a, m); mass spectrogram for given E
(b) NOID	hot ion	E-t spectrogram	JE(E, p/a, m); energy mass matrix
(c) NIMS	cold ion	Count/time plot	mass spectrogram
(d) CHEMS	energetic ion	E-t and Mass-t & Pitch angle spectrograms at selected E	JE(E, p/a, m); mass-t spectrogram for fixed energies (high resolution)
(e) MAG	magnetic field	spin or 30 sec averaged field	1Hz data, spin averaged data; power spectrogram for < 10 Hz
(f1) SLP-IS	SC potential	spin or 30 sec averaged SC pot.	spacecraft potential; estimated density
(g) Waves (h) SCM	EM waves	power spectrogram	power spectrogram for < 20 kHz
(i) PEACE	electron	E-t spectrogram	JE(E, p/a, m)
(j) STEIN	ENA	Count/time plot	JE(E, p/a, m)
(k) NUVO	emission line brightness	Count on detector (spectral and spatial) versus time	Column densities and density profiles
(l) CINMS	cold ion	Count/time plot	mass spectrogram
(m) CAAC	images	low resolution images	full resolution images
(n) MSA	hot ion	E-t, Mass-t spectrogram	JE(E, p/a, m)

*1differential energy flux (JE) vs energy and angle for each mass

5.4.2. Analyses program and data center

All programs related to limited telemetry processing (decompress and time ordering) to create level 0 and 1a files, as well as the production of quick-look plots are ESA's responsibility. The SI PIs will provide information on data formats and compression to ESA. Each PI is also responsible for developing the higher levels of data (2a, 3) from level 0 and 1a data, as well as the plot program that produces level 1b/2b data from level 1a/2a data. For data processing and analysis, within the PI teams, programs such as the cl program developed at IRAP for Cluster are expected to be used. While some deep analysis programs will be shared within the PI team or SWT, the programs to produce level 1b/2b will be provided to ESA and integrated in a mission-level web-interface program (like Cluster data center/archive) under ESA's responsibility. Such an integration of analysis programs also applies to level 3 data (like Cluster Active Archive and Cluster Science Archive). Because the dataset is somewhat similar to Cluster, this work will be

able to use some of the existing structure. The CDPP (http://cdpp.eu/) multi-mission data centre is also expected to hold a NITRO mission data archive, and to provide data access to the community.

5.4.3. Model-data comparison and Ground-based observations

Since the ionospheric ions start drifting in the inner magnetospheric after modest pitch-angle scattering, the semi-conjugate geometry of two spacecraft with 20° off in the orbital plane (10°-50° off in longitude when traversing the same latitude) makes an ion drift model a strong tool in understanding the fate of scattered ionospheric ions. The inner magnetospheric drift model has long history and is already quite advanced, and the proposing team has direct access to three such models. They are the Comprehensive Inner Magnetosphere-Ionosphere (CIMI) model (Fok et al., 2014), the Hot Electron and Ion Drift Integrator (HEIDI) model (Liemohn et al., 2004), and the Inner Magnetospheric Particle Transport and Acceleration Model (IMPTAM) (Ganushkina et al., 2011). These models can simulate the drift motion under any arbitrary magnetic and electric field models for any solar wind conditions and calculate a self consistent electric field, and is reliable tool in overviewing the the fate of ions at semi-conjugate region. Therefore, collaboration with modeling people are very important, and we have those people in the team (see Annex).

Ground-based optical observations will be performed regularly to compare with UV/Visible (NUVO) observations from the remote sensing SC. Although geomagnetic conjugacy with the spacecraft will not happen very often, NUVO can cover a large range of the upper ionosphere in the polar region through a limb observation with its 1-D scanning ability, so it is possible to compare these measurements with the vertical observations from the ground more often than ordinary conjugacy allows. Three ground stations from Scandinavia (Svalbard in Norway, IMAGE network in Finland, and Kiruna in Sweden) have agreed to try such observations.

5.4.4. Coordination of different disciplines

Coordination between different discipline and different science tools as mentioned above requires own coordinator, and SWT appoints Interdisciplinary Analyses Coordinator to assist such multi-disciplinary science. The task is not limited to demand-based coordination, but may take initiative for such coordination. In other words, this is outreach within scientific community.

5.4.5. Outreach

Nitrogen is familiar to everybody (including school children) and we do not need complicated explanations to the general public to persuade then of the importance of the nitrogen study. Atmospheric escape and evolution is also an issue on which there is substantial public interest. It is easy to make a single 10-min video in explaining the first three objectives of the mission to a wide level of audiences from school children to scientists in other fields. The last three objectives are also not difficult to explain at the public level . In this sense, we do not need different videos for different levels of audiences, and all members of the mission should be able to explain the video content. The major science that is targeted by the NITRO mission is thus simple.

6. Costing (1 page)

6.1. Overview cost for three options

Table 6.1 summarizes the total cost estimate of the mission for three options listed in §4.3.3. Since the mission does not require high precision attitude control for the optical telescopes measurements, both spacecraft designs can be made fairly standard. Furthermore, the mission does not require a high telemetry rate such that small LGA antennas with standard downlink rates are sufficient. Use of ESTRACK 13-m and 15-m antennas are baselined, rather than the more expensive 35-m antennas. Therefore, An allocation of 80 M€ for each spacecraft (70 M€ for spacecraft and 10 M€ for interface tests with multiple SI), including PFM AIT by the System Prime Contractor, is considered fully sufficient. The mass of each spacecraft is significantly below the full VEGA capacity, so the launch cost can be kept at 2x45 M€. The cost of the kick-motor is 3.5 MUSD ±20% (confirmation by ATK in January 2015). A conservative allocation of 5 M€ has been made to cater for motor, S/A device, transportation to launch site, and integration at the launch site.

The surplus cost comes from booms and ESA-provided instruments/subsystems, and these extra costs are explicitly stated in Table 6.1. We also included possible extra cost on operation/archiving that comes from multi-instrument dataset.

The table indicates that the baseline option costs less than the 450 M€ boundary with a good margin, and even the option including all optional SIs is about 450 M€. On the other hand, an extremely low-cost

option (highest science return per capital) can be achieved with the single spacecraft option, achieving about ~70% of the target science (Table 2.2) with only 240 M€.

Table 6.1: NITRO cost estimate for three options listed in §4.3.3.

	ESA funding (MEur)			**national funding**
options	**baseline option**	**enhanced option**	**one-SC option**	
Spacecraft & PFM AIT	70 x 2 = 140[*1]	70 x 2 = 140[*1]	70[*1]	
Integration tests with SI	10 x 2 = 20[*2]	10 x 2 = 20[*2]	10[*2]	travel
Kick motor (in-situ SC)	5	5	5	
Launcher	45 x 2 = 90	45 x 2 = 90	45	
2-D arm for solar panel	5[*3]	5[*3]	0	
Spacecraft DPU	3+3 = 6	3+3 = 6	3	
subtotal (system/lauunch)	**266**	**266**	**133**	
Science Instrument (SI)				all costs
ASPOC	5[*3]	5[*3]	5[*3]	
scanner for NUVO	5[*3]	5[*3]		
Booms and deployment	2 x 4 = 8	2 x 7 = 14	2 x 4 = 8	
subtotal (subsysem/payload)	**18**	**24**	**13**	
Data archive (ESOC/ESAC)	5	5	5	travel/ software
Operations (ESOC)	68 (450 x 15%)[*4]	68 (450 x 15%)[*4]	68 (450 x 15%)[*4]	travel/ command
extra cost for multiple SI	1 x 14=14	1 x 21=21	1x11=11	
subtotal (logistic)	**87**	**94**	**84**	
ESA management	**59** (450 x 13%)	**59** (450 x 13%)	**32** (207 x 15%)	
TOTAL	**430 MEur**[*5]	**443 MEur**[*5]	**239 MEur**[*5]	

*1: As a reference, the SMART-1 platform, a completely new development, costed 54 M€.
*2: This is normally included in the System Prime Contractors activities.
*3: New equipment developments (including EM+EQM) and ESA-lead SIs will typically cost around 5 M€ in an ESA environment. However, the all these are not new (e.g. ERS-1, 2 for two-axis mechanism).
*4: The 3-yr ESOC operations for SMART-1 costed 20 M€.
*5: Total ESA cost for SMART-1 lunar mission including 3-yr operations was 110 M€. The recurring Cluster mission (Cluster II) costed 154 MECU (roughly M€) in 1997 consisting of 4 satellites, excluding launchers, including 40% of the scientific payload cost.

6.2. Financial condition for payload

In Table 6.1, detailed costs for SIs are not listed because they are supported by national funding agencies. The cost for each SI (adding PI and CoI) is about 10-15 M€ for cold and energetic mass spectrometers, 2-5 M€ for the other SI depending on in-house manufacture or industrial sub-contracts, ending up with about 65-75 M€ for the baseline option and 90-100 M€ for the enhanced options. As summarized in the back front page and included in the Annex, all European SIs have already obtained the official endorsement from their national funding agencies to build the SIs.

For US participation, NASA has issued a letter of acknowledgement (see Appendix). Although this is not a firm commitment, NASA normally supports at least two instruments per mission. Therefore, the two baseline US SIs (CHEMS and CINMS) will most likely be supported by NASA. Considering that this is a two spacecraft mission, NASA might support two more instruments, which are at the moment listed as the optional SIs (STEIN and an alternative for NOID-RS). This should be confirmed during the Phase-A study.

For the Japanese participation (two PI contributions and one CoI contribution), JAXA is currently preparing the future roadmap (RFI document that will be submitted early February to the top level JAXA, written in Japanese, see Appendix), and all three contributions will be listed in this document (internal deadline was 22 December, 2014, and all are under processing). Therefore, their participation, if NITRO is selected, is quite safe.